To all my mentors

Abstract

Understanding the nature of photoinduced processes in organic molecules is essential for the design and synthesis of compounds with desired photochemical properties. This dissertation aims for gaining knowledge and mechanistic understanding of energy transfer in perylene-based systems. The investigations were performed using isomeric Donor-bridge-Acceptor systems, where perylene was used as an acceptor. Identifying the correlations between the molecular structure of the dyads and their photophysical properties allowed to gain an in-depth understanding of the mechanistic differences present in those. Both Förster and Dexter types of energy transfer were shown to be highly sensitive towards relative molecular orientations. This work shows the first experimental proof of triplet-to-singlet energy transfer that was verified within the theoretical framework of Förster formalism.

This thesis also demonstrates a new solubilising strategy for rylene-based chromophores using bay-alkylation of perylene. This allowed us to obtain soluble quaterrylene and subsequently form superradiant near-infrared J-aggregates. The delocalized nature of excited states in J-aggregates allowed to overcome the energy gap law and gain high fluorescence in the near-infrared region of the electromagnetic spectrum. That opens a previously unexplored pathway towards highly emissive near-infrared chromophores, where emission efficiency was restricted by the framework of the energy gap law.

The research results presented in this thesis contribute to the understanding of the fundamental photophysics behind processes such as multiplicity conversion, directional energy funnelling, switching between the energy transfer pathways and aggregation-induced enhanced emission. Such advanced molecular functions are of practical importance in smart materials of the future.

List of publications

The research results presented in this thesis is based on the findings reported in the following papers. The author contribution is mentioned for each paper.

Paper I

Modulating TTA efficiency through control of high energy triplet states

Andrew J. Carrod, Alexei Cravcenco, Chen Ye, Karl Börjesson, [Submitted to the Journal of Materials Chemistry C]

Synthesized the phenylperylenes and performed the DFT calculations. Contributed to the writing of the manuscript.

Paper II

Multiplicity conversion based on intramolecular triplet-to-singlet energy transfer [1]

Alexei Cravcenco, Manuel Hertzog, Chen Ye, Muhammad Naeem Iqbal, Uwe Müller, Lars Eriksson, Karl Börjesson, *Sci. Adv.,* **2019**, 5 (9), eaaw5978.

Synthesized and characterized all the molecules, performed steady-state measurements together with Manuel Hertzog and assisted in X-Ray experiments. Wrote the paper together with the other authors.

Paper III

Interplay between Förster and Dexter Energy Transfer Rates in Isomeric Donor–Bridge–Acceptor Systems [2]

Alexei Cravcenco, Chen Ye, Jürgen Gräfenstein, Karl Börjesson *J. Phys. Chem. A,* **2020**, 124, 7219–7227

Synthesized and characterized all molecules, performed steady-state measurements and time-resolved measurements together with Chen Ye, except transient absorption. Performed DFT calculations together with Jürgen Gräfenstein. Wrote the paper together with the other authors.

Paper IV

Exciton Delocalization Counteracts the Energy Gap: A New Pathway toward NIR-Emissive Dyes [3]

Alexei Cravcenco, Yi Yu, Fredrik Edhborg, Jonas F. Goebel, Zoltan Takacs, Yizhou Yang, Bo Albinsson, Karl Börjesson, *J. Am. Chem. Soc.* **2021**, 143, 45, 19232–19239.

Conceived the original project idea together with Karl Börjesson. Performed synthesis of the molecules together with Jonas F. Goebel and NMR experiments together with Zoltan Takacs. Performed steady-state measurements and time-resolved measurements together with Fredrik Edhborg. Wrote the paper together with the other authors.

The author has also published the following paper that is not included in the thesis:

Paper A

Vitrification of octonary perylene mixtures with ultralow fragility [4]

Sandra Hultmark, Alex Cravcenco, Khushbu Kushwaha, Suman Mallick, Paul Erhart, Karl Börjesson and Christian Müller, *Sci. Adv.,* **2021**, 7 (29), eabi4659.

Performed the synthesis of two bay-alkylated perylenes for the scope of the project.

List of abbreviations

9-BBN	9-Borabicyclo[3.3.1]nonane
A	Acceptor
AO	Atomic orbital
APCI	Atmospheric pressure chemical ionization
B3LYP	Becke three-parameter XC functional w. Lee-Yang-Parr correlation
B	Bridge
BOA	Born-Oppenheimer approximation
CCDC	Cambridge Crystallographic Data Centre
COD	Cyclooctadiene
COSY	Correlation spectroscopy
D	Donor
DBA	Donor-Bridge-Acceptor
dba	dibenzylideneacetone
DCM	Dichloromethane
DDQ	2,3-Dichloro-5,6-dicyano-1,4-benzoquinone
DFT	Density functional theory
DMF	*N, N*-Dimethylformamide
DMAA	*N, N*-Dimethylacetamide
DMPU	*N, N´*-Dimethylpropyleneurea
dppf	1,1'-Bis(diphenylphosphino)ferrocene
dtbpy	4,4´-Di-tert-butyl-2,2´-dipyridyl
DOSY	Diffusion ordered spectroscopy
EDG	Electron donating group
EET	Electronic energy transfer
ET	Energy transfer
EWG	Electron withdrawing group
GC/MS	Gas Chromatography / Mass Spectrometry
HMBC	Heteronuclear multiple-bond correlation spectroscopy

HOMO	Highest occupied molecular orbital
HRMS	High-resolution mass spectrometry
HSQC	Heteronuclear single-quantum correlation spectroscopy
FRET	Förster resonance energy transfer
IC	Internal conversion
IEA	International Energy Agency
IRF	Instrument response function
ISC	Intersystem crossing
$\mathbf{k_{nr}}$	non-radiative rate constant
$\mathbf{k_r}$	radiative rate constant
KS	Kohn and Sham
LCAO	Linear combination of atomic orbitals
LDA	Lithium diisopropylamide
LED	Light-emitting diode
LUMO	Lowest unoccupied molecular orbital
MO	Molecular orbital
MW	Microwave
NBS	*N*-Bromosuccinimide
NIR	Near-infrared
NMR	Nuclear magnetic resonance
NOESY	Nuclear Overhauser effect spectroscopy
ODCB	1,2-Dichlorobenzene
OLED	Organic light-emitting diode
Ph	Phenyl
PMT	Photomultiplier tube
PT	Proton transfer
QED	Quantum electrodynamical
QTRLN	Quaterrylene
RISC	Reverse intersystem crossing

RET	Resonant energy transfer
RT	Room temperature
SEC	Size-exclusion chromatography
SCRF	Self-consistent reaction field
SDG	Sustainable Development Goal
SDS	Sustainable Development Scenario
SOC	Spin-orbit coupling
TADF	Thermally activated delayed fluorescence
TCSPC	Time-correlated single photon counting
TD-DFT	Time-dependent density functional theory
TET	Triplet-triplet energy transfer
TfOH	Trifluoromethanesulfonic acid
THF	Tetrahydrofuran
THT	Tetrahydrothiphene
TM	Transition moment
TOCSY	Total correlation spectroscopy
tpit	Triphenyl phosphite
TRES	Time-resolved emission spectroscopy
TTA	Triplet-triplet annihilation
UC	Upconversion (photons)
UN	United Nations
UV	Ultraviolet
VIS	Visible
VR	Vibrational relaxation
VRE	Variable renewable resources
XC	Exchange and correlation

Contents

Chapter 1

Introduction

"If you want to find the secrets of the universe, think in terms of energy, frequency and vibration."

— Nikola Tesla

The projected population growth is expected to flatten around 2100 at ca. 11 billion people according to the predictions of the UN Population Division [[5]]. It is therefore reasonable to presume that the energy demand will grow in relation to the expanding population. In the light of these predictions and in consideration with the human environmental impact, many countries are implementing net-zero agendas by 2050 [6]. Integrating higher shares of variable renewable energy (VRE) technologies, is essential for decarbonising the power sector while continuing to meet the growing energy demand. Sustainable energy production goes hand in hand with sustainable energy consumption, thus allowing the users to implement smart ways of energy use.

1.1. Electricity and Light

"There are two ways of spreading light: to be the candle or the mirror that reflects it."

— Francis Bacon

As of today, electricity only accounts for a fifth of the total final energy consumption, however its share is rising rapidly [7]. According to the IEA Sustainable Development Scenario (SDS), electricity could surpass oil as the main energy source by 2040 [8]. The electricity demand increases by roughly 50% in just 20 years in all scenarios of the IEA World Energy Outlook [8, 9]. About 20% of the consumed electricity is used for lighting purposes [10], thus making efficient light sources a good example of sustainable energy consumption. In response to that, the light sources have undergone a rapid technological evolution. In 2015 LED sources accounted for 15% of global light source sales, while in 2020 51% of the light sources sold globally were LED-based [11]. The rapid evolution of OLED technologies has paved the way to market and establish themselves in electronic devices. Despite the rapid progress, technological advancement in LED technology is expected to plateau soon [11], whereas OLEDs still have vast potential. However, to become commercially desirable, they must overcome limitations including relatively short lifetimes and high costs [12]. Approaching such research challenges requires a fundamental understanding of the mechanisms of light-induced processes at the molecular level.

Light

Light is a synchronised combination of two oscillating fields, one electrical and one magnetic propagating through space perpendicularly as graphically exemplified in **Figure 1**. Being a subject to the wave-particle duality, light is characterized by discrete energy packets, photons (or quanta). The energy of a photon is described by its frequency (or wavelength). The term visible light refers to the tiny fraction of the electromagnetic spectrum that can be perceived by the human eye which is typically in the range of 400 nm to 750 nm. Molecules interact with light, which forms the basis of light sources and solar cells for instance. It is therefore of fundamental importance to learn to control the absorption and emission of light by organic molecules.

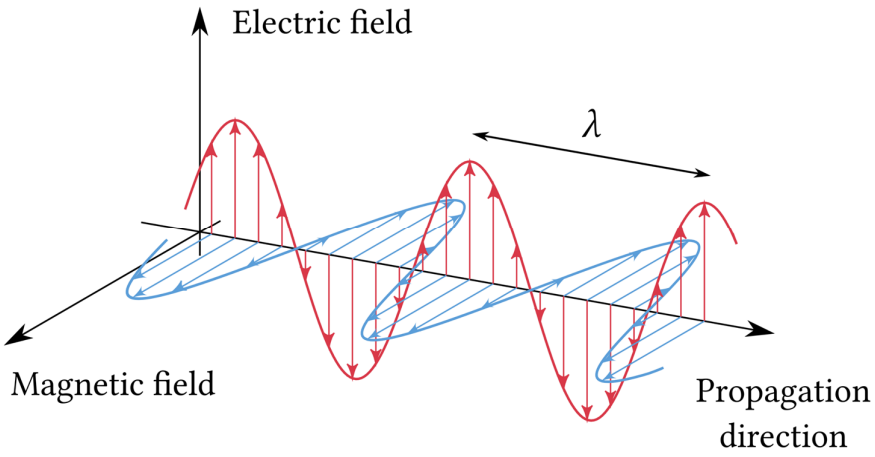

Figure 1. *An electromagnetic spectrum consists of an oscillating magnetic field (blue) and an oscillating electric field (red) perpendicularly propagating through space in the same direction. The spatial period λ, also called wavelength.*

1.2. Defining research questions

Molecules can emit light either by fluorescence or by phosphorescence. Fluorescence comes from the excited singlet states and phosphorescence occurs from the excited triplet states. In light sources, fluorescence is preferred to phosphorescence as it occurs significantly faster. It is possible to transfer the energy from triplets to singlets using spin conversion methods (triplet harvesting) that are discussed in **Section 2.3**. Methods of spin conversion are of interest fundamentally, but also for the design and production of molecules with precise function. For instance, triplet harvesting is of practical importance in the field of organic light-emitting diodes (OLEDs) where electrically excited molecules undergo a charge recombination process [13, 14]. Charge recombination results in a statistical mixture of 25% of the excited molecules being in the singlet states and 75% of the excited molecules being in the triplet states.

Due to the slow emission from the excited triplet states, a significant efficiency roll-off is observed in OLEDs [13, 14], thus making triplet harvesting strategies an important topic for research in photochemistry.

Another research topic to explore is making efficient light-emitting molecules in the near-infrared (NIR) region of the electromagnetic spectrum. The current progress in this area is limited by the framework of the energy gap law. According to Kasha's rule, the light emission in any molecule always comes from the lowest excited state of a given multiplicity [15]. The absorption and the emission in the NIR regime are associated with the photons of lower energy, meaning that the energy gap between the excited state and non-excited (ground) state is small. Reducing the energy gap between the ground state and the excited state results in an exponentially increased probability for the molecule to return to the ground state without photon emission. Developing strategies for overcoming the energy gap law is therefore essential for being able to achieve high emission quantum yields in the NIR region of the electromagnetic spectrum [16]. This is of particular interest for OLEDs [17], bioimaging [18] photodetection [19], and solar energy harvesting [20].

The research challenges mentioned in this section highlight the need for theoretical and experimental methods that can aid in a greater understanding of the fundamental processes involved in light-matter interactions. Such methods could equip scientists with relevant strategies in making materials for efficient light-harvesting, energy conversion and especially within the spectral regions where it is of most relevance.

1.3. Research hypotheses and goals

The research presented in this thesis started with one hypothesis. The research hypothesis addressed the probability of the energy transfer from the excited triplet state to the excited singlet state, potentially enhancing the rate of emission. Experiments showing triplet-to-singlet energy transfer were reported in the 60s [21, 22] using freely diffusing donors and acceptors. However, the probability of the energy transfer is sometimes discussed within the angular momentum conservation [23]. Testing this hypothesis could be done using a molecular dyad of a specific design that can potentially perform intramolecular triplet-to-singlet energy transfer. Performing energy transfer within the molecule allows executing the experiments in a controlled way by linking the experiment and the theory. This is important not only from a fundamental perspective but also can potentially address the charge recombination in OLEDs that was mentioned in the previous section. This hypothesis is addressed in **Paper II** and **Paper III.**

Based on the observations made in **Paper II** and **Paper III**, new research interest has emerged. The new theory suggested that the general photophysics of perylene derivatives can be modulated in relation to the derivatisation position. This is investigated in **Paper I**, where a series of positional isomers of phenylperylene were synthesised and studied using optical spectroscopy.

Finally, based on earlier reports showing that the bay-alkylation of perylene results in increased solubility [24] another research interest emerged. The bay-alkylation of perylene was explored as a solubilising strategy that could enable the making of extended rylene-based chromophores. The results of this research are discussed in **Paper IV** that demonstrates the synthesis of a soluble quaterrylene and explores its ability to form J-aggregates.

Concluding to the overall aim, this dissertation seeks to expand the fundamental understanding of the photophysical processes that occur in organic chromophores. By attempting to establish the correlations between the chemical structure and the intrinsic molecular properties of rylene based chromophores, this thesis strives to identify important parameters in making efficient light-emitting molecules and excitation energy transport systems. Therefore, the long-term goal of this research can be seen in the framework of the Sustainable Goals Development (Goal 7: Clean and affordable energy) as adopted by the UN Agenda 2030 [25].

Chapter 2

Background and methods

This chapter describes the core concepts that are necessary to understand the photophysical processes in organic molecules. **Section 2.1** describes electronic and vibrational states in organic molecules. **Section 2.2** covers photoinduced processes, providing the basics of fluorescence and phosphorescence, whereas **Section 2.3** describes the experimental methods that were used to study them. **Section 2.4** discusses energy transfer mechanisms and details the spin states involved. In **Section 2.5** quantum-mechanical computational methods are described in brief. Finally, **Section 2.6** covers the fundamentals of the NMR spectroscopy techniques that are described in this thesis.

2.1. Electronic and vibrational states in organic molecules

Understanding the nature of the electronic states in organic molecules is essential for making molecules with desired photochemical properties. To describe these electronic states, the behaviour of the smallest components in the molecules should be addressed first.

Schrödinger equation, stationary states

Organic molecules are comprised of atomic assemblies and atoms consist of positively charged nuclei, neutrons that have no electrical charge, and negatively charged electrons. Electrons resemble photons in their behaviour, meaning that they can be described both as particles and as waves. Due to the wave-particle duality, electrons and photons cannot be described in terms of classical mechanics, raising the need for quantum-mechanical description. An organic molecule could be therefore seen as a quantum system that is formed by the quantum-size particles (electrons). The quantum systems (molecules) thus require a quantum-theoretical description Most generally, this description is provided by the time-dependent Schrödinger equation, shown in **Equation 2.1a**,

$$\frac{\hbar}{i}\frac{\partial}{\partial t}\Psi(t) = \widehat{H}\Psi(t) \quad (2.1a)$$

where, $\hbar$ is reduced Planck constant, the constant i is the imaginary unit, the wave function $\Psi(t) = \Psi(q_{el}, q_{nucl}, t)$ depends, apart from the time, on the coordinates of the electrons q_{el} and of the nuclei q_{nucl} in the molecule (three coordinates per particle). The quantum-mechanical Hamiltonian operator $\widehat{H}$ is a differential operator that corresponds to the total energy of the system, including kinetic energy and

potential energy. The interpretation of Ψ is probabilistic: $|\Psi(t)^2|$ describes the probability of finding one electron each at the positions given by q_{el} and the nuclei at the positions given by q_{nucl}. **Equation 2.1a** can describe any process involving the molecule. However, of particular interest are so-called stationary states where $|\Psi(t)^2|$ is time-independent. The stationary states, also referred to as quantum states are limited to a set of discrete energy levels E, that could be defined by the time-independent Schrödinger equation [26] that reads,

$$\widehat{H}\Psi = E\Psi \qquad (2.1b)$$

Solving **Equation 2.1b** amounts to finding both those values for the energy E for which the equation has proper solutions Ψ and to find the corresponding Ψ. The E values (eigenvalues) are then the possible energy levels of the molecule and Ψ the corresponding eigenfunctions (states).

The wave function $\Psi = \Psi(q_{el}, q_{nucl})$ describes both electrons and nuclei as quantum-mechanical objects. However, since the nuclei are heavier than the electrons by a factor of ~10^5, their quantum character is considerably less distinct. Furthermore, the electrons will follow changes in the motion of the nuclei nearly immediately. Therefore, most quantum-chemical interpretations employ the zero-order Born-Oppenheimer approximation (BOA) [27], where the nuclei are described as classical charged particles at fixed positions. This approximation simplifies the description of the molecule because geometry parameters have fixed values in the zero-order BOA, whereas they follow a probability distribution in the full quantum-mechanical description.

Quantum numbers, spin

The stationary states of a system are commonly characterized with the help of quantum numbers. For example, for a single electron in an atom, there are four quantum numbers that are used to determine the energy, total angular momentum and its orientation, and spin. The principal quantum number (n) has an integer value starting from $1, n = 1, 2, 3 \ldots$ and is related to the energy of the state. The second quantum number (l) is used to describe the angular momentum of the atomic orbital where the electron is located. The angular momentum values start from $0, l = 0, 1, 2, 3 \ldots, n-1$. Then, each atomic orbital in their n and l states can be oriented in different directions that are described by the third quantum number, which is a magnetic quantum number $m_l = 0, \pm 1, \pm 2 \ldots, \pm l$. Finally, the fourth quantum number is used to describe the direction of the electron spin angular momentum. The spin of an electron is $1/2$ and it can be oriented in two different directions, which are usually denoted as $m_s = +1/2$ or $m_s = -1/2$ or with $\uparrow$ or $\downarrow$, respectively [28-31].

Quantum numbers can be specified both for individual electrons and for the molecule as a whole. An important example for the latter is the total electron spin S of the molecule momentum [32, 33]. For a molecule with $2N$ electrons, the possible total spin quantum numbers are $S = 0,1,2,3 \dots, N$. The spin multiplicity (M) is the number of possible spin states for the respective electronic state can be expressed by **Equation 2.2**,

$$M = 2S + 1 \qquad (2.2)$$

States of $M = 1, 2, 3, 4, 5$ are called singlets, doublets, triplets, quartets, quintets respectively (abbreviated as S, D, T, Q correspondingly). In most cases the ground state of a molecule has zero net spin ($S = 0$), due to paired spins of the electrons on the same orbital (Pauli principle). This explains why most of the molecules have singlet ground state configuration (S_0) with molecular oxygen (O_2) being a notable exception [29]. Spin states will be discussed extensively in this thesis.

Orbitals

If there were no mutual repulsion between the electrons, they would move independently of each other and could be investigated and described one by one. The possible one-electron wave functions are called *orbitals*. An orbital is a stationary state (or an approximation thereof) of a one-electron system, and thus can be described by the time-independent one-electron Schrödinger equation (**Equation 2.1b**) for the given arrangement of the nuclei. For an electron in an atom, it is called atomic orbital (AO), and for an electron in a molecule it is called molecular orbital (MO) [34]. Wave functions with orbital angular momentum $l = 0, 1, 2, 3 \dots$ are described as s, p, d, f orbitals. The s orbitals are spherically symmetric while others (p, d, f) have specific angular orientations. The structure of some AOs is shown in **Figure 2**.

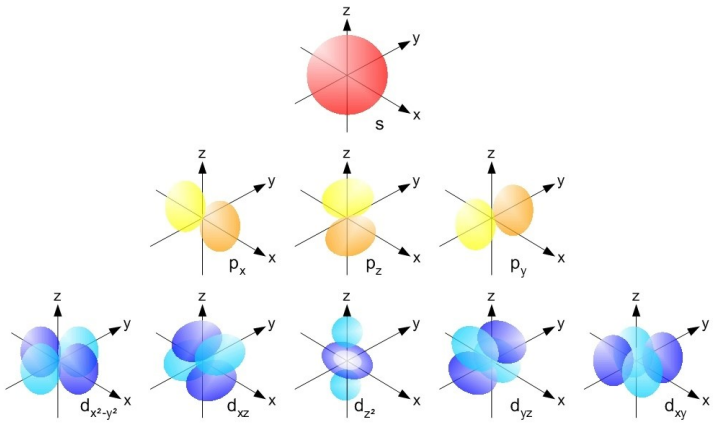

***Figure 2**. The 1s orbital (red), the 2p orbitals (yellow), the 3d orbitals (blue). Image source: [35].*

The orbitals are filled with electrons according to the Aufbau principle, meaning that orbitals with the lowest energy are filled first. Each orbital can contain a maximum of two electrons, and according to the Pauli exclusion principle [36], these electrons should have opposite spins, in that case, spins are considered paired. However, if there is more than one orbital of the same energy level, the orbitals will be filled with one electron each as far as possible, as postulated by Hund's rule. In this case, all electrons would have the same spin, and the spins are considered unpaired.

The many-electron wave function is rather complex and difficult to determine. Determining eigenvalues and eigenfunctions is usually done for each electron independently under a single-electron approximation. Of particular interest are the so-called frontier orbitals, i.e. the highest occupied molecular orbital (HOMO) and the lowest unoccupied molecular orbital (LUMO). An excitation (i.e. HOMO to LUMO transition) can be described in the way that one (or more) of the electrons is promoted into one or more of the unoccupied orbitals; the excitation energy can then be determined from the differences between the respective orbital energies. Although the orbital picture is based on the idea of non-interacting electrons it proves a good starting point for a qualitative understanding in real atoms and molecules (where electron-electron repulsion is present) as well. Furthermore, suitable types of orbitals can be defined exactly for systems with interacting electrons and can be used as tools for quantitative investigations. For instance, excitations can still be described as an electron moving from one orbital to a higher one; however, the excitation energy will no longer follow from the orbital energies. Therefore, the qualitative description of electronic transitions is commonly done using energy states.

Molecular vibrations

The nuclei in a molecule are not at rest but vibrate around their equilibrium positions. The molecular vibrations are quantized, which has two consequences. First, the nuclei can never be fully at rest. Even in the lowest energy state, they perform so-called zero-point vibrations, which make a positive contribution to the total energy of the molecule. Second, the possible levels for the vibrational energy are discrete, where the spacing between the vibrational energy levels is much smaller than the electronic excitation energies. As a consequence of these molecular vibrations, for each electronic state of the molecule there exists a series of vibrational levels that are associated with that state.

2.2. Photoinduced processes in organic molecules

Light-matter interaction

The electrons in atoms and molecules can interact with electromagnetic radiation. The radiation can induce an electronic transition if it perturbs the electron wave function

of an atom or a molecule in such a way that it converts to another wave function. For instance, an electronic transition can occur when a molecule absorbs a photon. A molecule that has absorbed a photon, changes its configuration, leaving one electron in the ground state (also denoted as a hole) and another electron is promoted to the (higher energy) excited state. Such an electron-hole pair is also called an exciton. A full-fledged description of such interactions goes beyond quantum mechanics and a requires quantum electrodynamical (QED) description [37]. QED description is significantly more complex and thus is beyond the scope of this thesis. An adequate description of electron-photon interactions can be accomplished using quantum mechanics. In this case, the light is described as an electromagnetic field that oscillates with the frequency of the photon as represented in **Figure 1**. To describe the photon absorption, one starts with the molecule in its ground state. As the external electric field (of the photon) is applied, the wave function of the electron generally undergoes just small temporary changes. However, if the photon energy matches the energy difference (ΔE) between the ground state and some of the excited states of the molecule, the photon frequency ν fulfils the Bohr frequency condition which is given by **Equation 2.3,**

$$\Delta E = h\nu \qquad (2.3)$$

where, h is Planck's constant and ν is frequency. The wave function is then in resonance with the oscillating field, similar to a pendulum that is pushed periodically with its resonance frequency. In this case, there is a finite probability that the system converts from its ground state to the respective excited state.

Transition dipole moment

The Bohr frequency condition as stated in **Equation 2.3** is necessary but is not sufficient on its own for an absorption process. In addition, initial and final electronic states must suit an excitation by an electric field. This condition can be formulated mathematically with the help of the *transition dipole moment* $\boldsymbol{M}_{n\rightarrow m}$ between the initial and final states, and is given by **Equation 2.4**,

$$\boldsymbol{M}_{n\rightarrow m} = e\langle\Psi_{el,n}|\Sigma r_i|\Psi_{el,m}\rangle \qquad (2.4)$$

where, e is the elementary charge, $\Psi_{el,n}$ and $\Psi_{el,m}$ are the electronic wave functions of the corresponding states, Σr_i is the sum of the vectors that define the positions of the electrons. For an absorption process to be possible at all $\boldsymbol{M}_{n\rightarrow m}$ must be non-zero; the absorption probability is proportional to $\boldsymbol{M}_{n\rightarrow m}$. In addition to this, the orientation of the oscillating electric field must not be orthogonal to $M_{n\rightarrow m}$. However, for molecules in solution or in the gas phase whose orientation is randomly distributed and permanently changing, this implies no restriction. The requirement

that $\boldsymbol{M}_{n\to m}$ is non-zero implies a number of rules that define which transitions are likely in a given system and which are not.

Selection rules

Selection rules are used to predict the probability and the intensity of the electronic transitions. These rules are crucial both to comprehend the behaviour of a given system and to design systems with specific properties. Selection rules are used to predict the intensity of electronic transitions and are typically discussed within the framework of symmetry and spin.

Symmetry. If the molecule under consideration has a centre of inversion, then all of its eigenstates are either symmetric (even parity) or antisymmetric (odd parity). In this case, $M_{n\to m}$ can only be non-zero for states with different parities, i.e. radiative transitions are only possible from a symmetric to an antisymmetric state or vice versa, not between two symmetric or two antisymmetric states. In practice, the symmetry-forbidden transition can still occur, however at considerably lower rates than symmetry-allowed transitions. This phenomenon is called vibronic coupling (vibrational and electronic), and it is neglected within the BOA. Vibronic coupling arises because the vibrations of appropriate symmetry lead to an admixture of the 'forbidden' excited state by some 'allowed' state.

Spin. The transition $M_{n\to m}$ can be non-zero only if m and n are in the same spin state, i.e. have the same multiplicity and the same orientation of the total electron spin. Electronic transitions between the states of the same multiplicity are referred to as *spin-allowed* transitions. This spin selection rule is valid to the extent to which spin and orbital functions can be separated. Deviations from this can induce transitions between states of different multiplicity, i.e. *spin-forbidden* transitions that arise due to the spin-orbit coupling (SOC) [38]. SOC is a relativistic effect that results from the interaction of the spin magnetic moment with the magnetic moment induced by its orbiting in the nuclear electrostatic field [39]. High SOC is usually observed in elements with high nuclear charge (where relativistic effects are strongest) and hence is sometimes denoted as 'heavy-atom effect'. SOC is essential in photochemistry allowing spin-forbidden processes such as phosphorescence to take place in organic molecules. The symmetry selection rule applies to radiative processes, whereas the spin selection rule applies to both radiative and non-radiative processes that are outlined below.

Radiative and non-radiative transitions

The absorption process discussed above is an example of a *radiative transition*, where the electronic transition is accompanied by the absorption or emission of a photon. While radiative transitions are at the heart of photochemistry, an important role is also played by *non-radiative transitions*, which use other mechanisms than photon

absorption or emission. For instance, an organic molecule that has absorbed a photon is subsequently promoted to the excited state and then can return to the ground state configuration through radiative or non-radiative decay.

Radiative decay occurs when a photon is emitted from the excited molecular state and the molecule returns to the ground state configuration. If the decay originates from the excited singlet state the process is then referred to as fluorescence, whereas if the decay originates from the excited triplet state the processes is denoted as phosphorescence.

Non-radiative decay occurs without photon emission and has several possible mechanisms. On the one hand, a system can convert to an isoenergetic vibrational level of another electronic state. On the other hand, a system can convert to a lower vibrational level belonging to the same electronic state. In this case, the released energy is dissipated e.g. by collisions with other molecules. Other potential mechanisms of non-radiative decay involve external conversion (i.e heat dissipation), Förster energy transfer, etc.

We have now summarized the typical photophysical processes that occur in organic molecules in consideration with the transition type and the spin states involved. Such processes are most often depicted using a Perrin-Jabłoński diagram shown in **Figure 3**. The diagram is followed by a brief description of the processes and their corresponding rates.

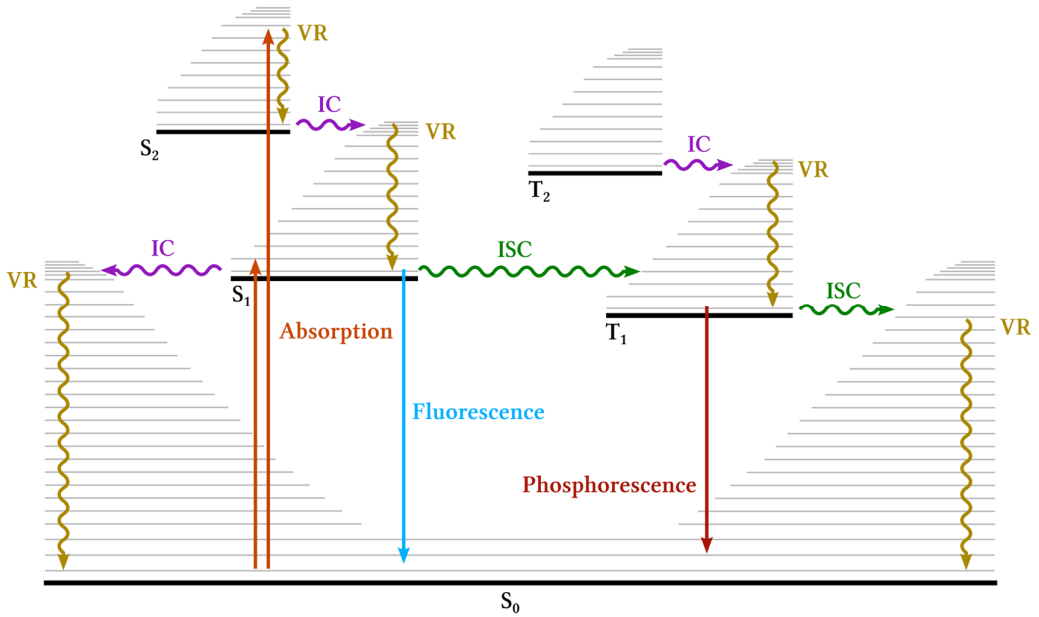

Figure 3. *Perrin-Jabłoński diagram illustrating common photophysical processes. Molecular electronic states are shown in black solid horizontal lines (i.e. S_0, S_1, etc.). The radiative transitions are shown with straight arrows, absorption – orange, fluorescence – blue and phosphorescence – red. Non-radiative processes are depicted using wiggly arrows, where intersystem crossing (ISC) is green, vibrational relaxation (VR) is yellow and internal conversion (IC) is purple.*

Absorption. It is considered that at room temperature most molecules are in the lowest vibrational level of their ground state (S_0). The absorption of a photon, therefore, starts from this level. Absorption of a photon occurs very fast, ca. 10^{-15} s.

Internal conversion (IC) is a spin-allowed radiationless transition that occurs between two isoenergetic states of the same multiplicity. For instance, IC conversion between $S_1 \leftarrow S_2$, as well as $T_1 \leftarrow T_2$ occurs very fast, ca. 10^{-12}-10^{-10} s and is regarded as an irreversible process because it is associated with an entropy increase. Additionally, the following process (vibrational relaxation) is very fast in solution.

Intersystem crossing (ISC) is a spin-forbidden isoenergetic radiationless transition between two electronic states of different multiplicity. ISC typically takes place from the excited singlet state to the excited triplet state and can be induced by high spin-orbit coupling. The rate of ISC depends on strength of spin-orbit coupling and typically lies within ca. 10^{-13}-10^{-6} s. The reverse process is also possible and can occur in two distinct ways. The transition can take place from the excited triplet state T_1 to the isoenergetic vibrational level of S_0 followed by vibrational relaxation. ISC is also considered to be an irreversible process because it is associated with an entropy increase (high density of the vibrational levels in the final lower energy electronic state). Moreover, the vibrational relaxation *(vide infra)* following ISC occurs very fast in solution. However, under certain conditions reverse ISC (RISC) is possible and will be discussed in more detail in **Section 2.4**.

Vibrational relaxation (VR) also called vibrational cooling covers all processes by which excess vibrational energy that a molecule has acquired by a vibronic transition (IC or ISC) is transferred to the surrounding media. Vibrational relaxation occurs very fast in solution, within ca. 10^{-13} to 10^{-15} s.

Fluorescence and phosphorescence. As mentioned above, emission is a radiative decay that can occur either by fluorescence or by phosphorescence. Fluorescence is a spin-allowed process originating from an excited singlet state, and occurs on a fast time scale, ca. 10^{-10}-10^{-7} s. In contrast, phosphorescence is a spin-forbidden process originating from an excited triplet state and occurs at a much slower rate ca. 10^{-3}-10^{1} s as compared to fluorescence. According to Kasha's rule [15], emission starts from the vibrationally relaxed state of the respective electronic level.

2.3. Experimental analysis of the photoinduced processes

This section describes experimental methods that were used to investigate steady-state absorption and emission in molecules that were studied in this thesis.

Absorption of a molecule is commonly expressed through Beer-Lambert-Bouguer law, shown in **Equation 2.5**,

$$A\,(\lambda) = \varepsilon(\lambda)cl \quad (2.5)$$

where, $A\,(\lambda)$ is the absorbance, $\varepsilon(\lambda)$ is the molar absorptivity, c is the molar concentration of the sample and l is the pathlength. In practice, the detector inside the UV spectrophotometer compares the light that comes through a sample to a light that comes through a reference. This is referred to as transmittance in **Equation 2.6**,

$$T = \frac{I}{I_0} \quad (2.6)$$

where, T is the transmittance, I_0 the intensity of light transmitted through the reference and I the intensity of the light transmitted through the sample. The detector transfers the transmittance data to the computer that expresses the sample absorbance, formulated by **Equation 2.7**,

$$A = \log\left(\frac{I_0}{I}\right) \quad (2.7)$$

Knowing the absorption properties of a molecule it is possible to determine its extinction coefficient $\varepsilon(\lambda)$ at a given wavelength. Using the **Equation 2.5**, $\varepsilon(\lambda)$ can be determined in solutions of known concentration.

The instrumental setup used for the absorption measurements

Steady-state absorption measurements are usually done using a spectrophotometer. The schematic diagram of a dual-beam UV-Vis spectrophotometer is shown in **Figure 4.**

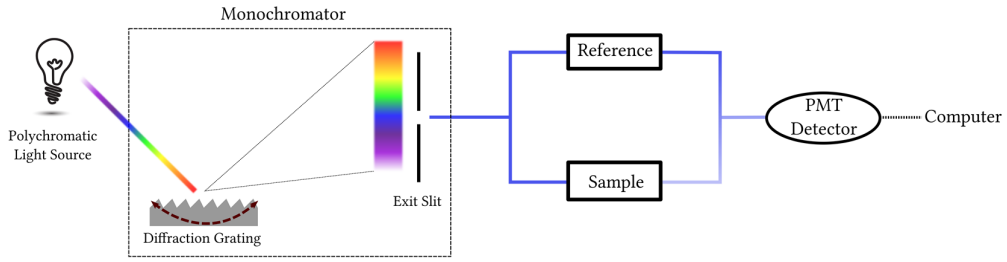

Figure 4. *Schematic diagram of a UV-VIS spectrophotometer.*

Most of the common spectrophotometers use a dual-beam design. Polychromatic light is obtained by means of deuterium arc lamps within the ultraviolet range (ca. 190 nm to 320 nm) and tungsten filament lamps cover visible to near-infrared range (ca. 320 nm to 2500 nm) of the electromagnetic spectrum. Inside the monochromator the white light is dispersed into its constitutional waves by a diffraction grating. The wavelength is selected by passing to an exit slit before reaching the sample and the reference. Thereafter, light reaches the detector where it is converted into an electrical signal. Photomultiplier tube (PMT) detectors are commonly used in spectrophotometry. The acquired data is then converted to an absorption spectrum by a computer.

The instrumental setup used for the emission measurement

The emission spectrum reflects the photon energies that are emitted by a molecule making the transition from the excited state to the ground state. Steady-state emission measurements are typically performed using a spectrofluorometer. The spectrofluorometer can record emission or excitation spectra, depending on which mode is used. During the acquisition of the emission spectrum, the grating in the excitation monochromator is fixed (λ_{exc} is fixed), whereas the grating in the emission monochromator is rotated to scan the emission wavelength (λ_{em} is scanned). The instrumental design of a spectrofluorometer recording emission spectrum is shown in **Figure 5**.

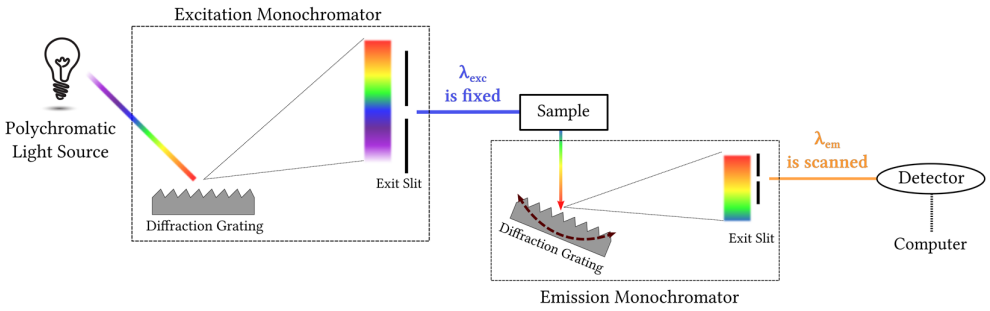

Figure 5. *The instrumental design of a spectrofluorometer recording emission spectrum.*

On the contrary, during the acquisition of the excitation spectrum the grating in the excitation monochromator is rotated to scan the excitation wavelength (λ_{exc} is scanned), whereas the grating in the emission monochromator is static (λ_{em} is fixed). In this way, the spectrum gives information about the wavelengths at which a sample will absorb so as to emit at the single emission wavelength chosen for observation. The excitation spectrum is superimposable of the absorption spectrum. The instrumental design of a spectrofluorometer recording the excitation spectrum is shown in **Figure 6**.

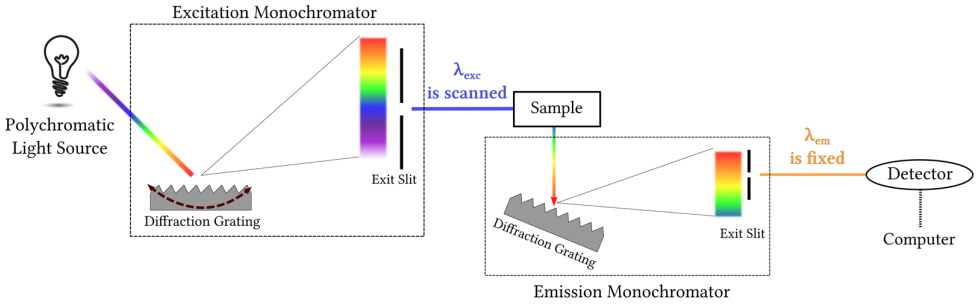

Figure 6. *The instrumental design of a spectrofluorometer recording excitation spectrum.*

2.3.1. Time-resolved measurements

This section describes experimental methods that were used to record time-resolved emission in molecules that were studied in this thesis.

The fluorescence lifetime τ_F is used to describe the average time that a population of molecules spend in an excited singlet state before the decay. The Time-Correlated Single Photon Counting (TCSPC) technique is commonly used to determine the fluorescence lifetimes. TCSPC is a digital counting technique, counting photons that are time-correlated in relation to a short excitation light pulse. In TCSPC the sample is repetitively excited using a pulsed light source with a high repetition rate. The time between excitation (start) and the first photon reaching the detector (stop) is then plotted in a histogram where the x-axis shows time from pulse to detection, and the y-axis shows a number of photons. In certain cases, an instrument response function (IRF) has to be recorded in the course of the measurement. The laser pulse and instrument response are recorded from a scattering sample and then IRF is deconvoluted from the fluorescent decay that is mathematically fitted to obtain the average lifetime of fluorescence. An example of a fluorescent emission lifetime (τ_F) measurement is shown in **Figure 7a**.

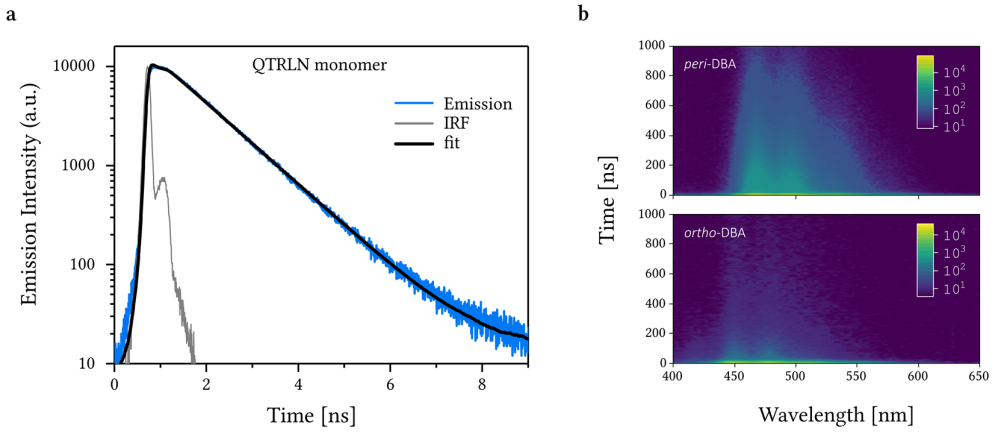

Figure 7. *a). The fluorescent emission decay (blue), monoexponential fit (black) and IRF (grey), reproduced from [3], b). TRES maps of peri-DBA and ortho-DBA recorded in toluene, reproduced from [2].*

TCSPC allows employing another technique that is called Time-Resolved Emission Spectroscopy (TRES). TRES is a technique that measures fluorescence decay at incremental wavelengths across the emission spectrum of a sample. A three-dimensional plot of intensity versus time versus wavelength is obtained. If a sample contains multiple emitters with overlapping spectra but different lifetimes, the individual spectra of these components can be separated using TRES. An example of the TRES spectra is shown in **Figure 7b**.

2.3.2. Quantum yields and rates determination

The quantum yield is normally used to describe the efficacy of a process in a system. The quantum yield Φ_x of a photoinduced process is typically used to describe the number of events N_x per number of absorbed photons in a system at a given wavelength λ and can be expressed using **Equation 2.8**,

$$\Phi_x\,(\lambda) = \frac{N_x}{N_p} \qquad (2.8)$$

This generic form could be then expanded further to calculate the efficiency of radiative processes (i.e. luminescence) as well as non-radiative processes (i.e. ISC, energy transfer, etc). The fluorescence quantum yield (Φ_F) describes the relationship between absorbed and emitted photons in a given system and is calculated using **Equation 2.9**,

$$\Phi_F = \frac{N_{em.\ photons}}{N_{abs.\ photons}} (2.9)$$

where, $N_{em.\ photons}$ is the number of emitted photons and $N_{abs.\ photons}$ is the number of absorbed photons. The Φ_F can be also expressed in rate constants as shown in **Equation 2.10**, because all the processes have first-order kinetics,

$$\Phi_F = \frac{k_F}{k_F + \sum k_{NR}} \qquad (2.10)$$

where k_F is the rate constant of radiative relaxation (fluorescence) and k_{NR} is the rate of all non-radiative relaxation processes. In cases when non-radiative decay is significantly lower than radiative decay, the values Φ_F can approach to unity (i.e. perylene).

Experimental determination of Φ_F could be done either using the absolute method or the relative method. The absolute method uses an instrumental module, such as integrating sphere, that allows to determine Φ_F directly in the course of the experiment. The relative method requires a reference compound with known Φ_F, with absorption and emission properties in a similar spectral region as the studied sample. The fluorescence quantum yield of a sample could then be determined using **Equation 2.11**,

$$\Phi_F(s) = \Phi_F(r)\,\frac{n_s^2\,A_r\,I_r\,F_s}{n_r^2\,A_s\,I_s\,F_r} \qquad (2.11)$$

where, (s) is the sample and (r) is the reference, $\Phi_F(i)$ is the fluorescence quantum yield, n_i is the refractive index of the solvent, A_i is the absorption at the excitation wavelength, I_i is the excitation intensity, F_i is the integrated emission intensity.

Quantum yields can be also used to determine radiative and non-radiative rates. For instance, if the Φ_F is known for a molecule with fluorescence lifetime τ_F, the radiative rate k_F can be expressed as shown in **Equation 2.12**,

$$k_F = \frac{\Phi_F}{\tau_F} \qquad (2.12)$$

Where fluorescence lifetime is then described using **Equation 2.13**,

$$\tau_F = \frac{1}{k_F + k_{NR}} \qquad (2.13)$$

whereas **Equation 2.14** shows how the non-radiative rate could be determined,

$$k_{NR} = \frac{1-\Phi_F}{\tau_F} \qquad (2.14)$$

The efficiency of the energy transfer event can also be expressed as a quantum yield. This is usually calculated by relating the probability of the energy transfer event per donor excitation event as shown in **Equation 2.20**.

2.4 Energy transfer and spin conversion methods

Excitation energy transfer events are essential processes in both natural and artificial light-harvesting systems [40, 41]. For instance, light-harvesting complexes contained in the antenna of photosynthetic organisms collect solar energy that is then transported to the reaction centre through a complex sequence of synchronised energy transfer events [41-43]. The direct funnelling of the energy observed in photosynthesis serves as a basis for creating artificial photosynthetic systems [44]. Energy transfer processes are isoenergetic, meaning that the energy lost by the donor reappears in the acceptor. If the excitation energy of the acceptor is below that of the donor, the isoenergetic vibrational level of the acceptor will be populated initially, followed by rapid excess energy dissipation to the medium. Energy transfer can occur by the radiative pathway or by the non-radiative pathway. The radiative energy transfer proceeds through electromagnetic radiation, a photon that is emitted by the excited donor is then absorbed by the ground state acceptor. This is a dominant process of energy transfer in dilute gases and interstellar space [45, 46]. Non-radiative energy transfer occurs without the emission of a photon and typically takes place between isoenergetic vibrational levels in the donor-acceptor pairs. It is important to note that although the energy transfer mechanisms that are described below are non-radiative themselves, they are usually followed by photon emission, a radiative decay. If the energy transfer takes place between the states of different multiplicity, the process is sometimes referred to as spin conversion. Triplet-to-singlet spin conversions (triplet harvesting) are of particular interest in photochemistry due to the

reasons that were covered in **Section 1.2**. The following subsections describe three methods that could be used for triplet-to-singlet energy transfer.

2.4.1 Förster Resonance Energy Transfer

Förster resonance energy transfer (FRET), sometimes also denoted as Coulombic mechanism or resonance energy transfer (RET) or electronic energy transfer (EET) is a mechanism describing energy transfer between two chromophores introduced by Theodore Förster in 1948 [47]. In FRET, the excitation energy is transferred from the excited donor chromophore to the acceptor chromophore through a dipole-dipole coupling [47]. No photon emission occurs during the transfer, therefore FRET is treated as a non-radiative mechanism of energy transfer [48]. Although, the FRET mechanism is often discussed using a notion of a virtual photon to illustrate the process [49]. A virtual photon is a temporary quantum fluctuation that exhibits certain characteristics of an ordinary free particle [50]. Recent interpretations of the mechanism show that radiationless FRET and radiative energy transfer could be seen as asymptotes of a single unified mechanism when analysed using quantum electrodynamical calculations [49, 51, 52]. Pictorial representation of FRET is shown in **Figure 8**.

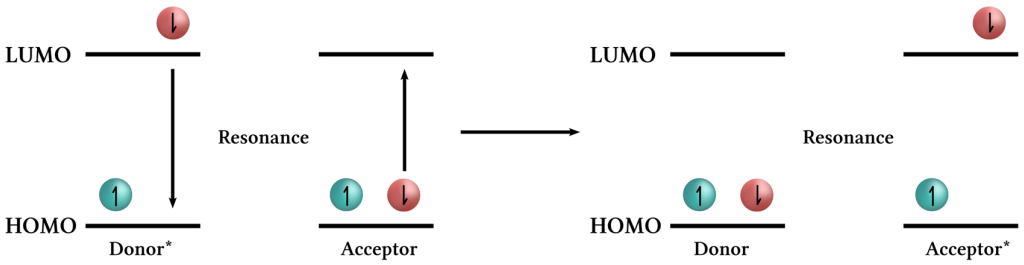

Figure 8. *Schematic diagram of Coulombic interactions in FRET mechanism.*

The energy transfer efficiency is inversely proportional to the sixth power of the distance between donor and acceptor, making FRET extremely sensitive to the small changes in the distance [53] as can be seen from **Equation 2.15**,

$$\Phi_{FRET} = \frac{1}{1+(r_{DA}/R_0)^6} \qquad (2.15)$$

where, r_{DA} is the distance between the donor and the acceptor, R_0 named critical transfer distance, is the distance in which energy transfer has 50% efficiency (meaning that half of the donor molecules decay through intrinsic pathways and half by energy transfer to the acceptor molecules). Due to its high distance sensitivity, FRET is widely used to determine the exact distances between the fluorescent markers in biological systems, denoting FRET as a ‘molecular ruler’ or a ‘spectroscopical ruler’ [53-55].

The probability and efficiency of FRET depend on several parameters: 1) the distance between the donor and the acceptor, 2) the spectral overlap between the donor emission and the acceptor absorption, 3) the relative orientation of the donor emission dipole moment and the acceptor absorption dipole moment, and 4) the strength of the transition dipole moments of the donor and the acceptor. These parameters are included in the time-dependent analysis of FRET, where the rate is used to evaluate the efficiency. The rate of Förster-type energy transfer is a function of the donor emission and the acceptor absorption J_{int}, and can be expressed using **Equation 2.16**,

$$k_{FRET}(r_{DA}) = k_D \frac{0.211^6 \kappa^2}{n^4 r_{DA}^6} J_{int} \qquad (2.16)$$

where k_D is the radiative rate constant of the donor in the absence of acceptor, n is the refractive index of the medium, r_{DA} is the donor–acceptor distance, κ^2 describes the relative orientation of the transition dipoles of the donor and the acceptor and J_{int} stands for spectral overlap integral. The spectral overlap integral is calculated using **Equation 2.17**,

$$J_{int} = \int_{\lambda_1}^{\lambda_2} F_D(\lambda)\, \varepsilon_A(\lambda) \lambda^4 \mathrm{d}\lambda \qquad (2.17)$$

where F_D is the area normalized emission of the donor and ε_A is the molar absorptivity of the acceptor. Pictorial exemplification of spectral overlap integral (J_{int}) is shown in **Figure 9**, where the distance between the absorption and the emission maxima in the molecule is called Stokes shift. With a good spectral overlap and appropriate molecular properties, the $1/r_{DA}^6$ distance dependence enables the energy transfer to occur efficiently over distances up to 10 nm [53, 56]. Although, Monte Carlo simulations show that the usable range of FRET can be extended up to 20 nm if multiple acceptors are used and the orientation factor is high [57]. The correlation between the rate of FRET and the size of spectral overlap integral is essential and is exemplified in **Paper III**.

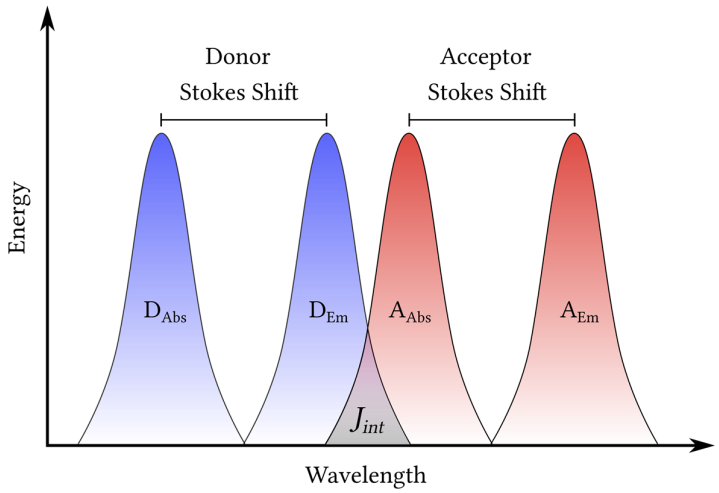

Figure 9. *Spectral overlap integral (J_{int}) is shown in grey. The distance between absorption and emission maxima in the molecule is called Stokes shift.*

As covered in **Section 2.1** the alignment of the transition dipole moment of the electron with the electric field of the electromagnetic wave has to take place for a transition event to occur. Similarly in FRET, the alignment between the transition dipole moments of the donor and the acceptor must be in place for a successful excitation energy transfer event. The orientation factor κ considers the directional orientation of the dipole-dipole interaction and is represented using a spherical model in **Figure 10**. It is usually assumed that both donor and acceptor undergo rapid Brownian rotation during the transfer event. Averaging all the possible orientations of the transition dipoles gives $\kappa^2 = 2/3$, which is used as a common value for molecules freely diffusing in solution. However, if the directional orientation of the chromophores is fixed (i.e., by means of a rigid linker) the orientation factor can be calculated using **Equation 2.18**,

$$\kappa^2 = [\cos\theta_T - 3\cos\theta_D \cos\theta_A]^2 \quad (2.18)$$

where, θ_T, θ_D and θ_A is the angle between the vectors $\vec{\mu}_D$ and $\vec{\mu}_A$, $\vec{\mu}_D$ and $\vec{r}$, and $\vec{\mu}_A$ and $\vec{r}$, respectively (where $\vec{\mu}$ is the transition dipole moment). If the orientation of the vectors is orthogonal, meaning that $\theta_D = 0$ and $\theta_T = \theta_A = 90°$, the $\kappa^2 = 0$. It is considered that the energy transfer event is not possible when the orientation factor is zero, since the dipoles seemingly have no interaction. However, there are examples showing the high quantum yield of FRET in dyads with orthogonal chromophore placing (orthogonal transition dipoles) [58-61].

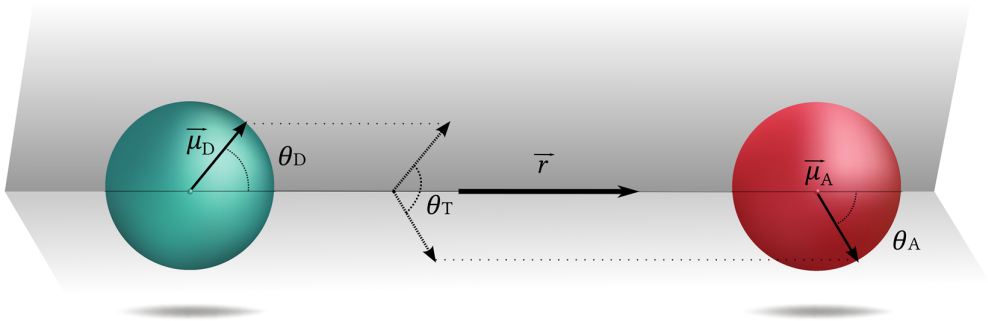

Figure 10. *Graphical representation of the orientation factor kappa squared.*

The FRET efficiency or quantum yield of the energy transfer is the probability of the energy transfer occurring per donor excitation event. Knowing the rates of the other processes, the FRET efficiency can be determined using **Equation 2.20**,

$$\Phi_{FRET} = \frac{k_{FRET}}{k_{RD}+k_{FRET}+\sum k_{NR}} \qquad (2.20)$$

where, k_{FRET} is the rate of energy transfer, k_{RD} is the radiative decay of the donor and k_{NR} is the rate of any other relaxation pathway that is not energy transfer event [31, 62].

The possibility of energy transfer by the FRET mechanism is sometimes discussed in terms of angular momentum conservation [23, 63-69]. Furthermore, this notion is also present in modern books on photochemistry [31, 34, 70]. Indeed, FRET predicts very short critical transfer distances R_0 for singlet-triplet transfer to organic acceptor molecules that have very low singlet-triplet absorption coefficients [31]. However, FRET from triplet donors with high quantum yields of phosphorescence and good spectral overlap with absorption of the singlet state of the acceptor can be fairly efficient and have been demonstrated in the 1960s [21, 22]. **Equation 2.21** conceptualizes triplet-to-singlet energy transfer,

$$^3D^* + A \rightarrow D + {}^1A^* \qquad (2.21)$$

Förster derived the energy transfer mechanism based on the Coulombic interactions, and thus the spin of the states involved should be of no consequence as seen in **Equation 2.16**. Therefore, as long as long as the right part in **Equation 2.16** is larger than 1, then triplet-to-singlet FRET outcompetes the radiative emission from the corresponding state. In this thesis, FRET mediated triplet-to-singlet energy transfer is addressed in **Paper II** and **Paper III** using perylene-based Donor-bridge-Acceptor systems.

2.4.2. Dexter-type energy transfer

The Dexter energy transfer, sometimes also denoted as a Dexter electron transfer is an energy transfer mechanism suggested by David Dexter in 1953 [71]. Similarly to FRET, Dexter-type energy transfer does not involve photon emission, and thus is regarded as a non-radiative energy transfer. It is treated as a synchronous dual exchange of electrons between the molecular orbitals of the donor (D) and those of the acceptor (A). The exchange mechanism is based on the spin conservation rule, and therefore the spin-allowed processes could be singlet-singlet, shown in **Equation 2.22** or triplet-triplet energy transfers, shown in **Equation 2.23**,

$$^1D^* + A \rightarrow D + {}^1A^* \qquad (2.22)$$

$$^3D^* + A \rightarrow D + {}^3A^* \qquad (2.23)$$

The Dexter energy transfer by electron exchange requires an appreciable overlap of the molecular orbitals of D and A, so that the critical transfer distance becomes essentially equal to the sum of the van der Waals radii of D and A. The electron density in the molecular orbital decreases exponentially with the distance from the nucleus, and thus the rate of energy transfer will decrease exponentially as well. This distance dependence of the energy transfer rates (k_{ET}) could be described using **Equation 2.24**,

$$k_{ET} \sim J exp(-\beta R_{DA}) \qquad (2.24)$$

where, R_{DA} is the distance between the donor and the acceptor, J is the integrated spectral overlap integral between the D and A and β describes the sensitivity to the distance separation [70, 72]. Essentially, two molecules must be in close contact with each other for the energy transfer to occur by the Dexter mechanism. This often occurs in solution when diffusing molecules collide [70, 73, 74].

Dexter mechanism of TET can be regarded as a double electron transfer process, one electron moves from the LUMO of the excited donor to the LUMO of the acceptor while the other electron moves from the acceptor HOMO to the donor HOMO. The pictorial representation of Dexter-type energy transfer could be seen in **Figure 11**.

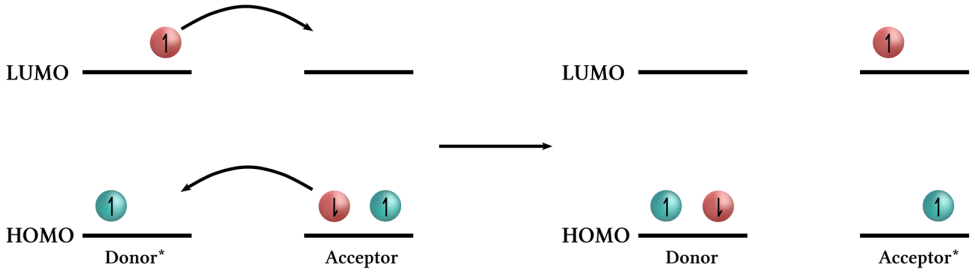

Figure 11. *Schematic diagram of simultaneous double electron transfer in Dexter-type energy transfer.*

In its original formulation Dexter mechanism was described in terms of direct overlap between donor and acceptor orbitals, however this can be extended to coupling mediated by the intervening medium. For instance, Dexter-type energy transfer can still occur without direct overlap of donor and acceptor orbitals, but rather by means of a 'conductive' bridge, that covalently links donor and acceptor. Bridge-mediated Dexter-type energy transfer is also referred to as 'through bond' energy transfer as to distinguish it from the 'through space' transfer that is a result of direct orbital overlap. The involvement of the bridge in Dexter energy transfer is often discussed in terms of hopping or superexchange mechanisms [75]. Through bond interactions that take place via connecting units (bridges) are common in supramolecular structures [76-81]. In the superexchange mechanism, the bridge energy is always higher than those of donor and acceptor, so the electron tunnels in a single step from donor to acceptor. On the other hand, in cases when the energy of the bridge is small, it acts as an intermediate step in transfer event being directly involved in the process. This is referred to as the hopping mechanism. Finally, if there is a complete mixing among the donor-bridge-acceptor orbitals (large coupling limit), the bridge acts as an incoherent 'molecular wire' as could be seen in the case of conjugated conducting polymers [82]. Triplet energy transfer is often used in energy upconversion (**Section 2.4.4**), preparative photochemistry and elucidation of the reaction mechanisms. **Paper III** addresses the interplay between Förster and Dexter Energy transfer mechanisms in isomeric Donor-bridge-Acceptor systems.

2.4.3. Delayed fluorescence

Delayed fluorescence describes an emission that has spectral characteristics of fluorescence but lifetimes much longer than that of prompt fluorescence. It typically occurs by the repopulation of the S_1 state following the initial ISC to the T_1 state. There are two types of delayed fluorescence; thermally activated delayed fluorescence (E-type delayed fluorescence) and triplet-triplet annihilation (P-type delayed fluorescence).

Thermally activated delayed fluorescence (TADF)

Thermally activated delayed fluorescence was first observed in eosin dye and was initially referred to as E-type delayed fluorescence [83]. Some organic dyes, for instance eosin and fluorescein demonstrate a small S_1-T_1 energy gap (ΔE = 20-40 kJ mol^{-1}). Light absorption by S_1 in eosin is then followed by prompt emission competing with ISC to T_1. By absorbing the nearby thermal energy, the eosin in its triplet state T_1 can undergo reverse intersystem crossing (RISC) allowing to repopulate singlet state S_1 which can then return to the ground state through fluorescent decay. The TADF process is graphically exemplified using an energy diagram in **Figure 12**.

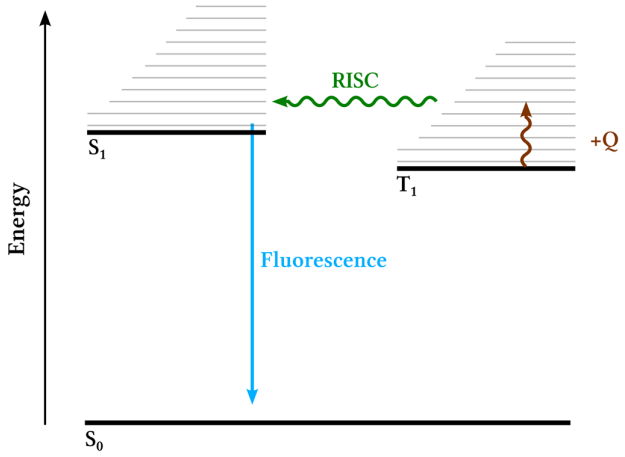

Figure 12. *Energy diagram showing thermally activated delayed fluorescence. Thermal energy (+Q) is shown in brown.*

Normally, T_1 to S_1 delayed fluorescence is observed, however there are some exceptions. Xanthone demonstrates an ultrafast 1 ps ISC rate to the T_2 that is nearly isoenergetic with S_1. The reverse intersystem crossing then occurs from T_2 to S_1 in competition with IC to T_1. [84]. The intensity of the TADF decreases strongly at reduced temperatures [85]. TADF did not get much attention until 2009 when Adachi and coworkers reported molecular design strategy for highly efficient green, orange and blue OLEDs using TADF [86-88]. The field escalated quickly showing systems of nearly unity external quantum efficiency [89, 90]. This approach towards OLEDs fabrication is sometimes referred to as the 3rd generation OLEDs after fluorescent and phosphorescent devices.

Triplet-triplet annihilation

TTA was initially denoted as P-type delayed fluorescence taking its name from pyrene [91] and later observed in many other aromatic compounds [92-94]. Parker and Hatchard in the 1960s established the field of sensitized triplet-triplet annihilation explaining the delayed fluorescence from anthracene and phenanthrene derivatives [83, 95-97].

TTA is a Dexter-type energy transfer mechanism that involves the recombination of two excited triplet states. This can be a sensitized process, but here we consider the TTA event with respect to only the annihilator molecule. TTA can occur both intramolecularly and intermolecularly. The recombination of two excited triplet states can result in higher excited singlet, triplet or quintet states. Taking into consideration the number of spin states in each possible configuration (singlet – 1, triplet – 3, quintet – 5), the plausibility of a singlet configuration is 1/9, triplet is 3/9 and quintet is 5/9 [98, 99].

$$^3E^* + {}^3E^* \leftrightarrow {}^1[EE]^* \rightarrow {}^1E^* + {}^1E \qquad 2.25$$

$$^3E^* + {}^3E^* \leftrightarrow {}^3[EE]^* \rightarrow {}^3E^{2*} + {}^1E \rightarrow {}^3E^* + {}^1E \qquad 2.26$$

$$^3E^* + {}^3E^* \leftrightarrow {}^5[EE]^* \rightarrow {}^5E^* + {}^1E \qquad 2.27$$

Several mechanisms can be envisaged for the relaxation of encounter complexes. Firstly, if the singlet encounter complex is formed, it can result in a higher singlet energy state ($^1E^*$) for one molecule and ground state configuration for the 'donating' molecule as shown in **Equation 2.25**. Secondly, for the triplet encounter complex the higher energy level formed would be the second triplet state $^3E^{2*}$ as illustrated in **Equation 2.26**. Thirdly, for the quintet encounter complex it is the first quintet state ($^5E^*$) as seen in **Equation 2.27**. All scenarios above are reversible processes, the encounter complex of any multiplicity can dissociate into two excited triplet states.

For most organic molecules, the quintet state is energetically inaccessible, and thus a quintet encounter complex is not likely to form [98, 99] We therefore consider only 4 possible encounter complexes and their products. Importantly, the probability of formation of $^1E^*$ and $^3E^{2*}$ is also determined by the accessibility of higher energy states of either spin-multiplicity. In an ideal case $^3E^{2*}$will be inaccessible and $^1E^*$ will be accessible thus forming the basis for the spin-statistical limit of triplet-triplet annihilation photon upconversion (TTA-UC) [100]. TTA-UC is graphically exemplified using Jabłoński diagram in **Figure 13** below.

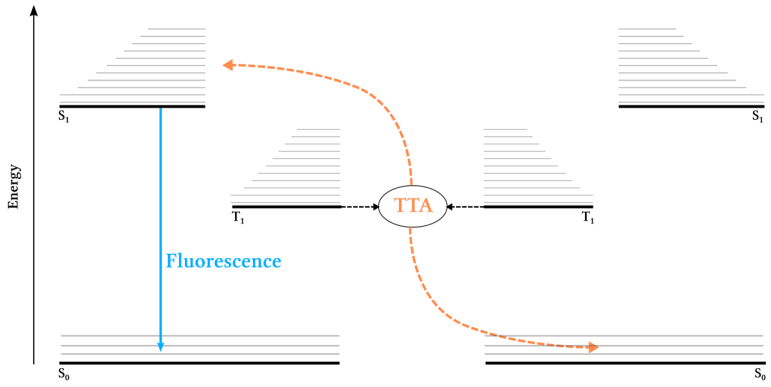

Figure 13. *Jabłoński diagram showing sensitized TTA-UC.*

The energetic requirements of the ideal scenario could be seen as a prerequisite for a successful TTA-UC annihilator. Photon upconversion through TTA is commonly used as a strategy for triplet harvesting and has been explored extensively in solar cells [100] and OLED systems [101]. Recent years have shown significant progress towards reaching the spin statistical limit of 50% [100, 102]. Recently, the precedents of exceeding the spin-statistical limit were rationalised [103].

2.5 Quantum-mechanical calculations

Quantum-mechanical calculations are often employed as a complement to experimental investigations, e.g. to predict structures and geometry of the molecules involved, excitation spectra and transition rates. Density-functional theory (DFT) is arguably the most common approach to quantum-mechanical modelling nowadays. The DFT method is based on a theorem postulated by Hohenberg-Kohn, stating that all properties of a given system are determined unambiguously by its electron density [104]. Starting from this theorem, Kohn and Sham (KS) [105] developed a computational scheme where the density of the system is represented by a set of orbitals (KS orbitals). This KS formalism involves the exchange and correlation (XC) energy of the system as a functional of its electron density. The mathematical expression of this functional is unknown and has to be approximated to make the KS formalism into an applicable computational scheme. Today, a wide variety of XC functionals are available, which allow reliable yet economical calculations of electronic structures.

In practical DFT calculations, a second approximation is necessary in addition to the choice of an approximate XC functional. The KS orbitals need to be described by a finite set of parameters, which can be handled by the computer. To this purpose, the orbitals are approximated as a linear combination of predefined atomic-centred functions (basis functions) [106]. The choice of a suitable basis set is a trade-off between numerical expenses and accuracy.

The geometry of the molecule, i.e. the set of coordinates for the nuclei, is specified in advance for a single DFT calculation. Typically, one needs to determine the equilibrium geometry of the molecule under investigation. This means finding that geometry for which the total energy of the molecule is minimal. To this end, one starts with a DFT calculation for a reasonable guess geometry. Based on the result of this calculation, the guess for the geometry is refined. This procedure is repeated until the geometry is sufficiently close to the equilibrium geometry. The procedure described is denoted as geometry optimization.

Standard KS-DFT describes only the ground state of the molecule and not its excited state. This limitation has been overcome by Gross and Runge [107], who proved that KS-DFT can be generalized to the case of a time-dependent external potential. Thus, the excitation of the molecule can be simulated by an oscillating external potential (modelling a photon), and the excited states of the molecule become available for DFT calculations [108].

A DFT or TD-DFT calculation as described above reflects the situation in the gas phase. However, solvent effects are known to have a substantial influence on the

properties of the molecule. It is possible to execute DFT calculations with consideration of at least some of the solvent effects, typically by some form of the self-consistent reaction field (SCRF) approach [109]. However, this significantly increases computational costs, and most often is disregarded. This sometimes raises concern that the output data for the ideal gas phase is not descriptive enough.

DFT calculations have been incorporated in several of the publications in this thesis. All of these calculations were performed using the Gaussian program package [110], using the Becke three-parameter (B3LYP) XC functional with Lee-Yang-Parr correlation [111-114] and the LANL2DZ basis set [115]. In **Paper I** and **Paper III** the ground state energies as well as the energies of the excited states in perylene-based molecules were determined using the B3LYP functional and LANL2DZ basis set. Furthermore, the Boltzmann probability density of the rotational degree of freedom in perylene acceptors was determined in **Paper III** using the Gaussian program package**.** This was done by changing a dihedral angle between the perylene and the phenyl ring and calculating the energy of the new conformer in a single point calculation. The probability density was then plotted against the energy of each conformer to derive the most plausible conformations of the molecules. Finally, the DFT method was used to determine the optimized geometry of dihexylquaterrylene in order to build the J-aggregate models for the diffusion coefficient simulation in the NMR study that is described in **Paper IV**.

2.6 NMR spectroscopy methods

Nuclear magnetic resonance is arguably the most common method of analysis in the toolkit of an organic chemist. Readers interested in the basic principles of the NMR methods are referred to the textbook [116]. In this thesis, 1D and 2D NMR methods were used for the structure determination and the diffusion NMR technique was used to estimate the physical size of the J-aggregates. All the NMR experiments in this thesis were carried out using 900 MHz, 800 MHz, 600 MHz and 400 MHz field strength spectrometers depending on the experiment.

2.6.1 Spectral assignment using 1D/2D experiments

To characterize the compounds synthesised in **Paper II** and **Paper III**, a set of ^{1}H, ^{13}C and ^{31}P NMR was performed. A set of 1D NMR measurements complemented by the HRMS results and single crystal X-ray data (only for *peri*-DBA) were used for the final structure determination. In **Paper IV**, in addition to 1D measurements, a set of 2D experiments was performed. Homonuclear COSY and anti-Z-COSY [117] experiments were performed in order to evaluate short-range proton-proton couplings and determine the J-coupling networks. Short-range heteronuclear

correlations were evaluated by HSQC experiments. HSQC spectra are widely used for investigating one-bond heteronuclear couplings, such as ^{1}H-^{13}C, ^{1}H-^{15}N, ^{1}H-^{31}P, etc. Long-range correlations between ^{1}H-^{13}C were investigated by IMPACT-HMBC [118]. The spin systems were identified with help of 2D-TOCSY experiments. TOCSY is a homonuclear experiment generally used for protons allowing to see correlations between spins that are connected by an unbroken chain of couplings. 2D NOESY experiments were done to be able to identify which homonuclear spins are close in space. In this way NOESY can be treated as a complementary experiment to COSY. Selective excitation 1D NOESY experiment was carried out to identify the interaction between particular aliphatic-aromatic protons. 1D NOESY experiment allows to set the excitation of a single site. 1D NOESY also provides a better signal to noise ratio as compared to 2D NOESY under shorter experiment times. Additionally, solvent and water peaks were suppressed using shaped pulse presaturation in order to obtain the spectra within a reasonable timeframe.

2.6.2 Diffusion NMR to estimate the molecular size

In **Paper IV** The physical size of the J-aggregates was estimated using diffusion-ordered spectroscopy (DOSY). DOSY allows performing both quantitative and qualitative types of analysis. The individual diffusion coefficients for the diffusing species could be determined in the experiment as a quantitative measure. During the diffusion experiment, the smaller species 'diffuse away' faster leaving the larger species (diffusing slower) present in the spectrum for a longer time. This can provide some qualitative insights into the composition of the investigated species.

Measured diffusion coefficients

The diffusion experiments for the aggregates were performed at the detection limits of the 900 MHz NMR system (10^{-4} M in $C_2D_2Cl_4$, 2 orders of magnitude higher than UV/Vis concentration). The indications of an exchange between monomers and aggregates were observed at the given concentration, indicating that the formed aggregates are in dynamic equilibrium. Luckily, the exchange was slow enough thus enabling to determine individual diffusion coefficients for the fast-diffusing species (monomers) and for the slow-diffusing species (aggregates). As seen in **Figure 14** the fast-diffusing species (monomers) demonstrate comparable diffusion rates at 10^{-4} M and 10^{-5} M, however the diffusion rates of the slow-diffusing species (aggregates) decrease as a function of concentration. This indicates the formation of larger aggregates at higher concentrations, whereas the diffusion rates of the monomers are concentration independent. Furthermore, the results obtained when carrying out exchange suppression sequences further reassured the slow exchange.

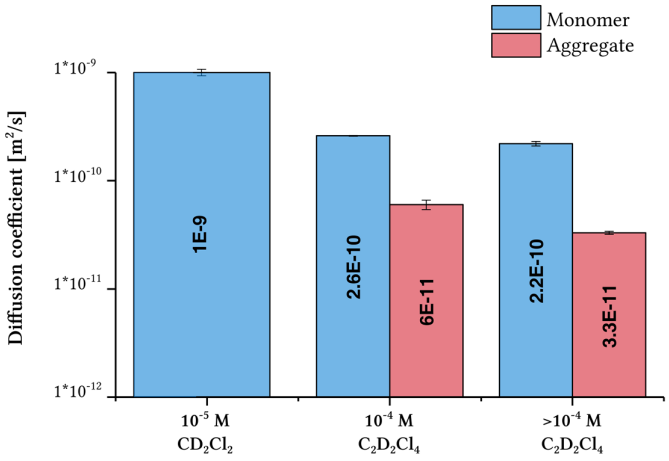

Figure 14. *The experimental diffusion coefficients for the dihyxylquaterrylene monomers and aggregates.*

Simulated diffusion coefficients

The diffusion coefficients could be translated to the molecular size using several methods. Typically, the Einstein-Stokes equation is used to describe the diffusion of the spherical particles, however this is not a very likely arrangement for the J-aggregates. Instead, J-aggregates are most-likely are in slip-stacked (staggered) orientation. Therefore, the diffusion coefficients for the J-aggregates were simulated using HYDRO++10 software [119, 120] that accounts for non-spherical J-aggregate geometry. The aggregate models consisting of up to 60 units were built in order to simulate the diffusion coefficients that could be later compared with the experimental ones. The experimental diffusion coefficients of the monomeric species were in good agreement with the simulated ones. The experimental diffusion coefficients for the J-aggregates match with the diffusion coefficient simulated for 14 units at 10^{-4} M concentration in $C_2D_2Cl_4$. At the higher concentration (>10^{-4} M) the recorded value matched the simulation for 34 units. These results correlated well with those obtained by the spectroscopical analysis, 6 units at 10^{-6} M concentration.

Chapter 3

Perylene as the common denominator

In this chapter, the choice of perylene as a 'parent chromophore' for this thesis is discussed. **Section 3.1** outlines a list of prerequisites a model system must meet to be relevant in answering the principal research questions formulated in this thesis. In this section, the choice of perylene as a model system is rationalised. **Section 3.2** covers a brief historic overview of perylene discovery and describes the generic chemical, and physical properties of the chromophore. **Section 3.3**. looks at the substitution pattern effect on the photophysics of perylene positional isomers. **Section 3.4** describes the design rationale and convergent synthetic approach towards perylene-based molecular dyads followed by their spectroscopical evaluation. **Section 3.5** is exploring bay-alkylation and longitudinal core expansion of perylene. Synthesis, photophysical evaluation and J-aggregation phenomena are discussed in this section as well.

3.1. Perylene as a model system

Unveiling the structure-to-properties correlations in organic chromophores requires a model system. The model system should satisfy a set of defined prerequisites to be able to address the research questions raised in **Section 1.2**. A brief overview of the prerequisites towards the model system and desired molecular properties are outlined below:

1. The model compound should be soluble in most organic solvents, allowing solution-based photophysical and NMR studies, the results of which are often more facile to interpret than solid-state experiments.
2. The relation between absorbed and emitted photons is reflected through emission quantum yields. High quantum yields can provide high signal-to-noise ratios that are beneficial to the instrumental methods of analysis.
3. Ideally, the molecule under investigation will absorb in a spectral region where laser sources are available. Furthermore, commonly used detectors are often most efficient in the visible segment of the electromagnetic spectrum, and therefore a visible light emitting molecule is adequate for our purpose.

Looking through the prism of these selection criteria, the attention was focused on the robust carbon-hydrogen framework of perylene. A versatile and soluble fluorescent chromophore with 4 nanoseconds excited state lifetime and emission quantum yield close to unity. Its aromatic network comprised of condensed phenyl

rings gives rise to a π-π* transition allowing us to work in the visible regime. It can offer a solid platform for investigating molecular properties and understanding the excited state interactions in composite chromophore assemblies.

3.2. Discovery and basic properties of perylene

History and nomenclature

In the early 1900s, a Swiss chemist named Roland Scholl was working on arene coupling reactions. Using sulphuric acid in the presence of aluminium chloride, he synthesized helianthron [121] and also perylene from naphthalene [122] in 1910 as shown in **Scheme 1**. Later, in 1913 perylene was also synthesized from 1,1'-binaphthalene [123]. Remarkably, the manufacturing process of perylene is basically unchanged since its discovery [124]. Emphasizing the relevance of Scholl's chemistry today, more than a hundred years later, we implemented a slightly modified reaction procedure to synthesize a soluble bay-alkylated quaterrylene that is able to form superradiant NIR J-aggregates (discussed in **Section 3.4**).

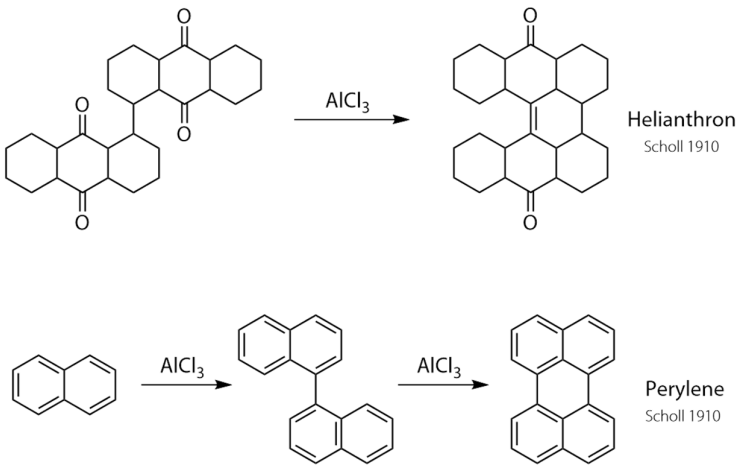

Scheme 1. *Scholl reaction and perylene synthesis.*

Perylene is soluble in most organic solvents and has three individual potential reactive sites. Positions 1, 6, 7, 12 are also referred to as *bay* positions, positions 2, 5, 8, 11 are also called *ortho,* and finally positions 3, 4, 9, 10 are labelled as *peri* positions as shown in **Figure 15**. All three positions could be functionalized through synthesis, however the reactivity of *bay, ortho* and *peri* regions varies.

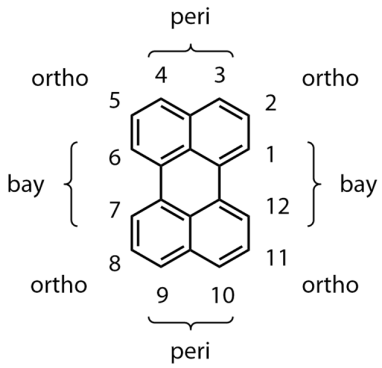

Figure 15. *Position numbering and region labelling in perylene.*

Reactivity

The reactivity of an organic molecule is often discussed in terms of energetics, electronic effects, steric effects, stereoelectronic effects and solvent effects. Some of these effects in relation to perylene are discussed below.

Electronic effects are usually determined using the Mulliken population analysis. The Mulliken method is used to estimate partial atomic charges in a molecule [125]. The method is based on a linear combination of atomic orbitals (LCAO) introduced by Lennard-Jones [126]. The Mulliken charges at *ortho*, *peri* and *bay* carbons of perylene are displayed in **Figure 16**.

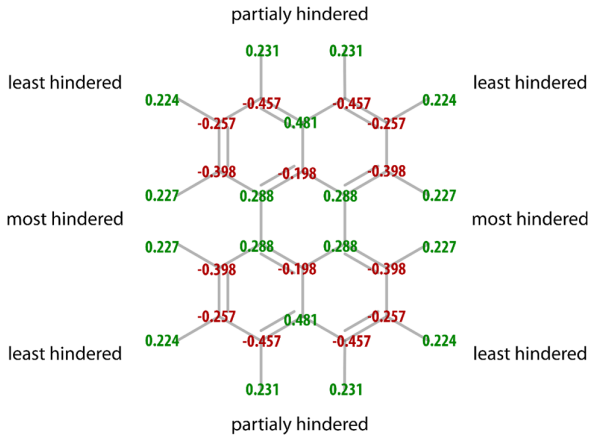

Figure 16. *Mulliken charge distribution in ground state perylene as calculated in the Gaussian 16 program package. The steric availability of each position is indicated.*

Steric effects. Steric factors play an important role in a predisposition towards certain reactions. The *bay* positions in perylene are the most sterically hindered due to the proximity of the neighbouring *bay* hydrogen. On the contrary, the ortho region has the best steric availability having negligible interactions with *peri* and *bay* hydrogens. *Peri* positions are partially hindered by the neighbouring hydrogen. The steric availability of each reactive site in perylene is indicated in **Figure 16**.

Stereoelectronic effects. The spatial orientation of filled and unfilled orbitals influences molecular reactivity. In many cases, electron pairs in atomic or molecular orbitals that are involved in the making or breaking of bonds have an optimal geometrical alignment that is critical for a reaction to occur. This alignment provides the best overall bonding of participating species during the reaction and reflects the fact that transition states having the greatest bonding energy have lower potential energies. The electronic densities around different positions in perylene are graphically exemplified using HOMO/LUMO orbitals in **Figure 17**.

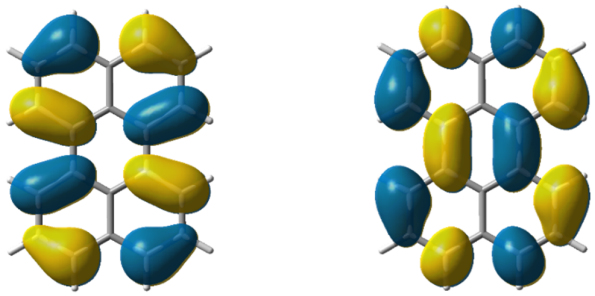

Figure 17. *HOMO-LUMO orbitals in perylene. Calculated in Gaussian 16, using B3LYP/LANL2DZ level.*

Reaction examples

Most of the examples listed below were used in the synthesis of perylene derivatives studied in this thesis. *Ortho* positions are the least sterically hindered regions in perylene, and easily react in Friedel-Crafts alkylations [127]. Even bulky substituents can be tolerated, allowing to introduce *tert*-butyl groups for instance, whereas that is not the case for the *bay* positions. Direct tertraborylation of perylene can also be done in *ortho* positions [128]. Sterically hindered *bay* positions could be alkylated upon exposure to organolithium agents. This applies to primary and secondary alkyllithiums, however *tert*-butyllithium (*t*-BuLi) will alkylate perylene in its *peri* position due to the steric hindrance of the *bay* region [24]. It is possible to expand the aromatic core using the Diels-Adler reaction, in that case the *bay* region acts as a diene [129]. Finally, *peri* positions readily undergo halogenation upon exposure to halogenated *N*-succinimides [130] allowing for a further functionalization in this position. Only a few examples are mentioned here, as the vastness of perylene chemistry deserves a book of its own.

Optical properties

Perylene has a very recognisable absorption spectrum that reaches a maximum at 438 nm and has a characteristic vibronic pattern with the second and third vibronic bands at 412 nm and 391 nm respectively as could be seen in **Figure 18**. The emission

spectrum is nearly a mirror image of the absorption spectrum reaching a maximum at 443 nm with second and third vibronic band at 472 nm and 505 nm respectively. Perylene shows a Stokes's shift is 5 nm and a molar absorption coefficient reaching 39000 $M^{-1}cm^{-1}$. Fluorescence quantum yield is close to unity in benzene (and toluene), showing excited state lifetimes of 4 ns. The assignment of the electronic spectrum of perylene was done by Tanizaki et al. in 1978 [131].

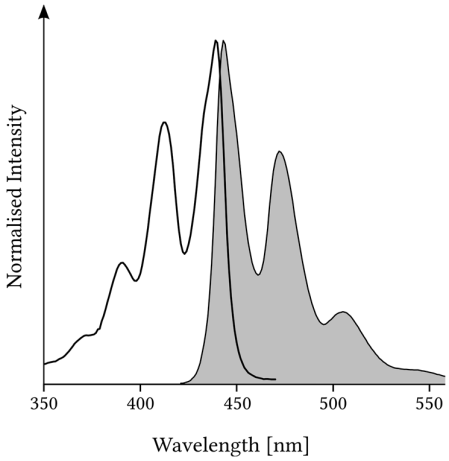

Figure 18. *Absorption (solid line) and emission (solid filled) spectra of perylene recorded in toluene.*

Physical properties

The crystal structure of perylene initially suggested planarity of the carbon skeleton and supposed that bay hydrogens may deviate from the general plane of symmetry. The central hexagon does not possess benzoid properties and demonstrates unusually long bond lengths connecting the two naphthalene cores [132]. Initial investigations assumed that the carbon skeleton is not ideally planar, however the distortion is practically negligible and often the molecule is considered to be planar [133] as seen in **Figure 19**. Perylene varies in appearance from a bright yellow/orange to a brown powder depending on the purity. The molecule has a melting point of 276-279˚C and sublimes at 350-400˚C, although purification of perylene via sublimation is usually performed under vacuum.

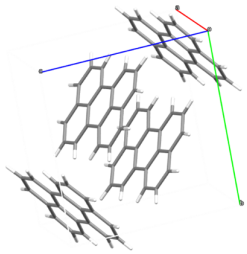

Figure 19. *The crystal structure of perylene showing the planarity of the molecule. Single crystal data from CCDC, deposition number 198723.*

Concluding this section one can say that unsubstituted perylene is a well-studied chromophore offering several synthetic strategies for derivatization. The chemical, optical and physical properties of perylene fit perfectly to our prerequisites and therefore comprise a good model system for understanding the intrinsic photophysical properties and unveiling structure-to-properties correlations. Lack of systematic studies on structure-to-properties dependence as a function of substitution position in perylene has sparked the interest to investigate the photophysical effects that could arise in *bay, ortho* and *peri* substituted perylenes. Furthermore, nanosecond lifetime as well as nearly quantitative fluorescence quantum yields would make it a good acceptor molecule when harvesting light in the blue regime of the electromagnetic spectrum.

In this thesis perylene-based chromophores were used in three separate pathways. **Paper I** investigates the substitution effect on general photophysics in positional isomers of perylene and evaluates their TTA-UC properties. In **Paper II** and **Paper III** perylene derivatives were used to make energy transfer systems for triplet harvesting in the deep-blue regime. In **Paper IV** twisted bay-alkylated perylene was used to make a soluble quaterrylene scaffold that forms superradiant J-aggregates with high emission efficiency in the NIR regime. The following sections summarise these findings.

3.3 Structure-to-properties correlations in phenylperylenes

With the model system at a hand, we can begin explorations of structure-to-properties correlations in perylene derivatives. This can be done by studying the photophysical properties of the perylene positional isomers. As it was covered in the previous section, perylene has three individual reactive sites, namely *bay, ortho* and *peri*. Functionalisation of perylene with the equivalent substituent in all three reactive sites would therefore result in three positional isomers. A phenyl substituent was chosen due to its near-zero Hammet value in any measurable position [134, 135]. This ensures that observed luminescence effects in the studied compounds arise due to the positional variability and not because of electron donating or withdrawing effects. Three regioisomers, namely 1-phenylperylene (1-PhPer), 2-phenylperylene (2-PhPer) and 3-phenylperylene (3-PhPer) were then synthesised as shown in **Scheme 2**.

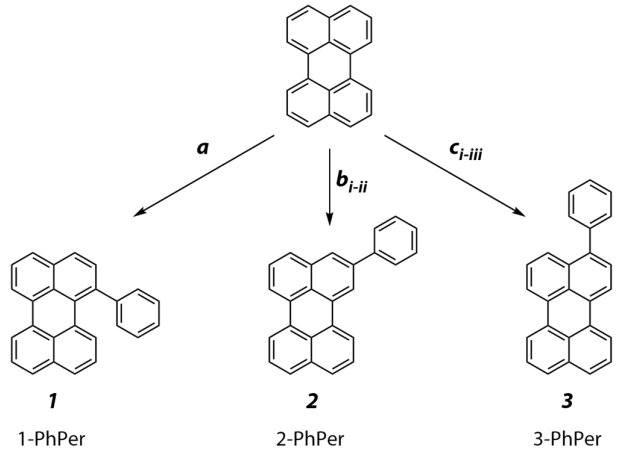

Scheme 2. *Synthesis of phenyl-substituted perylenes. Reactions conditions: a). PhLi, THF, -78 ˚C, b). (i) B_2Pin_2, dtbpy, $[Ir(COD)_2(OMe)_2]$, THF, 80 ˚C, (ii) PhBr, $Pd_2(dba)_3$, RuPhos, K_2CO_3, PhMe, 100 ˚C, c). (i) NBS, THF, RT, (ii) B_2Pin_2, KOAc, $Pd(dppf)_2Cl_2$, 1,4-dioxane, 70 ˚C, (iii) PhBr, $Pd_2(dba)_3$, RuPhos, K_2CO_3, PhMe, 100 ˚C.*

The *bay*-substituted molecule ***1*** was obtained by a direct use of phenyllithium. In the case of the *ortho*-substituted molecule ***2***, perylene was subjected to a direct pinacolation followed by Suzuki cross-coupling with 1-bromophenyl. To make the *peri*-derivative ***3***, perylene was halogenated using NBS and then converted to the corresponding borylated pinacol ester that was subjected to a Suzuki cross-coupling with 1-bromophenyl. Synthetic procedures are covered in **Paper I**, (Supplementary information, Section 4).

Naturally, the synthesis was followed by a photophysical evaluation. The absorption and emission spectra of phenyl-substituted perylenes are compared to unsubstituted perylene in **Figure 20**.

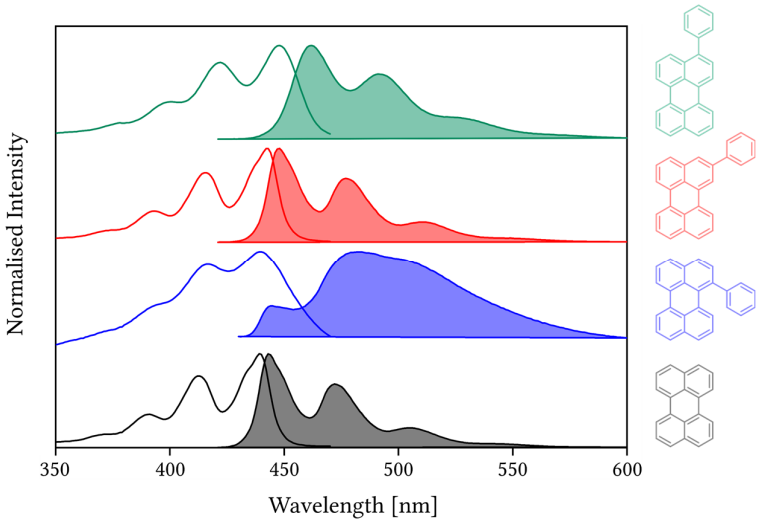

Figure 20. *UV-Visible absorption (solid line) and emission (solid filled, λ_{exc} = 410 nm) spectra of perylene derivatives in toluene. Structures of the compounds are displayed in the colour corresponding to their spectra.*

Ortho-substitution seemingly has the least influence over the spectral features in perylene, as 2-phenylperylene shows only a 5 nm red-shift of the absorption maxima and slightly lower emission quantum yields as compared to perylene. *Peri*-substitution induces a bathochromic shift of 10 nm in 3-phenylperylene when compared to perylene. The emission quantum yield is comparable to that of perylene, although the absorption signal is broader. Molar absorption coefficients of ***2*** and ***3*** are comparable to that of perylene and the emission profile of both compounds are in a mirror relationship with the absorption signals. Notably, 1-phenylperylene shows prominent differences when compared to the other compounds in the series. The absorption and emission spectra do not show a mirror relationship in the vibronic progression. The intensity ratio in the vibrational ladders of the emission profile of ***1,*** is significantly different to that of perylene, ***2*** and ***3***. The intensity of the vibrational progression depends on Huang-Rhys factors, indicating considerable translation of the excited state potential from the Frank-Condon state to the geometry relaxed excited state. This has been previously observed in other π-conjugated organic fluorophores [136]. Experimentally determined photophysical properties of the phenyl-substituted perylenes, as well as unsubstituted perylene are summarized in **Table 1.**

Table 1. *Experimentally determined photophysical properties of perylene derivatives.* [a]*Values are determined in toluene with* λ_{exc}*=410 nm, the value for the most intense peak is given.* [b]*Values are referenced using the reported value of perylene in benzene accurate to ±10 %,* [c]*Values are determined in toluene at 375 nm.*

Compound	λ_{max} / nm (ε / 10^4 M^{-1} cm^{-1})	λ_{em}[a] / nm	Φ_F[b] / %	τ[c] / ns	k_r / 10^8 s^{-1}	k_{nr} / 10^7 s^{-1}
Perylene	438 (3.9)	443	99	3.8	2.6	0.3
1	440 (1.8)	482	70	3.9	1.8	7.7
2	443 (3.6)	447	93	3.9	2.4	1.8
3	448 (3.7)	462	97	3.3	2.9	0.9

The distinct spectral appearance of 1-PhPer also translates to a lowered emission quantum yield and a significantly decreased molar absorption coefficient. The exact reasons for that are not yet established, but this could potentially be explained by the largely altered transition dipole vector of 1-PhPer as compared to 2-PhPer and 3-PhPer. The transition dipole density maps of the phenyl-substituted perylenes are shown in **Figure 21.**

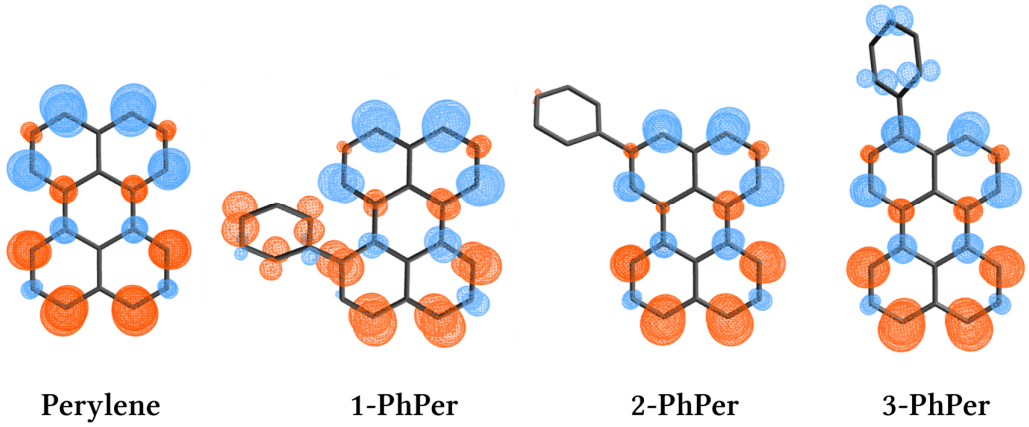

Figure 21. *Transition dipole moment density maps for perylene, 1-PhPer, 2-PhPer, 3-PhPer. Excited state transitions are calculated based upon a singlet ground state.*

In perylene, the transition dipole moment vector is oriented along the long axis of the molecule [137]. The vector orientation in 2-PhPer is similar to that of perylene. In 3-PhPer longitudinal elongation of the aromatic system consequentially extends the transition dipole moment, thus resulting in a red-shift as compared to perylene. Prominent electron delocalization extending to the phenyl ring in the *bay* position of perylene alters the vector direction from the long axis of the molecule. Even though, not being the aim of this particular study, consideration of the dipole moment orientation is of importance in energy transfer systems. It has been shown that strong electronic and vibrational mixing is achieved through co-aligned parallel transition dipole moments in perylene-terrylene diimide dyads resulting in ultrafast FRET rates (50 fs) [138]. Ultrafast energy transfer induced by the vibronic effect is also common in natural photosynthetic light-harvesting systems [139]. The triplet energies of the phenylperylenes were assessed in terms of their applications in TTA-UC, concluding that the *ortho*-substituted isomer has the best characteristics in the investigated series.

In conclusion, three positional isomers of perylene were synthesised and their photophysical properties were discussed in relation to the substitution position. The correlations between the phenyl attachment position, and alterations of the optical properties of the investigated perylenes were made. The compounds in the series were analysed in terms of their applications in TTA-UC, however this will not be discussed here as it lies outside of the scope of this thesis.

3.4 Molecular dyads for energy transfer

Having established that the substitution position influences the general photophysics of perylene, it is time to explore how the substitution effect translates to the energy transfer systems where perylene is used as an acceptor. **Section 3.4** summarises

results from **Paper II** and **Paper III**, where **Subsection 3.4.1** covers the design rationale, retrosynthesis and convergent approach towards Donor-Bridge-Acceptor systems, and **Subsection 3.4.2** describes the photophysics of the energy transfer mechanisms, rationalising their differences.

3.4.1 Design and synthesis of isomeric DBA systems

Concept. Intramolecular FRET-mediated triplet-to-singlet energy transfer in a Donor-Bridge-Acceptor dyad can be conceptualized using **Equation 3.1**,

$$^3D^* + {}^1A \longrightarrow {}^3D + {}^1A^* \qquad (3.1)$$

For this to occur, a triplet donor *(D)* and a singlet acceptor *(A)* are required. This concept with consideration to the energy levels of the donor and the acceptor counterparts are illustrated in **Figure 22** using the Jabłoński diagram. For a successful triplet-to-singlet energy transfer, the Donor-Acceptor dyad must perform a sequence of four distinct photophysical processes. The first process is the absorption of the photon (1) by the Donor chromophore, followed by an intersystem crossing (2) transferring the excitation energy to the excited triplet state. Next, the excitation energy should be transferred from the excited triplet state of the donor to the excited singlet state of the acceptor (3) using the FRET mechanism. Finally, the photon emission (4) from the excited singlet state of the acceptor finalises this sequence.

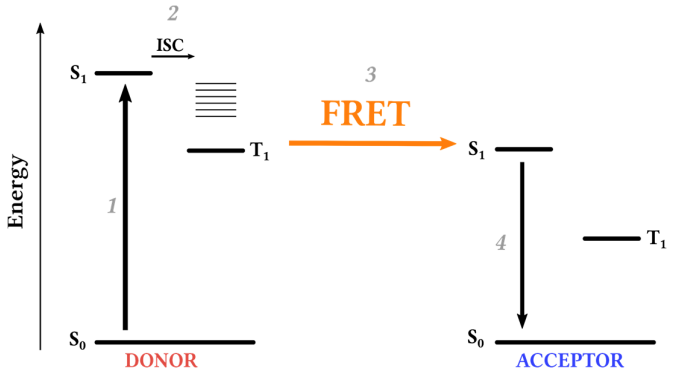

Figure 22. *Jabłoński diagram showing desired intramolecular triplet-to-singlet energy transfer.*

Building a model. The model should satisfy several design criteria in order to fulfil the sequence successfully. Having perylene in one hand as a potent singlet acceptor we can then turn our attention to the donor moiety. What makes a good donor for this purpose? Firstly, the donor should have a high population of triplet states. The population of triplet states is often achieved as a consequence of ISC that arises due to the high SOC effect that is a prominent feature of heavy atom complexes Furthermore, the energy of the triplet state of the donor should be isoenergetic to that of the acceptor for the FRET to occur. That also aligns with the first design criterion,

(1) the donor emission should overlap with the acceptor absorption. A large spectral overlap integral is essential for the FRET efficiency as shown in **Equation 2.16**.
Separating donor and acceptor in space could be done by a molecular linker. The rigid linker of a defined length allows to evaluate the FRET efficiency in a consistent manner, thereby bringing us to the second design criterion,
(2) the bridging unit should be of a rigid structure to avoid molecular flipping and to ensure the constant distance between the donor and the acceptor.
Finally, the bridging unit should not contain any π electrons, minimizing the possibility for electron communication in the dyad. Furthermore, the length of the linker should be sufficient for separating the electron clouds of the donor and the acceptor, establishing the last design parameter as,
(3) in order to mitigate the possibility of the Dexter triplet-triplet energy transfer between two chromophores the bridging unit should spatially separate the electronic clouds of the functional counterparts in the dyad.
In consideration to the design criteria a Donor-Bridge-Acceptor system with the desired properties could be envisioned. An example of such system using two isomeric dyads is presented in a retrosynthetic fashion in **Figure 23**. An iridium complex of suitable energy is linked to perylene using the stiff core of bicyclo[2.2.2]octane as a bridging unit that is connected to perylene either *peri* or *ortho* positions.

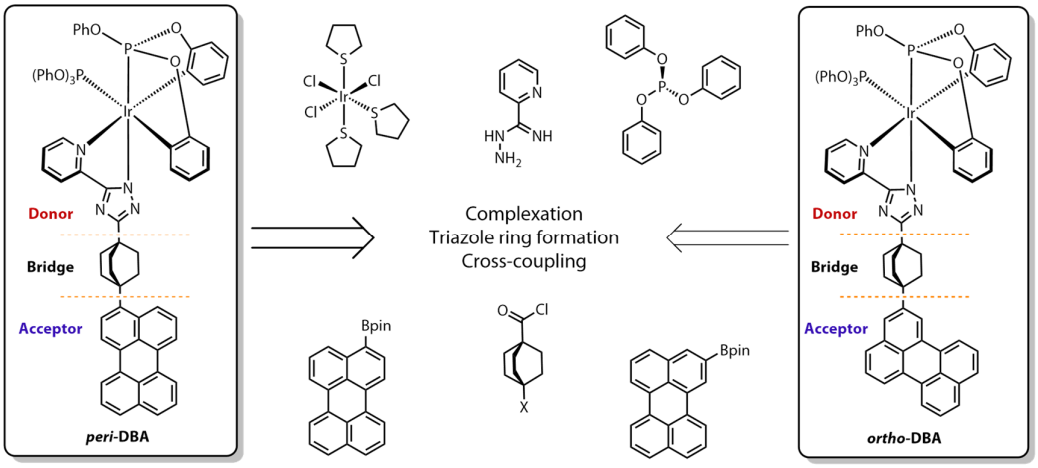

Figure 23. *Potential DBA systems for triplet-to-singlet FRET presented in a brief retrosynthetic way.*

The Donor (D). An Ir (III) complex with microsecond lifetimes, suitable energy levels and emission quantum yield of 78% was chosen as the donor [140]. The reported optical properties suggest a considerable spectral overlap between the emission of ***4*** and perylene absorbance. This satisfies design parameter **(1)** and ensures that J_{int}

component (**Equation 2.17**) is present. The donor reference *(D)* was synthesised using a slightly modified literature procedure [140] as shown in **Scheme 3**.

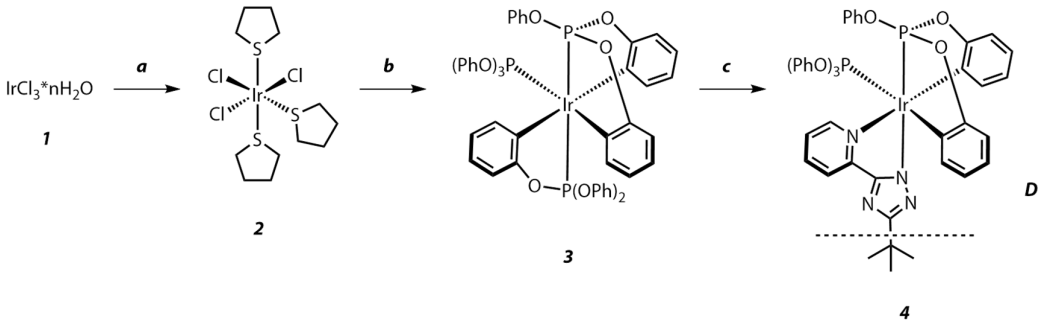

Scheme 3. *Iridium (D) reference compound synthesis. Reaction conditions:* ***a)*** *tetrahydrothiophene, 2-MeOEtOH, 130 °C, 6 h;* ***b)*** *$P(OPh)_3$, NaOAc, Decalin, MW 190 °C, 1h;* ***c)*** *NaOAc,* ***20****, Decalin, MW 190 °C, 6h.*

The Bridge (B). The rigid framework of the bicyclo[2.2.2]octane allows for a free rotation only along the sigma bonds of the long axis in the molecule (para position sigma bonds). This would keep the dyad's functional counterparts at a defined constant distance from each other avoiding varying distances between donor and acceptor during FRET efficiency evaluation. Additionally, sigma bonds in the stiff frame of the bicyclo[2.2.2]octane allow to spatially separate the electron clouds of the functional counterparts within the dyad. With this, conditions **(2)** and **(3)** were also satisfied.

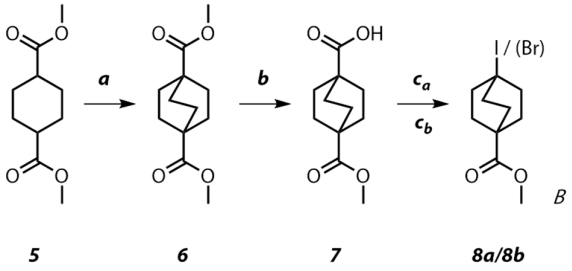

Scheme 4. *The Bridge synthesis. Reaction conditions:* ***a)*** *LDA (2 M), $Br(CH_2)_2Cl$, DMPU/THF, -78 °C, 12 h; then LDA (2 M), DMPU/THF, -78 °C, 12 h;* ***b)*** *KOH, MeOH, reflux, 5 h;* ***c_a)*** *HgO, I_2, $CHCl_3$, reflux, 6 h;* ***c_b)*** *$(Ir[dF(CF_3)ppy]_2(dtbpy))BF_4$, Cs_2CO_3, diethyl bromomalonate, hv (455 nm), PhCl, 4 h.*

When making the bridge, it is important to leave two non-identical synthetic handles for selective sequential coupling to the donor and the acceptor at a later stage. Keeping this in mind, one functionality was aimed to be a carboxylic acid that can subsequently be converted to the acid chloride then reacted with amidrazone forming a triazole ligand for complexation. Another functional handle was envisioned to be a halogen, such that it can be subjected to cross-coupling chemistry in reaction with perylenes *(vide infra)*. The synthesis of the bridging unit is shown in **Scheme 4**.

Deprotonation of the hydrogens adjacent to the ester functionality in dimethyl cyclohexane-1,4-dicarboxylate ***5*** was done using 2M LDA solution in dry THF at -78˚C. Next, 1-bromo-2-chloroethane was introduced in a two-step sequence [141]. Next, diester ***6*** was subjected to monosaponification using KOH in methanol [142]. Monitoring the reaction kinetics by frequent GC/MS analysis allowed to obtain the desired carboxyester ***7*** in 60% yield. The acid moiety was then subjected to halodecarboxylation procedure using the mercury (II) oxide modified Hunsdiecker-Borodin method [143]. Heating the starting material with mercury oxide and iodine in DCM in a sealed vial yielded iodocarboxylate ***8a***. An alternative method was then applied using a photoredox halodecarboxylation methodology reported in the literature [144]. The photocatalytic cycle of iridium-assisted halodecarboxyalation is shown in **Figure 24.**

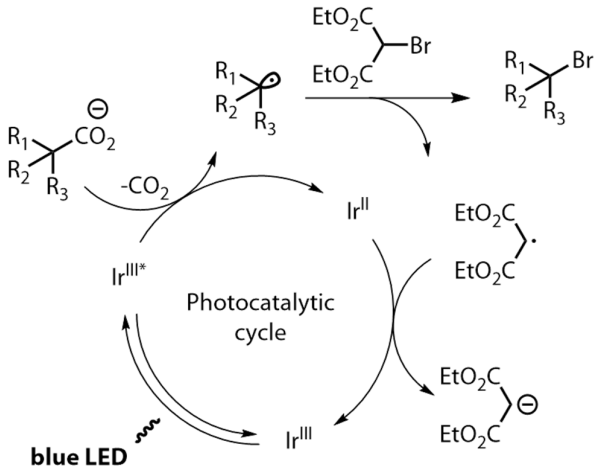

Figure 24. *Photoredox halodecarboxylation mechanism as suggested in ref. [98].*

Diethyl bromomalonate was used as a halogenating agent in presence of cesium carbonate and an iridium (III) catalyst in chlorobenzene. Irradiating the reaction mixture with 455 nm LED lamps allowed the conversion to the desired bromocarboxylate ***8b*** in a 65% yield. This method allowed to abstain from the mercury-assisted protocol, although the scalability of the photoredox protocol was not optimal under the given conditions. Recent reports of heterogeneous photoredox catalysis could potentially solve this issue [145].

Attempts to couple the bridge to the acceptor. Coupling the bridge to the acceptor appeared to be one of the most challenging transformations in the projected synthesis. The goal was to couple the electron deficient bicyclo[2.2.2]octane core to the aromatic and electron-rich perylene. A brief summary of the attempts is presented in **Scheme 5.**

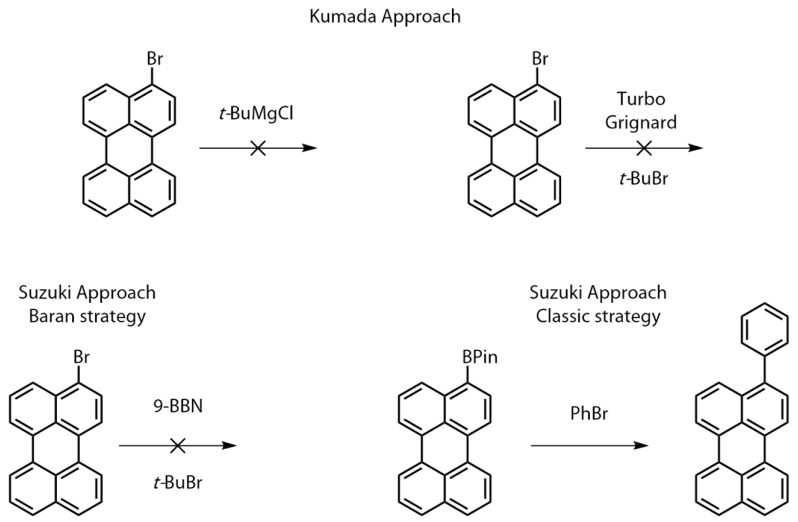

Scheme 5. *A short summary of attempts to couple perylene to bicyclo[2.2.2]octane.*

The initial strategy for coupling the bridge to the acceptor envisioned a Kumada coupling strategy [146]. However, the trials using tert-butyl magnesium chloride as a model substrate and 3-bromoperylene were deemed to be unsuccessful. Inversing the approach and attempting to make a Grignard reagent using 3-bromoperylene did not result in a positive outcome either. After this, we shifted our attention to the Suzuki-Miyaura coupling protocols [147]. There are very few reported procedures that succeeded in coupling unactivated tertiary alkyl halides to the electron-rich partners [148, 149]. Using the reported methodology, an attempt to make the 9-BBN derivative of perylene was followed by the addition of *t*-BuBr. Despite, the visual changes in the appearance of the mixture, the reaction did not proceed as desired. It is likely that the 9-BBN derivative of perylene is not stable and thus the coupling does not occur. After several unsuccessful attempts and facing challenges to trace the reaction intermediates this pathway was abandoned.

The modified system. At this point, the strategic decision of introducing another phenyl ring in the system was taken. This approach was justified for several reasons. Unlike the previously attempted coupling, Suzuki reactions between sp_2-sp_2 carbons are well-known and reported using perylenes as a substrate [150]. Besides, this transformation is successfully achieved in **Scheme 2**. The synthesis continued with a slight modification to the initial plan.

Coupling the bridge to the acceptor. The modified coupling partner was prepared according to **Scheme 6.** The bicyclo[2.2.2]octane scaffold was extended with a phenyl ring and then halogenated in the para position. The first transformation was achieved following a classic Friedel-Crafts protocol by alkylating benzene with haloester ***9*** in presence of $AlCl_3$ as a Lewis acid [151]. Next, methyl 4-phenylbicyclo[2.2.2]octane-1-

carboxylate ***10*** was then iodinated using $(CF_3COO)_2IPh$ and iodine in chloroform to yield the parahalide ***11*** [152].

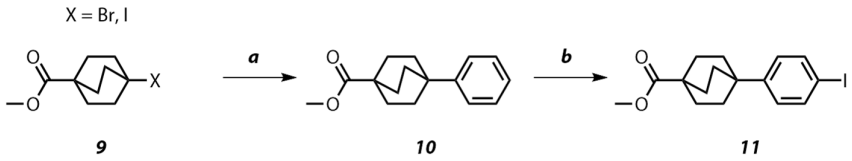

Scheme 6. *Preparing the modified bridge coupling partner for Suzuki coupling. Reaction conditions:* ***a)*** *$AlCl_3$, PhH, 12 h;* ***b)*** *$(CF_3COO)_2IPh$, I_2, $CHCl_3$, 1 h.*

The modified coupling partner was then coupled to perylene in *ortho* and *peri* positions. Perylene has to be selectively borylated in position 3 for the *peri* derivative and in position 2 for the *ortho* derivative. **Scheme 7** shows Suzuki coupling between the bridge and the perylene.

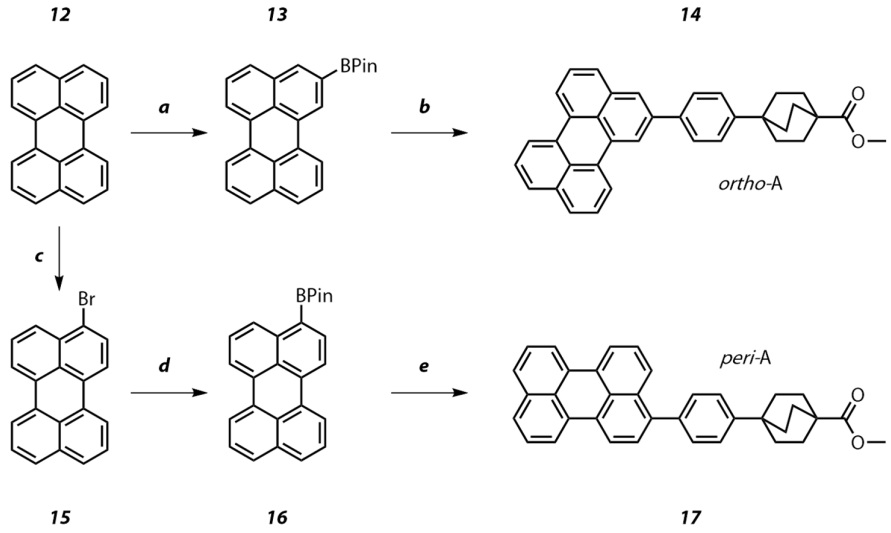

Scheme 7. *Coupling the bridge to the perylene via Suzuki coupling. Reaction conditions:* ***a)*** *B_2Pin_2, dtbpy, $[Ir(cod)(OMe)_2]$, THF, 80 ℃, 16h;* ***b)*** *$Pd_2(dba)_3$, RuPhos, K_2CO_3 (2 M), Aliquat 336 (cat.) PhMe, 100 ℃;* ***c)*** *NBS, THF, 24 h;* ***d)*** *$B_2(pin)_2$, $Pd(dppf)Cl_2$, KOAc, 1,4-dioxane, 80 ℃ 24 h;* ***e)*** *$Pd(Ph_3P)_4$, K_2CO_3 (2 M), Aliquat 336 (cat.), EtOH, PhMe 80 ℃, 40 h.*

Peri-Acceptor synthesis. Perylene was brominated using NBS in dry THF at room temperature [153]. The reaction product, 3-bromoperylene ***15*** was then subjected to borylation using B_2Pin_2 under $Pd(dppf)Cl_2$ catalysis in presence of KOAc as a base in 1,4-dioxane at 80˚C [154]. The target boropinacol ester ***16*** was subsequently used in the Suzuki cross-coupling reaction. Disappointingly, initial attempts of the cross-coupling procedure provided rather low yields (10-15%). Side product formation was observed as a result of dehalogenation. Dehalogenation pathways were observed previously in Suzuki-Miyaura couplings as a side reaction suggesting β-H elimination in the halide coupling partner [155]. The proposed reaction mechanism of Suzuki

cross-coupling with respect to the dehalogenation pathway is shown in **Scheme 8**. The undesired pathway likely arises because the base (2M K_2CO_3) is not delivered to the organic phase at a sufficient rate for the reaction to proceed towards the desired product. A phase transfer catalyst could be used to enhance the transfer rate. Addition of a few drops of Aliquat 336 to the reaction mixture containing $Pd(Ph_3P)_4$ as a catalyst and 2M K_2CO_3 as a base allowed to obtain higher reaction yields (>50%) for *peri*-A ***17***.

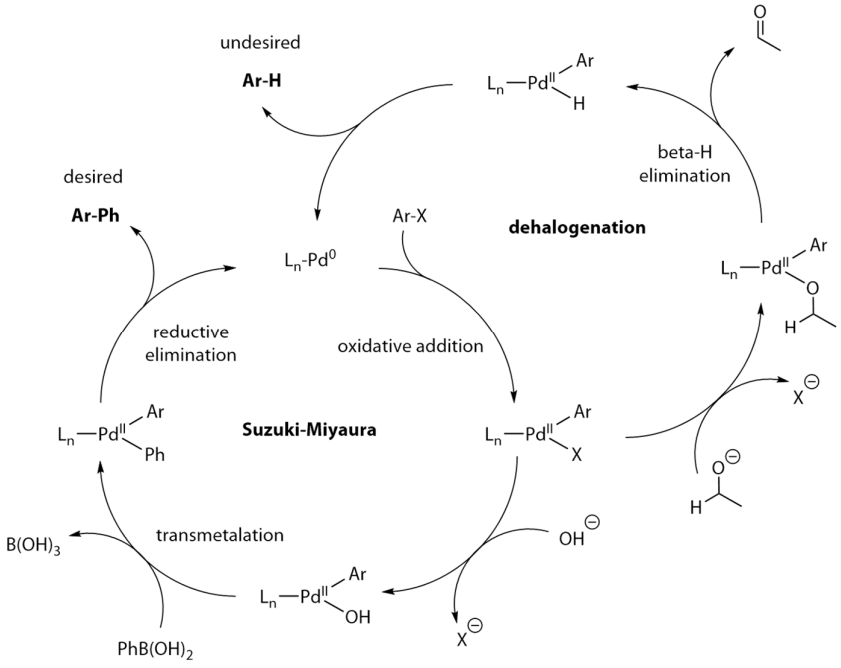

Scheme 8. *Suzuki cross-coupling generic mechanism.*

Ortho-Acceptor synthesis. Direct tetraborylation of perylene was previously reported in the literature [128]. Using a stochiometric amount of bis(pinacolato)diboron ester and following the conversion by the GC/MS it was possible to obtain monoborylated derivative ***13***. This was achieved by means of B_2Pin_2 under the catalysis of $[Ir(COD)OMe]_2$ in presence of dtbpy ligand in dry THF. The Suzuki coupling in the case of *ortho*-A was not straightforward either. Only poor conversion was observed when the same reaction conditions as for *peri*-A were applied to *ortho*-A. After screening several catalytic systems and ligands, the reaction was done under $Pd_2(dba)_3$ catalysis and using RuPhos as a ligand. The target product was obtained in a 31% yield.

Coupling of the acceptor to the donor. At this stage the triazole ring containing ligand has to be formed using the corresponding acceptor and amidrazone. This step was initially attempted on a model ligand that was then coordinated to the iridium complex in order to make a donor reference compound. **Scheme 9** shows the synthesis of the donor reference. Amidrazone (hydrazonamide) ***19*** was obtained from 2-cyanopyridine ***18*** that was treated with hydrazine [156]. Amidrazone then readily

reacts with pivaloyl chloride to give the triazole ligand ***20*** [157]. Reacting ***20*** with $Ir(THT)_3Cl_3$ ***2*** yields complex ***4***.

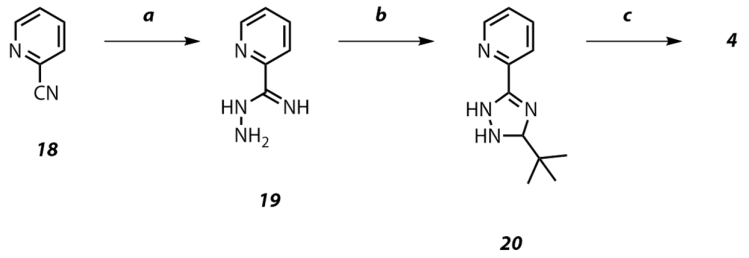

Scheme 9. *Synthesis of a model ligand for individual donor synthesis. Reaction conditions:* ***a)*** *$(NH_2)_2$, EtOH, 12h;* ***b)*** *Me_3CCOCl, Na_2CO_3, DMAA/THF, 4 h; then ethylene glycol, 190 ℃, 1 h;* ***c)*** *NaOAc,* ***3****, decalin, MW 190 ℃, 6h.*

Formation of the triazole ligand. First, the acceptor esters have to be hydrolysed to the corresponding acids. Considering the solubility of the target acids, hydrolysis was done in a THF/H_2O mixture. After 48h reflux the desired *peri*-acid ***22*** and *ortho*-acid ***27*** were isolated. Next, the acids must be converted to the corresponding acid chlorides. This was achieved by treating ***22*** and ***27*** with neat oxalyl chloride in presence of DMF as a catalyst [158]. The formation of a triazole ring is achieved by reacting acid chlorides (prepared *in situ*) with amidrazone ***19*** [157, 159]. The proposed reaction mechanism is shown in **Scheme 10** starting from the acid chloride. The nucleophilic addition of the amine to the carbonyl group is followed by the proton transfer (PT) resulting in HCl elimination. The second nucleophilic addition is from the imine and proceeds in a similar manner. Thermally assisted ring closure finalises this sequence forming *peri* ligand ***23*** *and ortho* ligand ***28***.

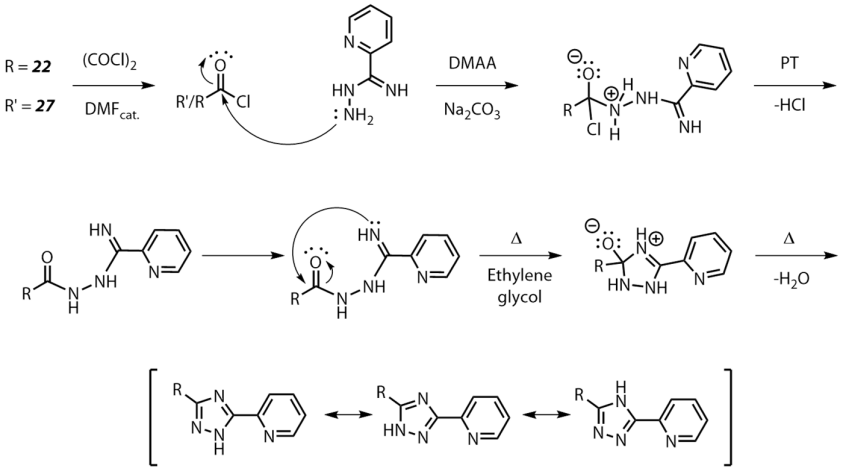

Scheme 10. *The proposed mechanism of triazole ligand formation.*

Coordination of the ligand to the iridium core. Finally, the obtained ligands were coordinated to the iridium complex ***3*** in order to obtain the target compounds *peri*-DBA and *ortho*-DBA. Due to the poor solubility of the ligands ***23*** and ***28*** in decalin, ODCB was used as a co-solvent. This allowed for a microwave-assisted procedure to grant the conversion to the desired products. **Scheme 11** shows the formation of the triazole ligand as well as coordination to the iridium core yielding the desired *peri*-DBA and *ortho*-DBA.

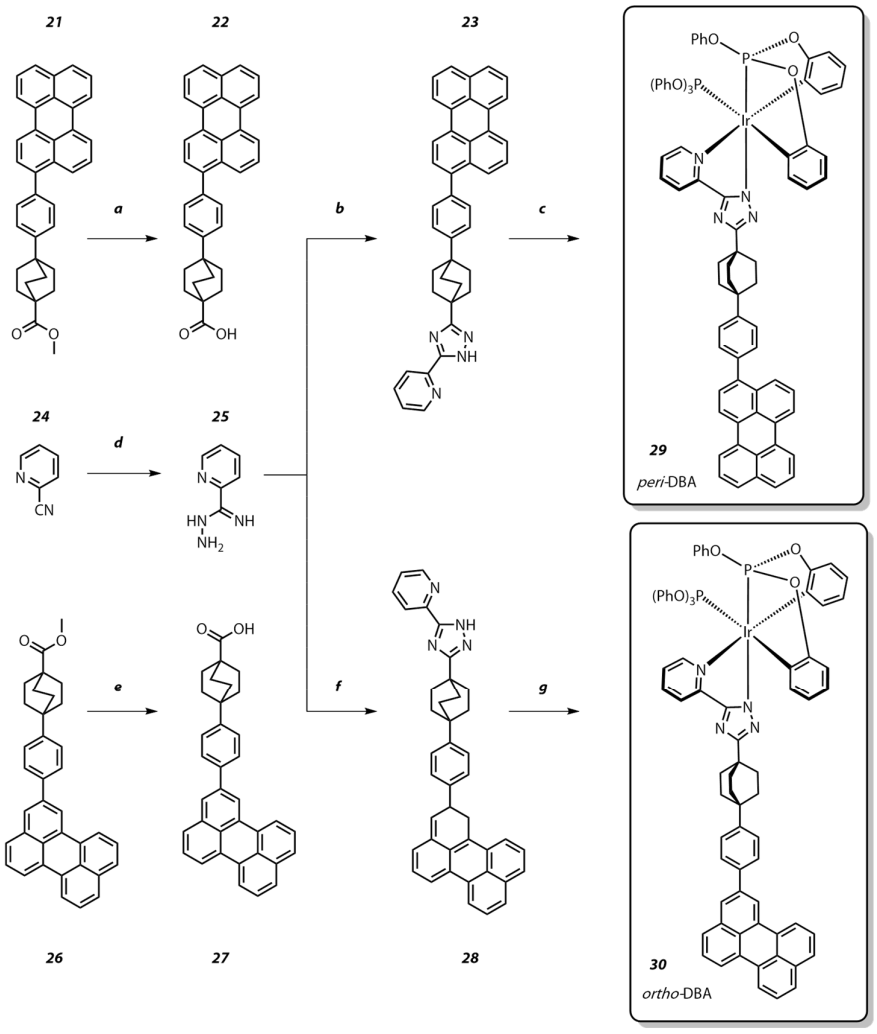

Scheme 11. *Formation of a triazole ligand and coordination to the iridium core. Reaction conditions:* ***a)/e)*** *$(COCl)_2$, DMF (cat.) then* ***b)/f) 25****, Na_2CO_3, DMAA/THF, 4 h; then ethylene glycol, 190 °C 1 h;* ***c)/g)*** *NaOAc, $Ir[P(OPh)_3](tpit)_2$, Decalin/ODCB, MW 190 °C, 6h;* ***d)*** *$(NH_2)_2$, EtOH, 12h;*

The final structures were characterized by ^{1}H, ^{13}C and ^{31}P NMR and HRMS. Additionally, single crystals of ligand ***23*** and *peri*-DBA were obtained and analysed using a synchrotron radiation source. The crystal data is available in the supplemental information of **Paper II** and in Cambridge Crystallographic Data Centre with the code CCDC 1886229.

3.4.2 Photophysics of the Donor-Bridge-Acceptor systems

Assessing preserved integrity of the functional components. After establishing the chemical structure of the target compounds, the optical properties of the dyads were investigated using the methods described in **Section 2.3**. Before starting the assessment of the energy transfer, it is crucial to verify that the integrity of the donating and the accepting chromophore is preserved within the dyads. To do so, reference compounds were synthesized, namely the donor reference *D* ***4***, *ortho*-A ***14*** and *peri*-A ***17***. The sigma bonds of the bicyclo[2.2.2]octane bridge do not affect the chromophore properties therefore both acceptor reference compounds contain the bridging unit. First, individual absorption of *D*, *peri*-A and *ortho*-A must be measured. Then absorption spectra of *peri*-DBA and *ortho*-DBA were recorded. The integrity was checked by plotting the spectra of the individual components, their arithmetic sum and the final dyads in relation to each other. The experimental data is in good agreement with the theoretical fit as seen in **Figure 25a**.

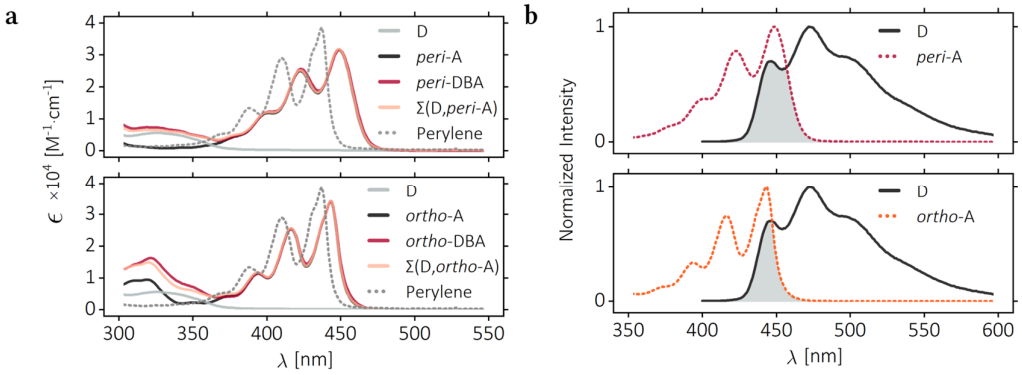

Figure 25. a) *Absorption spectra of D, peri-A, peri-DBA, arithmetic sum thereof and perylene (up), absorption spectra of D, peri-A, peri-DBA, arithmetic sum thereof and perylene (down);* ***b)*** *Spectral overlap between D and peri-A (up), spectral overlap between D and ortho-A (down). Reproduced from [2].*

Förster-type triplet-to-singlet energy transfer. The spectral overlap between *D* and peri-A/*ortho*-A is shown in **Figure 25b**. The spectral overlap integral was calculated for the *peri* and *ortho* systems using **Equation 2.17**. The J_{int} value was notably higher for the *peri*-DBA as compared to the *ortho*-DBA. Red-shifted absorption and emission observed for the *peri* system is the consequence of the longitudinal elongation of the aromatic system resulting in a large transition dipole moment. This observation is in line with the substitution effect (bathochromic shift of 3-PhPer) discussed in **Paper I**. The larger spectral overlap integral increases the rate of FRET as shown in **Equation 2.16**.

The emission in both dyads shows an emission envelope characteristic to perylene as could be seen in **Figure 7b.** Furthermore, no donor emission was observed irrespective of the excitation wavelength, indicating that the excitation energy has

been transferred from the triplet state of the donor to the acceptor. This observation signifies that FRET outcompetes phosphorescence in *peri*-DBA and *ortho*-DBA. The fluorescence lifetimes in the DBAs have a clear biexponential character suggesting that the emission can be attributed to two processes: firstly, from the direct excitation of the acceptor part (τ_F = 4 ns), secondly from excitation of the donor part followed by energy transfer to the acceptor from where the emission occurs (τ_F = 290 ns). It is impossible to avoid the direct excitation of the acceptor part during the measurements, however it is possible to perform a fractional analysis of the emission quantum yield to quantify the data. The emission quantum yield in DBAs can be thus divided into two fractions, the first fraction covers the direct excitation of the acceptors and the second fraction describes the emission as a consequence of triplet-to-singlet energy transfer. Using the fluorescence quantum yields of the dyads, it is possible to determine the quantum yields of FRET events in the corresponding molecules. The quantum yields of energy transfer by FRET mechanism was determined as Φ_{FRET} = 0.15 for *peri*-DBA and as Φ_{FRET} = 0.06 for *ortho*-DBA allowing to calculate the rates of the energy transfer. Summarizing the energy transfer rates using Förster formalism we conclude that triplet-to-singlet energy transfer is faster in *peri*-DBA, k_{FRET} = 5.33 × 10^5 s^{-1} as compared to *ortho*-DBA, k_{FRET} = 3.03 × 10^5 s^{-1}. This correlates well with the experimentally observed differences in the spectral overlap integral in *peri*-DBA and *ortho*-DBA. The J_{int} is larger for *peri*-DBA as compared to *ortho*-DBA, thus the kinetics of energy transfer in *peri*-DBA outcompete those of *ortho*-DBA. Readers interested in further details are referred to Supplementary Materials, Section S2 in **Paper II** and to Supporting information, Section 1 in **Paper III**.

Dexter-type triplet-to-triplet energy transfer. The quantum yields of the emission in both dyads were lower than the emission quantum yield of the donor. This indicates the plausibility of alternative energy transfer pathways opening up in the investigated DBA systems. The molecules were subjected to transient absorption experiments to evaluate the possibility of the Dexter type triplet-to-triplet energy transfer (TET). Indeed, the transient absorption signal recorded at 375 nm matches the literature value of perylene $T_n \leftarrow T_1$ absorption showing microsecond triplet lifetimes in DBAs, thus confirming that the non-emissive decay is due to the redundant donor-acceptor TET.

The rate of Dexter-type triplet–triplet energy transfer was then calculated in both systems. The decay lifetimes of triplet D can be calculated from the transient absorption decay. In the two DBA systems, the triplet lifetime of D is shortened by both FRET and triplet energy transfer. By knowing the lifetimes and the rate of FRET,

the rate of Dexter type triplet-triplet energy transfer was calculated with the help of **Equation 3.2**,

$$\frac{1}{\tau_D} - \frac{1}{\tau_{D0}} = k_{FRET} + k_{Dexter} \qquad (3.2)$$

where τ_{D0} is the triplet lifetime of the bare donor, τ_D is the triplet lifetime of the donor chromophore in DBA, and k_{Dexter} is the Dexter triplet-triplet energy transfer rate constant. The rates of Dexter-type energy transfer were determined, k_{Dexter} = 8.29 × 10^6 s^{-1} and k_{Dexter} = 2.92 × 10^6 s^{-1} for *ortho*-DBA and *peri*-DBA, respectively. Thus, Dexter-type energy transfer is occurring in both dyads, but at a much higher rate for *ortho*-DBA as compared to *peri*-DBA. This is rationalised through the conformational analysis of the rotational degree of freedom of the phenyl ring in both isomers. This was done by rotating the phenyl ring in respect to the plane of perylene and calculating the energy of each conformer as a function of dihedral angle. The Boltzmann probability density revealed a larger probability of finding *ortho*-A at dihedral angles deviating more from 90° as compared to *peri*-A as shown in **Figure 26a**. Furthermore, the rotational barrier is notably higher in *peri*-A as compared to *ortho*-A. This analysis indicates a larger perylene–phenyl conjugation for *ortho*-DBA, and thus electronic coupling that results in through bond Dexter-type energy transfer. Furthermore, this observation correlates with our examination of the HOMO/LUMO orbitals. The DFT calculations show that the HOMO and LUMO are to a higher extent delocalized on the phenyl substituent for *ortho*-A as compared to *peri*-A as seen in **Figure 26b**, creating more favourable conditions for Dexter-type energy transfer in *ortho*-DBA. Readers interested in further details are referred to the Supporting information, Sections 1, 2 in **Paper III**.

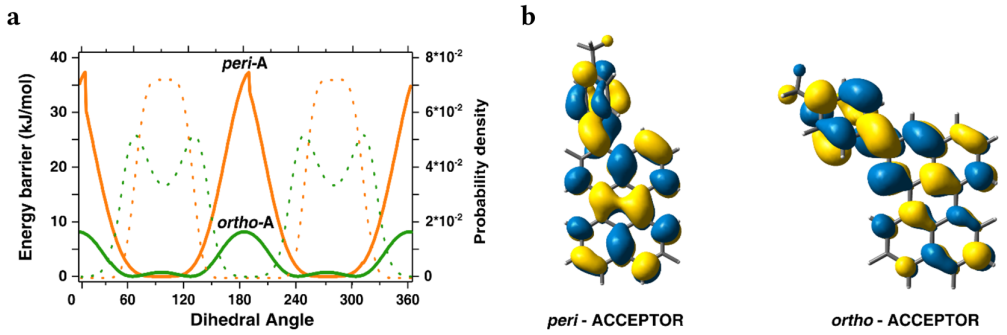

Figure 26. a) *Energy as a function of perylene–phenyl dihedral angle for peri-A (solid orange line) and ortho-A (solid green line). The Boltzmann probability density as a function of perylene–phenyl dihedral angle for peri-A (dashed orange line) and ortho-A (dashed green line).* ***b)*** *LUMO orbitals in peri-acceptor (left) and ortho-acceptor (right). Reproduced from [2].*

We now have investigated the differences between energy transfer mechanisms that arise in *peri* and *ortho* perylenes, confirming that by altering the attachment position,

it is possible to influence the nature of the energy transfer mechanism in composite molecular systems. The higher rate of FRET in *peri*-DBA is explained by the larger spectral overlap integral as compared to *ortho*-DBA. The intramolecular triplet-to-singlet FRET allowed to harvest the excitation energy 36 times faster as compared to the phosphorescence from *D* in the absence of the acceptor. The higher rate of Dexter TET in *ortho*-DBA is rationalised through a higher electronic coupling arising from the larger electron delocalization on the phenyl ring as compared to that of *peri*-DBA. This concludes to the possibility of influencing the energy transfer mechanism in isomeric perylene-based systems as a function of functionalization position. The next section explores the remaining position of perylene, the bay region.

3.5 Towards polyrylene

This section discusses the results from **Paper IV.** Synthesis and isolation of dihexylquaterrylene is described in **Subsection 3.5.1**, whereas the photophysical evaluation and the formation of superradiant NIR J-aggregates are covered in **Subsection 3.5.2**. The explorations of the perylene *bay* region chemistry are challenging due to its steric hindrance as mentioned in **Section 3.2**. Therefore, the investigations of the *bay* region chemistry and photophysics were performed in conjunction with the observation of increased solubility in *bay*-alkylated perylenes as mentioned in **Section 1.3**.

Solubility hurdles in oligorylenes

Limited solubility creates a major nuisance when it comes to the synthetic expansion of the rylene family of dyes complicating both synthesis and solution spectroscopy. For instance, a dication has to be produced in the case of unsubstituted quaterrylene to perform solution NMR characterization [160]. Multiple functionalization strategies attempt to tackle the solubility issues, making perylene diimides one of the most extensively studied polyaromatic hydrocarbons of the past decade [161]. The solubility enhancement strategies in non-imide rylenes are mostly focused on *bay/ortho* derivatizations [162, 163]. However, derivatising the *ortho* regions end-caps the molecule, thus limiting any further efforts in longitudinal elongation of the rylene scaffold. Therefore, we have set our focus on *bay*-functionalisation strategies [164]. Bay-alkylation of perylene introduces a twist to the symmetry plane of the long axis in perylene [24, 162]. The broken plane symmetry results in a lower π–π stacking as shown by a higher solubility of the *bay*-derivatives as compared to *ortho*-alkylated perylenes [102]. Bay-alkylation can be achieved by introducing linear or branched alkyl chains allowing to retain intrinsic optical properties of the chromophore [4, 24, 102]. The monoalkylated perylene could then be used as a building block for the synthesis of higher oligorylenes.

3.5.1 Synthesis and isolation of a soluble quaterrylene scaffold

The synthetic pathway towards soluble *bay*-alkylated quaterrylene is shown in **Scheme 12**. First, 1-hexylperylene was synthesized using a literature procedure established earlier in the group [24]. Perylene was alkylated using slow addition of n-hexyllithium in THF at -30 ℃. Product ***31*** was then subject to Scholl reaction using the literature method [160]. Dissolving 1-hexylperylene in DCM followed by subsequent addition of CF_3SO_3H and DDQ yielded dihexylquaterryelene ***32***.

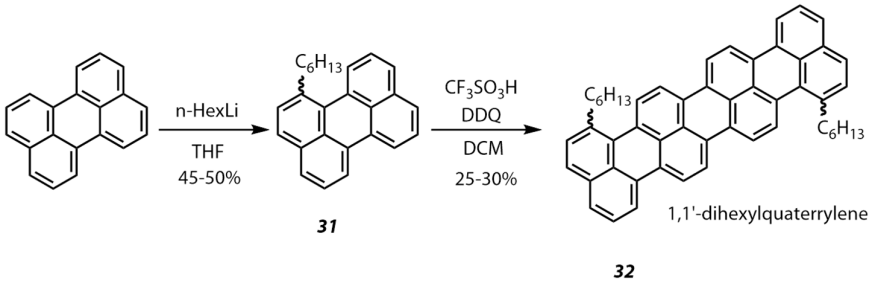

Scheme 12. *Synthesis of bay-alkylated quaterrylene.*

The MALDI-TOF spectrum of crude reaction mixture where 1-butylperylene was used as a starting material is shown in **Figure 27** (left). The signals at 916, 1220, 1524, 1829 and visible upon magnification 2132 correspond to the molecular weights of the alkylated hexarylene, octarylene, decarylene, dodecarylene and tetradecarylene respectively.

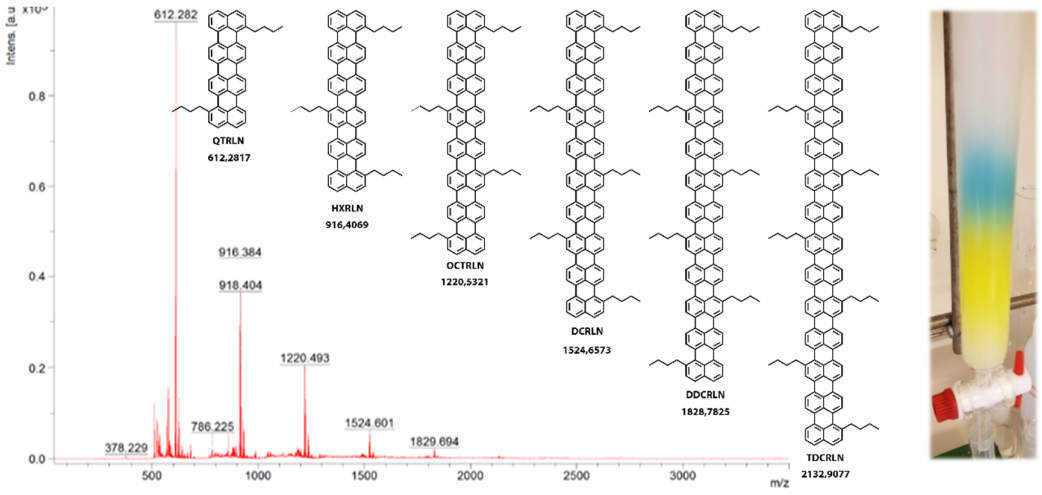

Figure 27. *The MALDI-TOF spectrum of the crude reaction mixture (left), SEC purification (right).*

Size exclusion chromatography (SEC) technique was used to purify the crude material. Using toluene or DCM as a mobile phase allowed for a visual separation of the fractions on the column as seen in **Figure 27** (right). Yellow fractions contained

mostly unreacted starting material and some unidentified compounds (possibly 1,1'-biperylene) the blue fractions contained the dihexylquaterrylene in up to 30% yield. The purified material was also analysed by HRMS (APCI source) to confirm the molecular weight of the target compound (see Supporting information, Section 2 in **Paper IV**).

Although, the mass analysis correlates to the dihexylquaterrylene molecule, the regioisomeric composition had to be determined. The asymmetrical starting material (1-hexylperylene) used in this reaction can produce up to 8 regioisomers that are shown in **Figure 28**.

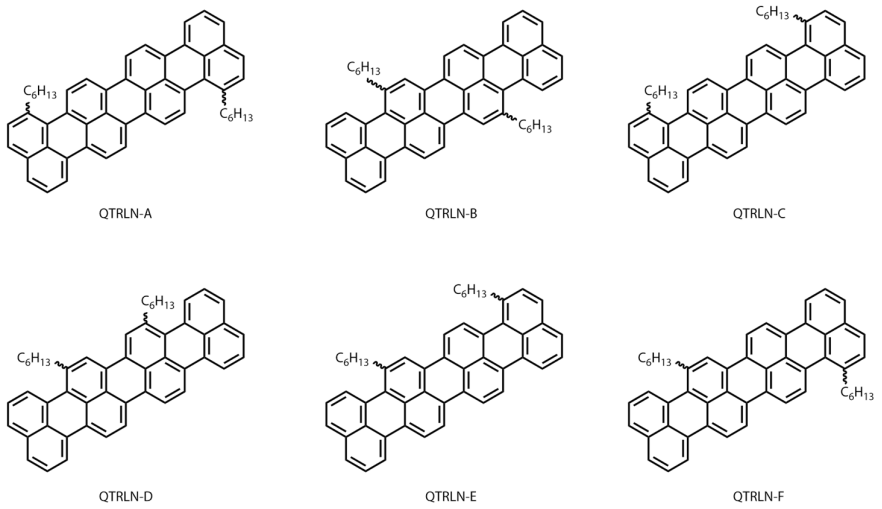

Figure 28. *The chemical structures of all the plausible dihexylquaterrylene regioisomers that could be produced during the Scholl condensation of 1-hexylperylene.*

To determine the structure, a series of NMR experiments were performed in collaboration with the Swedish NMR Centre. The experiments are described in Supporting information, Section 3 in **Paper IV**, defining the final structure as QTRLN-A or QTRLN-C (magnetically equivalent). The major component (QTRLN-A) is in ca. 90/10 ratio with the minor component (possibly regioisomer or atropisomer), the structure of which was not established. Hereafter, the reaction product will be referred to as 1,1'-dihexylquaterrylene (QTRLN-A).

Even though no rylene larger than dihexylquaterrylene was isolated in this experiment, the mass-spectrometry of the crude gave an important insight. The limitations of the Scholl coupling reaction are likely to be set by the solubility limits of the reaction products. Having established that 1,1'-dihexylquaterrylene is the major product formed when the reaction is executed in DCM, it was interesting to explore other chlorinated solvents. Performing the same reaction in 1,1,2,2-tetrachloroethane ($C_2H_2Cl_4$), the highest solvent power of any chlorinated

hydrocarbons [165] resulted in an unexpected outcome that is discussed in the next section together with the photophysical evaluation of 1,1'-dihexylquaterryelne.

3.5.2 Spectroscopical evaluation and the formation of J-aggregates

The improved solubility of the 1,1'-dihexylquaterrylene allowed to study the photophysical properties in toluene. Absorption and emission maxima are at 654 nm and 670 nm correspondingly, a moderate molecular absorption coefficient of 37000 $M^{-1}cm^{-1}$, and fluorescence quantum yields of 3-5% were in line with those reported earlier for other quaterrylenes [163]. The absorption (solid blue) and emission (dotted blue) spectra of 1,1'-dihexylquaterrylene are shown in **Figure 29**.

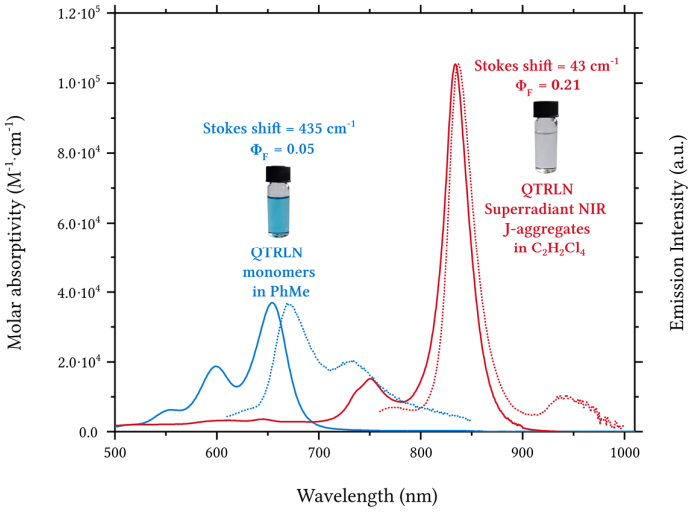

Figure 29. *Absorption and emission spectra of dihexylquaterrylene recorded in toluene (blue) and in $C_2H_2Cl_4$ (red) scaled according to their molar absorption coefficients. Dihexylquaterrylene is present in its monomeric form in toluene, while in $C_2H_2Cl_4$ it forms superradiant J-aggregates. Reproduced from [3].*

The summary of the photophysical properties of 1,1'-dihexylquaterrylene is presented in the first column of **Table 2**.

Table 2. *Photophysical properties of 1,1'-dihexylquaterrylene. The monomer was studied in toluene and the J-aggregate was studied in $C_2H_2Cl_4$. Reproduced from [3].*

	Monomer Toluene	J-aggregate $C_2H_2Cl_4$
$\lambda_{max,\ abs}$ [nm]	654	834
ε [$M^{-1}cm^{-1}$]	37000	105000
$\lambda_{max,\ em}$ [nm]	670	837
Stokes shift [cm^{-1}]	365	43
τ [ns]	1.05	1.50
Φ_F	0.05	0.21
k_r [s^{-1}]	$4.8 \cdot 10^7$	$1.4 \cdot 10^8$
k_{nr} [s^{-1}]	$9.05 \cdot 10^8$	$5.33 \cdot 10^8$

Aggregate formation

When the Scholl reaction was performed in $C_2H_2Cl_4$, the formation of some new species was observed. The absorption spectrum of the crude reaction mixture showed sharp signals around 840 nm and no signals corresponding to quaterrylene were observed. The narrow character of the absorption peak together with the significant bathochromic shift implied the possibility of aggregation. To analyse this phenomenon, we first looked at 1-hexylperylene in $C_2H_2Cl_4$. The absorption spectrum of 1-hexylperylene was not different to the one in toluene or DCM. However, when preparing 10^{-5} – 10^{-6} M concentration of dihexylquaterrylene in $C_2H_2Cl_4$ a discolouration was observed. This visible change indicated the formation of a new species and the composition thereof was then investigated by traditional spectroscopy methods. The absorption and the emission spectra for the newly formed species are shown in **Figure 29** using solid red lines (absorption) and dotted red lines (emission). The new species that form in $C_2H_2Cl_4$ show a bathochromic shift of 180 nm as compared to monomers, a significant decrease in Stokes shift (from 365 cm^{-1} to 43 cm^{-1}) and a drastic increase in the molar absorption coefficient (three-fold increase). A similar phenomenon was observed in the 1930s by Jelley and Schiebe [166-168]. Both scientists noticed that when dissolving pseudo isocyanine chloride in ethanol instead of water absorption and emission properties of the dye changed. The significant bathochromic shift of the absorption and the emission, reduced Stokes shift and largely increased molar absorptivity indicated the formation of staggered aggregates that were later called J-aggregates [166, 167]. The optical observations of the species formed in $C_2H_2Cl_4$ are in line with these characteristics, thus indicating that the newly formed species are dihexylquaterryelene J-aggregates.

The size of the J-aggregates

The physical size of the J-aggregates was estimated using two different methods: analysing the emission spectra and by using the diffusion NMR technique.

Spectral analysis. One potential way to estimate the physical size of the aggregate is by looking at the exciton delocalization over the individual molecules in the aggregate. This can be done by comparing the full width of the emission spectrum at 2/3 of a maximum of the monomer and the aggregate as represented in **Equation 3.3**,

$$N = \left(\frac{FW2/3M_{mon}}{FW2/3M_{agg}}\right)^2 \qquad (3.3)$$

Where N represents the coherence number, or in other words number of chromophore units the exciton is delocalised over in a coherent way. FW2/3M is the full width at two-thirds of the maximum of the emission of the monomer and the J-aggregate correspondingly. Using the values of the emission spectrum of the monomer and the aggregate from **Figure 29**, we can calculate the delocalisation

length with the help of **Equation 3.3**. The coherence number N equals to 6 for the given aggregate. This means that the aggregate is most likely composed of six dihexylquaterrylene units where the exciton is coherently delocalised.

Diffusion NMR. Another way of looking at the aggregate size is by diffusion NMR spectroscopy (DOSY). The experimental setup of the DOSY experiments was covered in **Section 2.6**. The specific models were built in order to simulate diffusion coefficients for dihexylquterrylene aggregates of 2 to 60 units. The models consisted of slip-stacked dihexylquaterrylenes (half molecular length) placed on a 3.5Å distance between each other, a typical stacking distance in perylenes [102]. The simulated diffusion coefficients were then compared to the experimentally obtained ones and are presented in **Table S3**.

Table S3. *Experimental and HYDRO++10 simulated diffusion coefficients. Reproduced from [3].*

Solvent	CD_2Cl_2 [m^2/s]		$C_2D_2Cl_4$ [m^2/s]	
Compound	experimental	simulated	experimental	simulated
1-hexylperylene	$1.5 \cdot 10^{-9} \pm 6 \cdot 10^{-12}$	$1.5 \cdot 10^{-9}$ / 1 unit	$3.6 \cdot 10^{-10} \pm 6 \cdot 10^{-12}$	$3.8 \cdot 10^{-10}$ / 1 unit
1,1'-dihexylquaterrylene	$1 \cdot 10^{-9} \pm 7 \cdot 10^{-11}$ [a]	$1 \cdot 10^{-9}$ / 1 unit	$6 \cdot 10^{-11} \pm 6 \cdot 10^{-12}$ [c]	$6.4 \cdot 10^{-11}$ / 14 units
	$1 \cdot 10^{-9} \pm 3 \cdot 10^{-11}$ [b]	$1 \cdot 10^{-9}$ / 1 unit	$3.3 \cdot 10^{-11} \pm 6 \cdot 10^{-12}$ [d]	$3.1 \cdot 10^{-11}$ / 34 units

[a] The diffusion constant was determined for 10^{-5} M sample in CD_2Cl_2, [b] The diffusion was determined for 10^{-4} M sample in CD_2Cl_2, [c] The diffusion constant was determined for 10^{-4} M sample in $C_2D_2Cl_4$, [d] The diffusion constant was determined for $>10^{-3}$ M sample in $C_2D_2Cl_4$. Reproduced from [3].

The experimental diffusion rates and the simulated values overlap at 14 units for 10^{-4} M concentrations. The diffusion rates are affected by the molecular concentrations, indicating the formation of larger aggregates at higher concentrations. This observation supports the values obtained by the spectral analysis at lower concentrations (N=6 units at 10^{-5} M). This concludes that within the investigated concentration range, the NMR assessment of the physical size of the aggregate is in reasonable agreement with the spectral assessment thereof.

Surpassing the energy gap law

An increased radiative rate constant was observed in the case of the J-aggregate (three-fold increase) as compared to monomer. The emission enhancement (superradiance) is a commonly observed phenomenon in J-aggregates [169]. However, what is less common is that the non-radiative rate has decreased in J-aggregates by 40% as compared to that of the monomer. Typically, the internal conversion is increasing as a function of red-shifted emission, resulting in an increased rate of non-

radiative relaxation. The energy gap law states that the non-radiative rate constant should increase exponentially as the energy gap decreases as can be expressed in **Equation 3.4** [170],

$$k_{nr} = \frac{C^2\sqrt{2\pi}}{\hbar\sqrt{\omega_{vib}\Delta E}} exp\left\{\frac{-\Delta E}{\omega_{vib}}\left[ln\left(\frac{\Delta E}{l\cdot\lambda}\right) - 1\right]\right\} \qquad (3.4)$$

where C is the effective electronic coupling constant between the excited state and ground state, ΔE is the energy difference between S_1 and S_0, ω_{vib} is the vibrational energy, l is the number of vibrational modes that induce the non-radiative transition (l is assumed to be 1) and λ is the reorganization energy of the promoting vibrational mode. Further derivations and calculation of the delocalization number and its effect on reorganizational energy is described in detail in **Paper IV.**

The decreased non-radiative rate is explained through the delocalized nature of the excited state. Exciton delocalization reduces the reorganization energy λ in the J-aggregates, consequentially decreasing the non-radiative rate. The deviation from the exponential increase in the non-radiative rate constant in the energy gap law was shown earlier using platinum complexes [16]. However, quaterrylene J-aggregates demonstrate a reduced non-radiative rate as compared to the monomers, therefore surpassing the energy gap law. Furthermore, the four-fold increase in fluorescence quantum yield is a direct consequence of both increased radiative rate (superradiance) and decreased non-radiative rate. The fluorescence quantum yields of 21% are not common in the NIR regime. Finding dyes with high emission quantum yields in the NIR regime is difficult because of the exponential increase of the nonradiative rate constant with decreasing energy of the excited state. The exciton delocalization can overcompensate for this by reducing the reorganization energy in highly ordered molecular assemblies. This strategy could potentially benefit the development of highly emissive dyes in the NIR region of the electromagnetic spectrum.

In conclusion, a promising solubilisation strategy (bay-alkylation) was established in oligorylene synthesis. Moreover, using the J-aggregation phenomenon it was concluded that the highly ordered nature of the aggregate reduces the reorganization energy, thus enabling to overcome the energy gap law.

Chapter 4

Summary and outlook

The work presented in this thesis strives to contribute to the fundamental understanding of the photoinduced processes that arise in perylene-based systems in relation to the molecular architecture thereof. Seeking to identify the correlations between the chemical structure and the intrinsic molecular properties, several important observations were made.

In **Paper I**, the general photophysics of phenylperylene isomers were discussed as a function of the derivatization position. In *ortho*-substituted phenylperylene the photophysical properties were similar to those of naked perylene, retaining the relative orientation of the transition dipole vector along the long axis of the molecule. In *peri*-substituted phenylperylene the red-shifted absorption and emission are explained by the elongated transition dipole vector because of the extended aromatic system along the long axis of the molecule. In *bay*-substituted phenylperylene the transition dipole vector deviates from the long molecular axis to a large extent. This could potentially explain the significantly altered relationship between the vibronic peaks in the emission spectrum. These results provide a generic insight on the modulation of the intrinsic photophysics of perylene derivatives as a function of the attachment position. This is of potential interest for the design of perylene-based dyes, energy transfer systems where the dipole moment orientation is of importance, as well as to the TTA-UC field where perylene could be used as an annihilator. In **Paper I**, perylene was functionalised with the electron neutral substituent (phenyl), however it might be relevant to explore the influence of EWG or EDG on the photophysics of perylene isomers. Moreover, the exploration of the transition dipole moment orientation influence could be taken further, for instance to multicomponent systems. This could potentially be done in covalently linked perylenes with aligned transition dipoles.

Paper II and **Paper III** discussed FRET-mediated triplet-to-singlet energy transfer and Dexter-type triplet-triplet energy transfer in two isomeric perylene-based dyads. In early studies, FRET-mediated triplet-to-singlet energy transfer was observed using freely diffusing donors and acceptors [21, 22]. However, recent studies have put this under doubt, discussing the energy transfer event in terms of angular momentum conservation [23]. To test the hypothesis of triplet-to-singlet FRET, the donor and the acceptor were covalently linked within a rigid molecular framework allowing to experimentally verify the theoretical predictions. The results confirmed intramolecular triplet-to-singlet energy transfer governed by the FRET mechanism.

This makes **Paper II** the first study that aligns the theoretical and experimental results of triplet-to-singlet FRET-mediated energy transfer in a fully controlled manner (controlled distances and transition dipole moment directions). Furthermore, this allowed to harvest the excitation energy from DBA systems 36 times faster as compared to the rate of phosphorescence from the pure donor. In *peri*-DBA the higher rate of FRET is rationalised by a larger spectral overlap integral as compared to *ortho*-DBA. On the other hand, the higher rate of Dexter-type energy transfer in *ortho*-DBA is explained by a larger electron delocalization on the phenyl ring and thus stronger electron coupling between the donor and the acceptor. When attaching the acceptor chromophore in the *ortho* position, the rate of Dexter-type TET increased but the rate of triplet-to-singlet FRET has decreased. Consequentially, attaching the acceptor in the *peri* position showed an increase in the rate of triplet-to-singlet FRET but the Dexter-type TET decreased. This interplay demonstrates the sensitivity of both Förster and Dexter types of energy transfer towards molecular alignment. Furthermore, it shows that it is possible to increase the rate of one energy transfer pathway, while simultaneously decreasing the other one. These results are of significance for the rational design of multiplicity conversion systems with controlled energy transfer pathways. Furthermore, these results are of relevance for the charge recombination in OLEDs that was discussed in **Section 1.2**.

Lastly, **Paper IV** demonstrates an efficient solubilisation strategy for the synthesis of higher oligorylenes. *Bay*-functionalization causes a molecular twist in the plane symmetry of the long axis of perylene, resulting in lower π–π stacking and therefore increased solubility [24, 102]. This allowed to synthesise *bay*-alkylated quaterrylene that is soluble in such neutral solvents as cyclohexane and toluene, whereas unsubstituted quaterrylene is insoluble in DCM. This observation opens a potential gateway towards the synthesis of linear oligorylenes where solubility is the major hurdle. Additionally, the *bay*-alkylated quaterrylene formed superradiant J-aggregates with high emission quantum yields in the NIR region of the electromagnetic spectrum. The J-aggregates demonstrated a 3-fold increase in radiative rate constant as well as a 40% decrease in non-radiative rate, consequentially resulting in a 4-fold increase of the emission quantum yield in the J-aggregates as compared to the monomers. Furthermore, the unprecedented decrease in the non-radiative rate indicates overcoming the limitations set by the energy gap law. This was achieved because of the reduced reorganization energy due to the delocalized nature of the excited state in J-aggregates. This emphasizes the importance of controlled aggregation strategies that could potentially open up a new approach towards highly emissive NIR dyes.

In conclusion, investigating the chemical, physical and photophysical properties of perylene-based systems provided a deeper understanding of some of the parameters guiding the excitation energy transfer pathways. A potentially new pathway towards highly emissive NIR chromophores was explored through the J-aggregation phenomenon. These results contribute to the understanding of the fundamental photophysics behind such processes as: multiplicity conversion, directional energy funnelling, switching between the energy transfer pathways and aggregation-induced enhanced emission. These functions are of practical importance in smart materials of the future.

Bibliography

1. Cravcenco, A., M. Hertzog, C. Ye, M.N. Iqbal, U. Mueller, L. Eriksson,K. Börjesson, Multiplicity conversion based on intramolecular triplet-to-singlet energy transfer. *Sci. Adv.* **2019,** *5* (9), eaaw5978.
2. Cravcenco, A., C. Ye, J. Gräfenstein,K. Börjesson, Interplay between Förster and Dexter Energy Transfer Rates in Isomeric Donor–Bridge–Acceptor Systems. *J. Phys. Chem. A* **2020,** *124* (36), 7219-7227.
3. Cravcenco, A., Y. Yu, F. Edhborg, J.F. Goebel, Z. Takacs, Y. Yang, B. Albinsson,K. Börjesson, Exciton Delocalization Counteracts the Energy Gap: A New Pathway toward NIR-Emissive Dyes. *J. Am. Chem. Soc.* **2021,** *143* (45), 19232-19239.
4. Hultmark, S., A. Cravcenco, K. Kushwaha, S. Mallick, P. Erhart, K. Börjesson,C. Müller, Vitrification of octonary perylene mixtures with ultralow fragility. *Science Advances* **2021,** *7* (29), eabi4659.
5. United Nations, D.o.E.a.S.A., Population Division, World Population Prospects. 2019.
6. IEA, Net zero by 2050 hinges on a global push to increase energy efficiency, IEA, Paris 2021.
7. IEA, Power Systems in Transition, IEA, Paris. 2020.
8. IEA, World Energy Model, IEA, Paris 2021.
9. IEA, World Energy Outlook 2021, IEA, Paris 2021.
10. Zissis, G., *Energy Consumption and Environmental and Economic Impact of Lighting: The Current Situation, Handbook of Advanced Lighting Technology*. Springer Reference Series.
11. IEA, Lighting, IEA, Paris. 2021.
12. Matsueda, Y., 52.1: Invited Paper: Next Generation Technologies for OLED displays. *SID Symposium Digest of Technical Papers* **2021,** *52* (S2), 615-618.
13. Roest, M.R., A.M. Oliver, M.N. Paddon-Row,J.W. Verhoeven, Distance Dependence of Singlet and Triplet Charge Recombination Pathways in a Series of Rigid Bichromophoric Systems. *J. Phys. Chem. A* **1997,** *101* (27), 4867-4871.
14. Baldo, M.A., D.F. O'Brien, Y. You, A. Shoustikov, S. Sibley, M.E. Thompson,S.R. Forrest, Highly efficient phosphorescent emission from organic electroluminescent devices. *Nature* **1998,** *395* (6698), 151-154.
15. Kasha, M., Characterization of Electronic Transitions in Complex Molecules. *Faraday Discuss.* **1950,** *9*, 14-19.
16. Wei, Y.-C., S.F. Wang, Y. Hu, L.-S. Liao, D.-G. Chen, K.-H. Chang, C.-W. Wang, S.-H. Liu, W.-H. Chan, J.-L. Liao, W.-Y. Hung, T.-H. Wang, P.-T. Chen, H.-F.

Hsu, Y. Chi,P.-T. Chou, Overcoming the energy gap law in near-infrared OLEDs by exciton–vibration decoupling. *Nat. Photonics* **2020,** *14* (9), 570-577.

17. Zampetti, A., A. Minotto,F. Cacialli, Near-Infrared (NIR) Organic Light-Emitting Diodes (OLEDs): Challenges and Opportunities. *Adv. Funct. Mater.* **2019,** *29* (21), 1807623.
18. Li, J., Y. Liu, Y. Xu, L. Li, Y. Sun,W. Huang, Recent advances in the development of NIR-II organic emitters for biomedicine. *Coord. Chem. Rev.* **2020,** *415*, 213318.
19. Wang, Y., H. Wu, W. Zhu, X. Zhang, Z. Liu, Y. Wu, C. Feng, Y. Dang, H. Dong, H. Fu,W. Hu, Cocrystal Engineering: Toward Solution-Processed Near-Infrared 2D Organic Cocrystals for Broadband Photodetection. *Angew. Chem. Int. Ed.* **2021,** *60* (12), 6344-6350.
20. Umeyama, T., K. Igarashi, D. Sasada, Y. Tamai, K. Ishida, T. Koganezawa, S. Ohtani, K. Tanaka, H. Ohkita,H. Imahori, Efficient light-harvesting, energy migration, and charge transfer by nanographene-based nonfullerene small-molecule acceptors exhibiting unusually long excited-state lifetime in the film state. *Chem. Sci.* **2020,** *11* (12), 3250-3257.
21. Ermolaev, V.L., Sveshnikova, E. V., Inductive-resonance Energy Transfer from Aromatic Molecules in the Triplet State. *Dokl. Akad. Nauk SSSR* **1963,** *149*, 1295-1298.
22. Kellogg, R.E.,R.G. Bennett, Radiationless Intermolecular Energy Transfer. III. Determination of Phosphorescence Efficiencies. *J. Chem. Phys.* **1964,** *41* (10), 3042-3045.
23. Guo, D., T.E. Knight,J.K. McCusker, Angular Momentum Conservation in Dipolar Energy Transfer. *Science* **2011,** *334* (6063), 1684-1687.
24. Kushwaha, K., L. Yu, K. Stranius, S.K. Singh, S. Hultmark, M.N. Iqbal, L. Eriksson, E. Johnston, P. Erhart, C. Müller,K. Börjesson, A Record Chromophore Density in High-Entropy Liquids of Two Low-Melting Perylenes: A New Strategy for Liquid Chromophores. *Adv. Sci.* **2019,** *6* (4), 1801650-1801650.
25. Assembly, U.G., Transforming out world: the 2030 Agenda for Sustainable Development. 2015.
26. Schrödinger, E., An Undulatory Theory of the Mechanics of Atoms and Molecules. *Phys. Rev.* **1926,** *28* (6), 1049-1070.
27. Born, M.,R. Oppenheimer, Zur Quantentheorie der Molekeln. *Ann. Phys. (Berl.)* **1927,** *389* (20), 457-484.
28. Anslyn, E.V., & Dougherty, D. A., *Modern physical organic chemistry*. University Science Books: 2006.

29. Atkins, P., de Paula, J., Friedman, R. , *Quanta, matter, and change : a molecular approach to physical chemistry*. Oxford University Press: 2009.
30. Juris, A., P. Ceroni,V. Balzani. *Photochemistry and Photophysics: Concepts, Research, Applications*. 2014.
31. Klan, P., Wirz, J., *Photochemistry of Organic Compounds: From Concepts to Practice*. Wiley: 2009.
32. Levine, I.N., *Quantum Chemistry (4th ed.)*. United States: Prentice-Hall: 1991.
33. Atkins, P., de Paula, J., *Atkins' Physical Chemistry (8th ed.)*. Oxford University Press: 2006.
34. Atkins, P.W., *Physical Chemistry*. Oxford University Press: 1978.
35. *Electronic Orbitals*. 2020/6/22/; Available from: https://chem.libretexts.org/@go/page/1650.
36. Pauli, W., Über den Zusammenhang des Abschlusses der Elektronengruppen im Atom mit der Komplexstruktur der Spektren. *Z. Phys.* **1925,** *31* (1), 765-783.
37. Feynman, R., *QED: The Strange Theory of Light and Matter*. Princeton Univeristy Press: 1985.
38. Foldy, L.L.,S.A. Wouthuysen, On the Dirac Theory of Spin 1/2 Particles and Its Non-Relativistic Limit. *Phys. Rev.* **1950,** *78* (1), 29-36.
39. Dirac, P.A.M.,R.H. Fowler, The quantum theory of the electron. *Proc. Math. Phys. Eng. Sci.* **1928,** *117* (778), 610-624.
40. Balzani, V., A. Credi,M. Venturi, Photochemical Conversion of Solar Energy. *ChemSusChem* **2008,** *1* (1-2), 26-58.
41. Mirkovic, T., E.E. Ostroumov, J.M. Anna, R. van Grondelle, Govindjee,G.D. Scholes, Light Absorption and Energy Transfer in the Antenna Complexes of Photosynthetic Organisms. *Cherm. Rev.* **2017,** *117* (2), 249-293.
42. Barber, J., Photosystem II: an enzyme of global significance. *Biochem Soc Trans* **2006,** *34* (Pt 5), 619-31.
43. Pullerits, T., S. Hess, J.L. Herek,V. Sundström, Temperature Dependence of Excitation Transfer in LH2 of Rhodobacter sphaeroides. *J. Phys. Chem. B* **1997,** *101* (49), 10560-10567.
44. McConnell, I., G. Li,G.W. Brudvig, Energy Conversion in Natural and Artificial Photosynthesis. *Chem.* **2010,** *17* (5), 434-447.
45. Kannan, R., F. Marinacci, M. Vogelsberger, L.V. Sales, P. Torrey, V. Springel,L. Hernquist, Simulating the interstellar medium of galaxies with radiative transfer, non-equilibrium thermochemistry, and dust. *Mon. Notices Royal Astron. Soc.* **2020,** *499* (4), 5732-5748.
46. Lunttila, T., Radiative transfer modelling of interstellar clouds. University of Helsinki: 2012; Vol. PhD.

47. Förster, T., Zwischenmolekulare Energiewanderung und Fluoreszenz. *Annalen der Physik* **1948,** *437* (1-2), 55-75.
48. Valeur, B.a.B.-S., M.N., *Excitation Energy Transfer*. 2012; p 213-261.
49. Andrews, D.L.,D.S. Bradshaw, Virtual photons, dipole fields and energy transfer: a quantum electrodynamical approach. *European Journal of Physics* **2004,** *25* (6), 845-858.
50. Jaeger, G., Are Virtual Particles Less Real? *Entropy* **2019,** *21* (2), 141.
51. Andrews, D.L., A unified theory of radiative and radiationless molecular energy transfer. *Chem. Phys.* **1989,** *135* (2), 195-201.
52. Jones, G.A.,D.S. Bradshaw, Resonance Energy Transfer: From Fundamental Theory to Recent Applications. *Front. Phys.* **2019,** *7* (100).
53. Lakowicz, J.R., *Principles of Fluorescence Spectroscopy (3rd Edition)*. Springer: 2006.
54. Stryer, L.,R.P. Haugland, Energy Transfer: A Spectroscopic Ruler. *Proc. Natl. Acad. Sci. U.S.A.* **1967,** *58* (2), 719-726.
55. Selvin, P.R.,J.E. Hearst, Luminescence Energy Transfer Using a Terbium Chelate: Improvements on Fluorescence Energy Transfer. *Proc. Natl. Acad. Sci. U.S.A.* **1994,** *91* (21), 10024-10028.
56. Vekshin, N.L., *Energy Transfer in Macromolecules*. SPIE Press: 1997.
57. Bojarski, P., L. Kulak, K. Walczewska-Szewc, A. Synak, V.M. Marzullo, A. Luini,S. D'Auria, Long-Distance FRET Analysis: A Monte Carlo Simulation Study. *J. Phys. Chem. B* **2011,** *115* (33), 10120-10125.
58. Pugliesi, I., H. Langhals,E. Riedle. *Förster Resonant Energy Transfer (FRET) in Orthogonal Chromophores*. in *CLEO/Europe and EQEC 2011 Conference Digest*. 2011. Munich: Optical Society of America.
59. Langhals, H.,A. Walter, FRET in Dyads with Orthogonal Chromophores and Minimal Spectral Overlap. *J. Phys. Chem. A* **2020,** *124* (8), 1554-1560.
60. Langhals, H., C. Dietl,P. Mayer, FRET in Orthogonal, Increasingly Strain-Rigidified Systems. *Isr. J. Chem.* **2021,** *n/a* (n/a).
61. Schweighöfer, F., L. Dworak, C.A. Hammer, H. Gustmann, M. Zastrow, K. Rück-Braun,J. Wachtveitl, Highly efficient modulation of FRET in an orthogonally arranged BODIPY–DTE dyad. *Sci. Rep.* **2016,** *6* (1), 28638.
62. Schaufele, F., I. Demarco,R.N. Day, *4 - FRET Imaging in the Wide-Field Microscope*, in *Molecular Imaging*, A. Periasamy and R.N. Day, Editors. 2005, American Physiological Society: San Diego. p. 72-94.
63. Skaisgirski, M., X. Guo,O.S. Wenger, Electron Accumulation on Naphthalene Diimide Photosensitized by [Ru(2,2′-Bipyridine)3]2+. *Inorg. Chem.* **2017,** *56* (5), 2432-2439.

64. Chang, Y.-L., Y. Song, Z. Wang, M.G. Helander, J. Qiu, L. Chai, Z. Liu, G.D. Scholes,Z. Lu, Highly Efficient Warm White Organic Light-Emitting Diodes by Triplet Exciton Conversion. *Adv. Funct. Mater.* **2013,** *23* (6), 705-712.
65. Chang, Y.L., S. Gong, X. Wang, R. White, C. Yang, S. Wang,Z.H. Lu, Highly efficient greenish-blue platinum-based phosphorescent organic light-emitting diodes on a high triplet energy platform. *Appl. Phys. Lett.* **2014,** *104* (17), 173303.
66. Chang, Y.-L.,Z.-H. Lu, White Organic Light-Emitting Diodes for Solid-State Lighting. *J. Display Technol.* **2013,** *9* (6), 459-468.
67. Cerdán, L., E. Enciso, V. Martín, J. Bañuelos, I. López-Arbeloa, A. Costela,I. García-Moreno, FRET-assisted laser emission in colloidal suspensions of dye-doped latex nanoparticles. *Nat. Photonics* **2012,** *6* (9), 621-626.
68. Barbour, J.C., A.J.I. Kim, E. deVries, S.E. Shaner,B.M. Lovaasen, Chromium(III) Bis-Arylterpyridyl Complexes with Enhanced Visible Absorption via Incorporation of Intraligand Charge-Transfer Transitions. *Inorg. Chem.* **2017,** *56* (14), 8212-8222.
69. Bonn, A.G.,O.S. Wenger, Photoinduced charge accumulation by metal ion-coupled electron transfer. *Phys. Chem. Chem. Phys.* **2015,** *17* (37), 24001-24010.
70. Turro, N.J., Ramamurthy, V., & Scaiano, J. C., *Principles of molecular photochemistry: An introduction.* University Science Books: 2009.
71. Dexter, D.L., A Theory of Sensitized Luminescence in Solids. *J. Chem. Phys.* **1953,** *21* (5), 836-850.
72. Gilbert, M.,B. Albinsson, Photoinduced charge and energy transfer in molecular wires. *Chem Soc. Rev.* **2015,** *44* (4), 845-862.
73. Balzani, V., F. Bolletta,F. Scandola, Vertical and "nonvertical" energy transfer processes. A general classical treatment. *J. Am. Chem. Soc.* **1980,** *102* (7), 2152-2163.
74. Scandola, F., Balzani, V., Energy-Transfer Processes of Excited States of Coordination Compounds *J. Chem. Educ.* **1983,** *60* (10), 814-823.
75. Piotrowiak, P., *Relationship between Electron and Electronic Excitation Transfer*, in *Electron Transfer in Chemistry*. 2001. p. 215-237.
76. Balzani, V., A. Credi,M. Venturi. *Molecular Devices and Machines: Concepts and Perspectives for the Nanoworld.* 2008.
77. Vura-Weis, J., S.H. Abdelwahed, R. Shukla, R. Rathore, M.A. Ratner,M.R. Wasielewski, Crossover from Single-Step Tunneling to Multistep Hopping for Molecular Triplet Energy Transfer. *Science* **2010,** *328* (5985), 1547-1550.
78. Renaud, N., Y.A. Berlin, F.D. Lewis,M.A. Ratner, Between Superexchange and Hopping: An Intermediate Charge-Transfer Mechanism in Poly(A)-Poly(T) DNA Hairpins. *J. Am. Chem. Soc.* **2013,** *135* (10), 3953-3963.

79. Voityuk, A.A., Long-Range Electron Transfer in Biomolecules. Tunneling or Hopping? *J. Phys. Chem. B* **2011,** *115* (42), 12202-12207.
80. Hines, T., I. Diez-Perez, J. Hihath, H. Liu, Z.-S. Wang, J. Zhao, G. Zhou, K. Müllen,N. Tao, Transition from Tunneling to Hopping in Single Molecular Junctions by Measuring Length and Temperature Dependence. *Journal of the American Chemical Society* **2010,** *132* (33), 11658-11664.
81. Lloveras, V., J. Vidal-Gancedo, T.M. Figueira-Duarte, J.-F. Nierengarten, J.J. Novoa, F. Mota, N. Ventosa, C. Rovira,J. Veciana, Tunneling versus Hopping in Mixed-Valence Oligo-p-phenylenevinylene Polychlorinated Bis(triphenylmethyl) Radical Anions. *J. Am. Chem. Soc.* **2011,** *133* (15), 5818-5833.
82. Brédas, J.-L., J. Cornil, D. Beljonne, D.A. dos Santos,Z. Shuai, Excited-State Electronic Structure of Conjugated Oligomers and Polymers: A Quantum-Chemical Approach to Optical Phenomena. *Acc. Chem. Res.* **1999,** *32* (3), 267-276.
83. Parker, C.A.,C.G. Hatchard, Triplet-singlet emission in fluid solutions. Phosphorescence of eosin. *Trans. Faraday Soc.* **1961,** *57* (0), 1894-1904.
84. Heinz, B., B. Schmidt, C. Root, H. Satzger, F. Milota, B. Fierz, T. Kiefhaber, W. Zinth,P. Gilch, On the unusual fluorescence properties of xanthone in water. *Phys. Chem. Chem. Phys.* **2006,** *8* (29), 3432-3439.
85. Parker, C.A., *Photoluminescence of Solutions*. Elsevier: 1968.
86. Uoyama, H., K. Goushi, K. Shizu, H. Nomura,C. Adachi, Highly efficient organic light-emitting diodes from delayed fluorescence. *Nature* **2012,** *492* (7428), 234-238.
87. Endo, A., K. Sato, K. Yoshimura, T. Kai, A. Kawada, H. Miyazaki,C. Adachi, Efficient up-conversion of triplet excitons into a singlet state and its application for organic light emitting diodes. *Appl. Phys. Lett.* **2011,** *98* (8), 083302.
88. Endo, A., M. Ogasawara, A. Takahashi, D. Yokoyama, Y. Kato,C. Adachi, Thermally Activated Delayed Fluorescence from Sn4+−Porphyrin Complexes and Their Application to Organic Light Emitting Diodes — A Novel Mechanism for Electroluminescence. *Adv. Mater.* **2009,** *21* (47), 4802-4806.
89. Ravinson, D.S.M.,M.E. Thompson, Thermally assisted delayed fluorescence (TADF): fluorescence delayed is fluorescence denied. *Mater. Horizons* **2020,** *7* (5), 1210-1217.
90. Hamze, R., J.L. Peltier, D. Sylvinson, M. Jung, J. Cardenas, R. Haiges, M. Soleilhavoup, R. Jazzar, P.I. Djurovich, G. Bertrand,M.E. Thompson, Eliminating nonradiative decay in Cu(I) emitters: >99% quantum efficiency and microsecond lifetime. *Science* **2019,** *363* (6427), 601-606.

91. Parker, C.A.,C.G. Hatchard, Delayed fluorescence of pyrene in ethanol. *Trans. Faraday Soc.* **1963,** *59* (0), 284-295.
92. Nickel, B., Delayed Fluorescence from Upper Excited Singlet States Sn (n > 1) of the Aromatic Hydrocarbons 1,2-benzanthracene, fluoranthene, pyrene, and chrysene in methylcyclohexane. *Helv. Chim.* **1978,** *61* (1), 198-222.
93. Liu, D.K.K.,L.R. Faulkner, Delayed fluorescence efficiencies of anthracene and phenanthrene. *J. Am. Chem. Soc.* **1978,** *100* (9), 2635-2639.
94. Nickel, B.,H.-J. Karbach, Complete spectra of the delayed luminescence from aromatic compounds in liquid solutions: On the observability of direct radiative triplet-triplet annihilation. *Chem. Phys.* **1990,** *148* (1), 155-182.
95. Parker, C.A.,E.J. Bowen, Sensitized P-type delayed fluorescence. *Proc. Math. Phys. Eng. Sci.* **1963,** *276* (1364), 125-135.
96. Parker, C.A., C.G. Hatchard,E.J. Bowen, Delayed fluorescence from solutions of anthracene and phenanthrene. *Proc. Math. Phys. Eng. Sci.* **1962,** *269* (1339), 574-584.
97. Parker, C.A.,T.A. Joyce, Delayed fluorescence of anthracene and some substituted anthracenes. *Chem. Commun.* **1967,** (15), 744-745.
98. Schmidt, T.W.,F.N. Castellano, Photochemical Upconversion: The Primacy of Kinetics. *J. Phys. Chem. Lett.* **2014,** *5* (22), 4062-4072.
99. Fagnoni, M., Modern Molecular Photochemistry of Organic Molecules. By Nicholas J. Turro, V. Ramamurthy and Juan C. Scaiano. *Angew. Chem. Int. Ed.* **2010,** *49* (38), 6709-6710.
100. Gray, V., K. Moth-Poulsen, B. Albinsson,M. Abrahamsson, Towards efficient solid-state triplet–triplet annihilation based photon upconversion: Supramolecular, macromolecular and self-assembled systems. *Coordination Chemistry Reviews* **2018,** *362*, 54-71.
101. Kukhta, N.A., T. Matulaitis, D. Volyniuk, K. Ivaniuk, P. Turyk, P. Stakhira, J.V. Grazulevicius,A.P. Monkman, Deep-Blue High-Efficiency TTA OLED Using Para- and Meta-Conjugated Cyanotriphenylbenzene and Carbazole Derivatives as Emitter and Host. *J. Phys. Chem. Lett.* **2017,** *8* (24), 6199-6205.
102. Ye, C., V. Gray, K. Kushwaha, S. Kumar Singh, P. Erhart,K. Börjesson, Optimizing photon upconversion by decoupling excimer formation and triplet triplet annihilation. *Phys. Chem. Chem. Phys.* **2020,** *22* (3), 1715-1720.
103. Bossanyi, D.G., Y. Sasaki, S. Wang, D. Chekulaev, N. Kimizuka, N. Yanai,J. Clark, Spin Statistics for Triplet–Triplet Annihilation Upconversion: Exchange Coupling, Intermolecular Orientation, and Reverse Intersystem Crossing. *JACS Au* **2021**.
104. Hohenberg, P.,W. Kohn, Inhomogeneous Electron Gas. *Phys. Rev.* **1964,** *136* (3B), B864-B871.

105. Kohn, W.,L.J. Sham, Self-Consistent Equations Including Exchange and Correlation Effects. *Phys. Rev.* **1965,** *140* (4A), A1133-A1138.
106. Woods, N.D., M.C. Payne,P.J. Hasnip, Computing the self-consistent field in Kohn–Sham density functional theory. *J. Phys. Condens.* **2019,** *31* (45), 453001.
107. Runge, E.,E.K.U. Gross, Density-Functional Theory for Time-Dependent Systems. *Phys. Rev. Lett.* **1984,** *52* (12), 997-1000.
108. Petersilka, M., U.J. Gossmann,E.K.U. Gross, Excitation Energies from Time-Dependent Density-Functional Theory. *Phys. Rev. Lett.* **1996,** *76* (8), 1212-1215.
109. Tomasi, J., B. Mennucci,R. Cammi, Quantum Mechanical Continuum Solvation Models. *Cherm. Rev.* **2005,** *105* (8), 2999-3094.
110. Frisch, M.J., G.W. Trucks, H.B. Schlegel, G.E. Scuseria, M.A. Robb, J.R. Cheeseman, G. Scalmani, V. Barone, G.A. Petersson, H. Nakatsuji, X. Li, M. Caricato, A.V. Marenich, J. Bloino, B.G. Janesko, R. Gomperts, B. Mennucci, H.P. Hratchian, J.V. Ortiz, A.F. Izmaylov, J.L. Sonnenberg, Williams, F. Ding, F. Lipparini, F. Egidi, J. Goings, B. Peng, A. Petrone, T. Henderson, D. Ranasinghe, V.G. Zakrzewski, J. Gao, N. Rega, G. Zheng, W. Liang, M. Hada, M. Ehara, K. Toyota, R. Fukuda, J. Hasegawa, M. Ishida, T. Nakajima, Y. Honda, O. Kitao, H. Nakai, T. Vreven, K. Throssell, J.A. Montgomery Jr., J.E. Peralta, F. Ogliaro, M.J. Bearpark, J.J. Heyd, E.N. Brothers, K.N. Kudin, V.N. Staroverov, T.A. Keith, R. Kobayashi, J. Normand, K. Raghavachari, A.P. Rendell, J.C. Burant, S.S. Iyengar, J. Tomasi, M. Cossi, J.M. Millam, M. Klene, C. Adamo, R. Cammi, J.W. Ochterski, R.L. Martin, K. Morokuma, O. Farkas, J.B. Foresman, and D.J. Fox, Gaussian 16 Rev. C.01. Wallingford, CT, 2016.
111. Becke, A.D., Density-functional thermochemistry. III. The role of exact exchange. *J. Chem. Phys.* **1993,** *98* (7), 5648-5652.
112. Lee, C., W. Yang,R.G. Parr, Development of the Colle-Salvetti correlation-energy formula into a functional of the electron density. *Phys. Rev. B.* **1988,** *37* (2), 785-789.
113. Vosko, S.H., L. Wilk,M. Nusair, Accurate spin-dependent electron liquid correlation energies for local spin density calculations: a critical analysis. *Can. J. Phys.* **1980,** *58* (8), 1200-1211.
114. Stephens, P.J., F.J. Devlin, C.F. Chabalowski,M.J. Frisch, Ab Initio Calculation of Vibrational Absorption and Circular Dichroism Spectra Using Density Functional Force Fields. *J. Phys. Chem.* **1994,** *98* (45), 11623-11627.
115. Hay, T.H.D.J.a.P.J., *Methods of Electronic Structure Theory, Vol. 2*. Plenum Press: 1977.
116. Keeler, J., *Understanding NMR spectroscopy*. Wiley: Hoboken, N.J., 2005.
117. Pell, A.J., R.A.E. Edden,J. Keeler, Broadband proton-decoupled proton spectra. *Magn. Reson. Chem.* **2007,** *45* (4), 296-316.

118. Furrer, J., A robust, sensitive, and versatile HMBC experiment for rapid structure elucidation by NMR: IMPACT-HMBC. *Chem. Commun.* **2010,** *46* (19), 3396-3398.
119. Garcia de la Torre, J., S. Navarro, M.C. Lopez Martinez, F.G. Diaz,J.J. Lopez Cascales, HYDRO: a computer program for the prediction of hydrodynamic properties of macromolecules. *Biophys. J.* **1994,** *67* (2), 530-531.
120. García de la Torre, J., G. del Rio Echenique,A. Ortega, Improved Calculation of Rotational Diffusion and Intrinsic Viscosity of Bead Models for Macromolecules and Nanoparticles. *J. Phys. Chem. B* **2007,** *111* (5), 955-961.
121. Scholl, R.,J. Mansfeld, meso-Benzdianthron (Helianthron), meso-Naphthodianthron, und ein neuer Weg zum Flavanthren. *Berichte der deutschen chemischen Gesellschaft* **1910,** *43* (2), 1734-1746.
122. Scholl, R., C. Seer,R. Weitzenböck, Perylen, ein hoch kondensierter aromatischer Kohlenwasserstoff C20H12. *Ber. Dtsch. Chem. Ges.* **1910,** *43* (2), 2202-2209.
123. Weitzenböck, R.,C. Seer, Zur Kenntnis des Perylens und seiner Derivate. (2. Mitteilung). *Ber. Dtsch. Chem. Ges.* **1913,** *46* (2), 1994-2000.
124. Fritz Ullmann, M.B., *Ullmann's encyclopedia of industrial chemistry (7th edition).* Wiley Online Library: 2009.
125. Mulliken, R.S., Electronic Population Analysis on LCAO–MO Molecular Wave Functions. I. *J. Chem. Phys.* **1955,** *23* (10), 1833-1840.
126. Lennard-Jones, J.E., The electronic structure of some diatomic molecules. *Trans. Faraday Soc.* **1929,** *25* (0), 668-686.
127. Harmer, R., H. Fan, K. Lloyd, S. Doble, J. Avenoso, H. Yan, L.G.C. Rego, L. Gundlach,E. Galoppini, Synthesis and Properties of Perylene-Bridge-Anchor Chromophoric Compounds. *J. Phys. Chem. A* **2020,** *124* (31), 6330-6343.
128. Coventry, D.N., A.S. Batsanov, A.E. Goeta, J.A.K. Howard, T.B. Marder,R.N. Perutz, Selective Ir-catalysed borylation of polycyclic aromatic hydrocarbons: structures of naphthalene-2,6-bis(boronate), pyrene-2,7-bis(boronate) and perylene-2,5,8,11-tetra(boronate) esters. *Chemical Communications* **2005,** (16), 2172-2174.
129. Kurpanik, A., M. Matussek, P. Lodowski, G. Szafraniec-Gorol, M. Krompiec,S. Krompiec, Diels–Alder Cycloaddition to the Bay Region of Perylene and Its Derivatives as an Attractive Strategy for PAH Core Expansion: Theoretical and Practical Aspects. *Molecules* **2020,** *25* (22), 5373.
130. Kodama, K., A. Kobayashi,T. Hirose, Synthesis and spectral properties of ruthenium(II) complexes based on 2,2′-bipyridines modified by a perylene chromophore. *Tetrahedron Letters* **2013,** *54* (40), 5514-5517.

131. Tanizaki, Y., T. Yoshinaga,H. Hiratsuka, Assignment of electronic spectrum of perylene. *Spectrochimica Acta Part A: Molecular Spectroscopy* **1978,** *34* (2), 205-210.
132. Donaldson, D.M., J.M. Robertson,J. White, The crystal and molecular structure of perylene. *Proc. Math. Phys. Eng. Sci.* **1953,** *220* (1142), 311-321.
133. Botoshansky, M., F.H. Herbstein,M. Kapon, Towards a Complete Description of a Polymorphic Crystal: The Example of Perylene. *Helvetica Chimica Acta* **2003,** *86* (4), 1113-1128.
134. E. V. Anslyn and D. A. Dougherty, *Modern Physical organic Chemistry*. University Science Books: 2006.
135. Hansch, C., A. Leo,R.W. Taft, A survey of Hammett substituent constants and resonance and field parameters. *Cherm. Rev.* **1991,** *91* (2), 165-195.
136. Heimel, G., M. Daghofer, J. Gierschner, E.J.W. List, A.C. Grimsdale, K. Müllen, D. Beljonne, J.-L. Brédas,E. Zojer, Breakdown of the mirror image symmetry in the optical absorption/emission spectra of oligo(para-phenylene)s. *The Journal of Chemical Physics* **2005,** *122* (5), 054501.
137. Rangel, T., A. Rinn, S. Sharifzadeh, F.H. da Jornada, A. Pick, S.G. Louie, G. Witte, L. Kronik, J.B. Neaton,S. Chatterjee, Low-lying excited states in crystalline perylene. *Proc. Natl. Acad. Sci.* **2018,** *115* (2), 284-289.
138. Pugliesi, I., H. Langhals, H. Kauffmann,E. Riedle, New perspectives on ultrafast Förster Resonant Energy Transfer. *EPJ Web of Conferences* **2013,** *41*, 05015.
139. Arsenault, E.A., Y. Yoneda, M. Iwai, K.K. Niyogi,G.R. Fleming, Vibronic mixing enables ultrafast energy flow in light-harvesting complex II. *Nat. Commun.* **2020,** *11* (1), 1460.
140. Cheng-Huei, L., C. Yao-Yuan, H. Jui-Yi, L. Chih-Yuan, C. Yun, C. Min-Wen, L. Chia-Li, C. Pi-Tai, L. Gene-Hsiang, C. Chih-Hao,L. Wei-Chieh, Iridium(III) Complexes of a Dicyclometalated Phosphite Tripod Ligand: Strategy to Achieve Blue Phosphorescence Without Fluorine Substituents and Fabrication of OLEDs. *Angew. Chem. Int. Ed.* **2011,** *50* (14), 3182-3186.
141. Chang, H., W.F. Kiesman,R.C. Petter, Convenient One-Pot Preparation of Dimethyl Bicyclo[2.2.2]octane-1,4-dicarbolylate, a Key Intermediate for a Novel Adenosine A1 Receptor Antagonist. *Synth. Commun.* **2007,** *37* (8), 1267-1272.
142. Bandak, D., O. Babii, R. Vasiuta, I.V. Komarov,P.K. Mykhailiuk, Design and Synthesis of Novel 19F-Amino Acid: A Promising 19F NMR Label for Peptide Studies. *Organic Letters* **2015,** *17* (2), 226-229.
143. Al Hussainy, R., J. Verbeek, D. van der Born, A.H. Braker, J.E. Leysen, R.J. Knol, J. Booij,J.D.M. Herscheid, Design, Synthesis, Radiolabeling, and in Vitro and in Vivo Evaluation of Bridgehead Iodinated Analogues of N-{2-[4-(2-

Methoxyphenyl)piperazin-1-yl]ethyl}-N-(pyridin-2-yl)cyclohexanecarboxamide (WAY-100635) as Potential SPECT Ligands for the 5-HT1A Receptor. *Journal of Medicinal Chemistry* **2011,** *54* (10), 3480-3491.

144. Candish, L., E.A. Standley, A. Gómez-Suárez, S. Mukherjee,F. Glorius, Catalytic Access to Alkyl Bromides, Chlorides and Iodides via Visible Light-Promoted Decarboxylative Halogenation. *Chemistry – A European Journal* **2016,** *22* (29), 9971-9974.
145. Materna, K.,L. Hammarström, Photoredox Catalysis Using Heterogenized Iridium Complexes. *Chem. Eur. J.* **2021**.
146. Tamao, K., K. Sumitani,M. Kumada, Selective carbon-carbon bond formation by cross-coupling of Grignard reagents with organic halides. Catalysis by nickel-phosphine complexes. *J. Am. Chem. Soc.* **1972,** *94* (12), 4374-4376.
147. Miyaura, N., K. Yamada,A. Suzuki, A new stereospecific cross-coupling by the palladium-catalyzed reaction of 1-alkenylboranes with 1-alkenyl or 1-alkynyl halides. *Tetrahedron Lett.* **1979,** *20* (36), 3437-3440.
148. Zultanski, S.L.,G.C. Fu, Nickel-Catalyzed Carbon–Carbon Bond-Forming Reactions of Unactivated Tertiary Alkyl Halides: Suzuki Arylations. *J. Am. Chem. Soc.* **2013,** *135* (2), 624-627.
149. Zhou, J.,G.C. Fu, Suzuki Cross-Couplings of Unactivated Secondary Alkyl Bromides and Iodides. *Journal of the American Chemical Society* **2004,** *126* (5), 1340-1341.
150. Cui, X., A. Charaf-Eddin, J. Wang, B. Le Guennic, J. Zhao,D. Jacquemin, Perylene-Derived Triplet Acceptors with Optimized Excited State Energy Levels for Triplet–Triplet Annihilation Assisted Upconversion. *The Journal of Organic Chemistry* **2014,** *79* (5), 2038-2048.
151. Birch, A.M., S. Birtles, L.K. Buckett, P.D. Kemmitt, G.J. Smith, T.J.D. Smith, A.V. Turnbull,S.J.Y. Wang, Discovery of a Potent, Selective, and Orally Efficacious Pyrimidinooxazinyl Bicyclooctaneacetic Acid Diacylglycerol Acyltransferase-1 Inhibitor. *Journal of Medicinal Chemistry* **2009,** *52* (6), 1558-1568.
152. Barlind, J.G., U.A. Bauer, A.M. Birch, S. Birtles, L.K. Buckett, R.J. Butlin, R.D.M. Davies, J.W. Eriksson, C.D. Hammond, R. Hovland, P. Johannesson, M.J. Johansson, P.D. Kemmitt, B.T. Lindmark, P. Morentin Gutierrez, T.A. Noeske, A. Nordin, C.J. O'Donnell, A.U. Petersson, A. Redzic, A.V. Turnbull, and J. Vinblad, Design and Optimization of Pyrazinecarboxamide-Based Inhibitors of Diacylglycerol Acyltransferase 1 (DGAT1) Leading to a Clinical Candidate Dimethylpyrazinecarboxamide Phenylcyclohexylacetic Acid (AZD7687). *J. Med. Chem.* **2012,** *55* (23), 10610-10629.

153. Torres, É., M.N. Berberan-Santos,M.J. Brites, Synthesis, photophysical and electrochemical properties of perylene dyes. *Dyes and Pigments* **2015,** *112*, 298-304.
154. Avlasevich, Y.,K. Müllen, An Efficient Synthesis of Quaterrylenedicarboximide NIR Dyes. *The Journal of Organic Chemistry* **2007,** *72* (26), 10243-10246.
155. Navarro, O., N. Marion, Y. Oonishi, R.A. Kelly,S.P. Nolan, Suzuki–Miyaura, α-Ketone Arylation and Dehalogenation Reactions Catalyzed by a Versatile N-Heterocyclic Carbene–Palladacycle Complex. *J. Org. Chem.* **2006,** *71* (2), 685-692.
156. Case, F.H., The Preparation of Hydrazidines and as-Triazines Related to Substituted 2-Cyanopyridines1. *The Journal of Organic Chemistry* **1965,** *30* (3), 931-933.
157. Ahn, S.Y.,Y. Ha, The Blue Phosphorescent Iridium Complexes Containing New Triazole Ligands for OLEDs. *Mol. Cryst.* **2009,** *504* (1), 59-66.
158. Adams, R.,L.H. Ulich, THE USE OF OXALYL CHLORIDE AND BROMIDE FOR PRODUCING ACID CHLORIDES, ACID BROMIDES OR ACID ANHYDRIDES. III. *Journal of the American Chemical Society* **1920,** *42* (3), 599-611.
159. Ahn, S.Y.,Y. Ha, Color Tuning of Blue Phosphorescence: New Iridium Complexes Containing a Bipyridine Derivative and Various Ancillary Ligands. *Mol. Cryst.* **2010,** *530* (1), 116/[272]-122/[278].
160. Thamatam, R., S.L. Skraba,R.P. Johnson, Scalable synthesis of quaterrylene: solution-phase 1H NMR spectroscopy of its oxidative dication. *Chem. Commun.* **2013,** *49* (80), 9122-9124.
161. Nowak-Król, A.,F. Würthner, Progress in the synthesis of perylene bisimide dyes. *Org. Chem. Front.* **2019,** *6* (8), 1272-1318.
162. Miletić, T., A. Fermi, I. Papadakis, I. Orfanos, N. Karampitsos, A. Avramopoulos, N. Demitri, F. De Leo, S.J.A. Pope, M.G. Papadopoulos, S. Couris,D. Bonifazi, A Twisted Bay-Substituted Quaterrylene Phosphorescing in the NIR Spectral Region. *Helv. Chim.* **2017,** *100* (11), e1700192.
163. Meyer, Y.H., P. Plaza,K. Müllen, Ultrafast spectroscopy of soluble terrylene and quaterrylene. *Chemical Physics Letters* **1997,** *264* (6), 643-648.
164. Fujimoto, K., M. Takahashi, S. Izawa,M. Hiramoto, Development of Perylene-Based Non-Fullerene Acceptors through Bay-Functionalization Strategy. *Materials* **2020,** *13* (9), 2148.
165. *Merck Index, 11th Edition.*
166. Jelley, E.E., Molecular, Nematic and Crystal States of I: I-Diethyl--Cyanine Chloride. *Nature* **1937,** *139* (3519), 631-631.
167. Jelley, E.E., Spectral Absorption and Fluorescence of Dyes in the Molecular State. *Nature* **1936,** *138* (3502), 1009-1010.

168. Schiebe, G., Über die Veränderlichkeit der Absorptionsspektren in Lösungen und die Nebenvalenzen als ihre Ursache. *Angew. Chem.* **1937,** *50*, 212-219.
169. Rodrigues, A.C.B.,J.S. Seixas de Melo, Aggregation-Induced Emission: From Small Molecules to Polymers—Historical Background, Mechanisms and Photophysics. *Top. Curr. Chem.* **2021,** *379* (3), 15.
170. Englman, R.,J. Jortner, The energy gap law for radiationless transitions in large molecules. *Mol. Phys.* **1970,** *18* (2), 145-164.

Acknowledgements

First of all, I would like to thank my supervisor Prof Karl Börjesson. Your insightful feedback pushed me to sharpen my thinking and brought my work to a higher level. I value the pedagogical approach you took to introduce me to the world of photophysics that I fear no longer. Your creative and constructive thinking taught me a lot about what means to be a Scientist. Thanks for being patient with me and handling my stubbornness. I also would like to thank my co-supervisor Prof Göran Hilmersson for never forgetting to mention the importance of physical exercise, for Thursday's running club where I learned how to run properly and for your mentorship advice. I would like to thank my examiner Morten Grøtli, whose invaluable input and advice always cleared the skies above my head. Your thoughtful guidance made me understand and even appreciate my ISP.

I would like to express my gratitude to Dr Hugo Bronstein for accepting to be my opponent, Prof Nina Kahn, Ass Prof Henrik Ottoson, Prof Ergang Wang and Prof Joakim Andreasson for accepting the to participate in my thesis jury and for constructive comments that are coming.

To all my collaborators who contributed significantly to work, Dr Fredrik Edhborg, Sandra Hultmark, Prof Lar Eriksson, Dr Naeem Iqbal, Prof Uwe Müller, Prof Bo Albinsson, Dr Ulrika Brath. Thanks to Prof Jürgen Gräfenstein for explaining the quantum world to me and teaching me about quantum-mechanical calculations. Special thanks to my collaborators in the Swedish NMR Centre, Dr Ulrika Brath and to Dr Zoltan Takacs, who showed me how to use the force of the magnets. Zoltan, your enthusiasm and undying desire to find out the truth resonates with me at a high frequency.

I would like to express my gratitude to all the colleagues from the 8th floor, past and present. To all my group members, past and present: Amritha, Andrew, Arpita, Clara, Chen, Jürgen, Kati, Khushbu, Mao, Manuel, Martin, Suman, Rahul, Yi and Yizhou. Clara, it was fun to be in the same lab with you and I appreciate that we both know what music is right for the lab. Thanks to my past colleagues: Ivana, Cassandra, Mark, Carlo, Giulia, Per-Martin, Alavi, Emma, Tina, Umberto, Yongjin, Bea. And of course, to the present ones: Amalyn, Sara, David, Marcus, Diego Anna, Sara, Hanna, Luisa, Karan, Rickard, Alica, Emil, Andreas, Monica, Jeemol and everyone else who works on the 8th floor, and special thanks goes to the biking club: Alica, Manuel and Rickard. We had some truly unforgettable trips together. Thanks to the lunch climbing team: Prof Henrik Sundén, Diego, David, Amalyn, Alica, Sara, Karan, Clara, August and many others. Pull-ups club: Diego, Manuel, Mao, David, Prof Emeritus Åke Nilsson and everyone else who joined us. Bijan and Patrik for keeping our NMR magnets energized. Many thanks to all the administrative staff, who are absolutely great at relieving the burdens of PhD paperwork, Linn, Ingrid, Catarina, Johanna thanks a lot for what you do. I also want to thank many great chemists from Chalmers that I had the pleasure of knowing

during my PhD. Firstly, a talented chemist and artist Mariza for making this great cover and for high-grade oregano, Cedrik for your great sense of humour and yoga sessions, Ambra for great climbs and trips with La Negrita, Anna for great hikes, Zhihang, Martyn and Mads for introducing me to Gammel Dansk. Additionally, I would like to thank my colleagues who did and still do student representational work at all levels. Thanks to the CMB PhD council, NDR PhD council, and GUDK PhD Committee at GU, and all the other boards I have been a part of. Special thanks to Malin Podlevskikh-Carlström, Veronica Ideböhn, Katharina Keuenhof and Denis Sukhino-Khomenko. Furthermore, to the SFS-DK, aka the most pleasant board to be a member of. Pil, I think you should be nominated for an interstellar PhD committee when they make one. Linnea, Daniel, Sebastian, Chris, Marvin, Katharina, Lakshmi, Gustav I am happy to be working with you all, you make a great team.

Thanks to my friends with whom I have been climbing, running and doing all sorts of stuff. You all have been a great support to me during my PhD studies. Thanks to Sandra, Bas, Johanna, Aila, Maude, Alex, Tanya, Matthias, Eden, Sabino. Special thanks to Fredrik Schubert, we had a great kombucha run. To all my workout buddies and pubmates. To my great friends from Stockholm, Helene, Slavik, Alona, Pavel, Anna, Slava, Vera and others. You all made my first year in Sweden absolutely fantastic. Special thanks to my best travel buddies, Daniel, Max and Helene. Thanks to Niklas, because of who I ran my first ultramarathon in the snow. Thanks to my friends in Moldova, Oleg, Sashulya, Sasha, Ira, Mazan, Igor, Yura and many-many others. Thank you for still being here. Thanks to my friends who live all over the world, Andrew, Yulia, Max, Daniel, it was great visiting you all during my PhD times.

A separate acknowledgement goes to my mentors and people who were inspirational to me. Thanks to Anneli Brännström who gave me enormous support, useful advice and engaged in great discussions. Thanks to my supervisors in KTH, Stockholm, Prof Anna-Karin Borg-Karlsson and Dr Raimondas Mozuraitis, I appreciate your guidance and support. To my mentor, Dr Sukhanya Raghavan who gave me the motivation to search for the answers myself. Thomas Olsson, for unveiling the potential of Python skills for an organic chemist, great discussions about toxic and hazardous chemicals and for your great support. Thanks to Jerker Ligthart and ChemSec for giving me the opportunity to contribute with my knowledge and skills in driving the industries towards safer chemicals. Thanks to Cedrik Wiberg for giving me the chance to contribute to the field of organic flow batteries. A distinct acknowledgement goes to the staff of Biochemtech, especially to Shimiket Abegaz, Ivan and Rustam. My chemistry carrier began with all of you guys and those times were simply the best. Thanks to Prof Boris Kovalev for teaching me everything about the total synthesis of insect pheromones. And great thanks to my high-school chemistry teacher Vladlena Alexandrovna, you sparked my interest in chemistry and I give you a big credit for that.

Special thanks to Andrew Carrod, Clara Schäfer, Cedrik Wiberg and Jürgen Gräfenstein for proofreading this thesis. Thanks to SI for welcoming me to Sweden, proud to be your alumni. Throughout the years I have been working on this thesis I have received a great deal of support and assistance from all of you, and since I am writing this literally before sending it to print there is a chance, I have forgotten to mention some names. I apologise for that.
Many thanks to Vladimir, your energy and motivation are truly inspirational. My greatest acknowledgement and appreciation go to my Mother. You have been an eternal source of inspiration to me. You give me a lot of strength. I appreciate enormously the education you gave me and the love and patience you still have (hopefully) for me. This would not have been possible without you. Literally.

Appended papers I-IV